DE86014658

NTIS
One Source. One Search. One Solution.

CO + H SUB 2 REACTION OVER NITROGEN-MODIFIED IRON CATALYSTS. FINAL TECHNICAL REPORT, AUGUST 1, 1982-DECEMBER 31, 1985

PURDUE UNIV., LAFAYETTE, IN. SCHOOL OF CHEMICAL ENGINEERING

1985

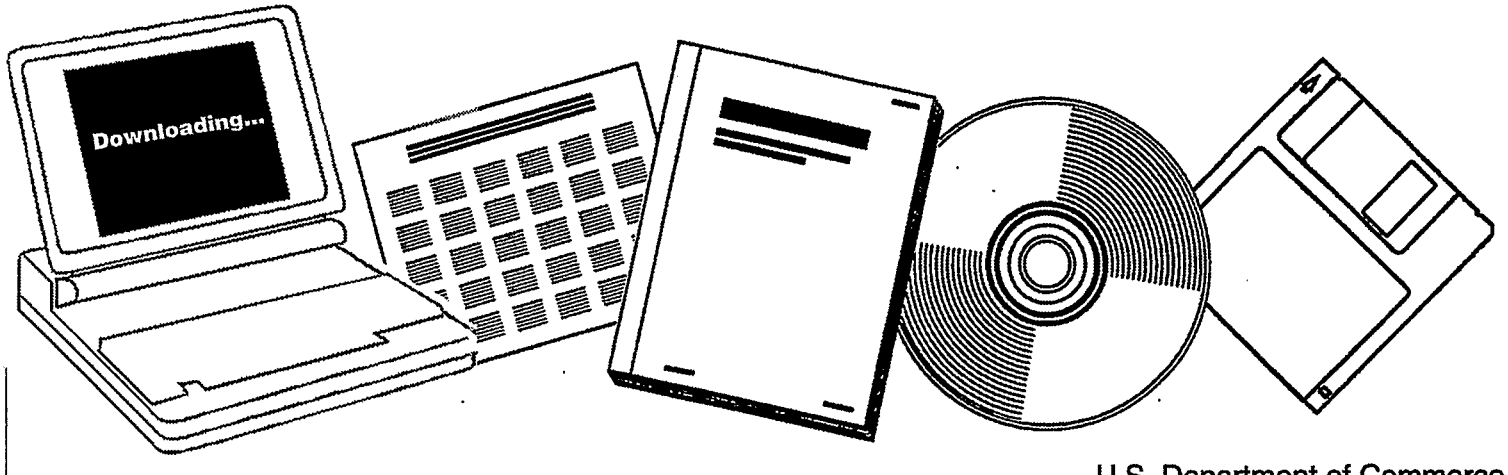

U.S. Department of Commerce
National Technical Information Service

One Source. One Search. One Solution.

NTIS

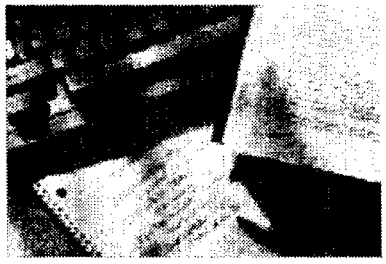

Providing Permanent, Easy Access to U.S. Government Information

National Technical Information Service is the nation's largest repository and disseminator of government-initiated scientific, technical, engineering, and related business information. The NTIS collection includes almost 3,000,000 information products in a variety of formats: electronic download, online access, CD-ROM, magnetic tape, diskette, multimedia, microfiche and paper.

Search the NTIS Database from 1990 forward

NTIS has upgraded its bibliographic database system and has made all entries since 1990 searchable on **www.ntis.gov.** You now have access to information on more than 600,000 government research information products from this web site.

Link to Full Text Documents at Government Web Sites

Because many Government agencies have their most recent reports available on their own web site, we have added links directly to these reports. When available, you will see a link on the right side of the bibliographic screen.

Download Publications (1997 - Present)

NTIS can now provides the full text of reports as downloadable PDF files. This means that when an agency stops maintaining a report on the web, NTIS will offer a downloadable version. There is a nominal fee for each download for most publications.

For more information visit our website:

www.ntis.gov

U.S. DEPARTMENT OF COMMERCE
Technology Administration
National Technical Information Service
Springfield, VA 22161

DOE/PC/50804--14

DE86 014658

DE86014658

DOE/PC/50804-14

$CO+H_2$ Reaction Over Nitrogen-Modified Iron Catalysts

Final Technical Report
for the Period Aug. 1, 1982 - Dec. 31, 1985

W. Nicholas Delgass
Purdue University
West Lafayette, Indiana 47907

PREPARED FOR THE

U.S. DEPARTMENT OF ENERGY

DISCLAIMER

This report was prepared as an account of work sponsored by an agency of the United States Government. Neither the United States Government nor any agency thereof, nor any of their employees, makes any warranty, express or implied, or assumes any legal liability or responsibility for the accuracy, completeness, or usefulness of any information, apparatus, product, or process disclosed, or represents that its use would not infringe privately owned rights. Reference herein to any specific commercial product, process, or service by trade name, trademark, manufacturer, or otherwise does not necessarily constitute or imply its endorsement, recommendation, or favoring by the United States Government or any agency thereof. The views and opinions of authors expressed herein do not necessarily state or reflect those of the United States Government or any agency thereof.

MASTER

DISTRIBUTION OF THIS DOCUMENT IS UNLIMITED

Disclaimer

This report was prepared as an account of work sponsored by the United States Government. Neither the United States nor any agency thereof, nor any of their employees, makes any warranty, express or implied, or assumes any legal liability or responsibility for the accuracy, completeness, or usefulness of any information, apparatus, product, or process description disclosed, or represents that its use would not infringe privately owned rights. Reference herein to any specific commercial product, process or service by trade name, mark, manufacturer, or otherwise, does not necessarily constitute or imply its endorsement, recommendation, or favoring by the United States Government or any agency thereof. The views and opinions of authors expressed herein do not necessarily state those of the United States Government or any agency thereof.

TABLE OF CONTENTS

	page
Disclaimer	ii
TABLE OF CONTENTS	iii
LIST OF FIGURES	iv
LIST OF TABLES	viii
ABSTRACT	1
1. OBJECTIVE AND SCOPE	3
1. Background	3
2. Objectives	4
2. TECHNICAL PROGRESS	5
2.1 Summary of Results	5
2.2 Stability of Iron Nitride Catalysts	6
2.2.1 Introduction	6
2.2.2 Experimental Techniques	8
2.2.3 Preparation of Iron Nitride Catalysts	11
2.2.4 Iron Nitride Stability	21
2.2.5 Nitride Stability During Fischer-Tropsch Synthesis	27

page

2.3 Iron Nitrides as Fischer-Tropsch Catalysts 30

2.3.1 Introduction 30

2.3.2 Steady State Fischer-Tropsch Reaction over the Iron Nitrides 32

2.3.3 Kinetic Behavior at 458 K 37

2.3.4 Phase Behavior at 458 K 41

2.3.5 α-Fe Carburization at 458 K 41

2.3.6 γ'-Fe_4N Carburization at 458 K 45

2.3.7 ϵ-Fe_xN Carburization at 458 K 48

2.3.8 ζ-Fe_2N Carburization at 458 K 50

2.3.9 Effect of CO Pretreatment on FTS 52

2.3.10 Kinetic Behavior of Preoxidized ζ-Fe_2N 58

2.3.11 Phase Behavior of Preoxidized ζ-Fe_2N 60

2.3.12 Hydrogenation of Catalysts After Reaction 65

2.3.13 Carburization of Iron and Iron Nitrides at 523 K 70

2.4 Modification of Iron Nitride Chemistry by Supports and by Gas Pha.. Ammonia 93

2.4.1 Selectivity and Stability of Synthesis Reactions Over Iron Nitrides 93

2.4.2 Catalyst Preparation 94

2.4.3 Addition of Ammonia to Synthesis Gas 95

2.4.4 Small Particle Iron on Carbon 101

page

3. REFERENCES 108

4. APPENDICES 110

1. Report Distribution List 110

2. DOE Form RA 427 112

List of Figures

page

Figure 1 Nitriding Conditions 12

Figure 2 Mössbauer Spectra of Single Phase Nitrides 13

Figure 3 Mössbauer Spectra of ϵ–Fe_xN 17

Figure 4 Fits of ϵ nitrides using 25 point distribution 20

Figure 5 Mössbauer Spectra of ς–Fe_2N during nitriding and denitriding 22

Figure 6 *In-Situ* Analysis of ς–Fe_2N Stability at 523 K 24

Figure 7 Decomposition of Iron Nitrides in Hydrogen Sequence: He→H_2 at 523 K 25

Figure 8 Decomposition of Fe_2N in Deuterium at 523 K 28

Figure 9 First Minute of Synthesis over ϵ–$Fe_{2.7}N$ Sequence: He→$3H_2$/CO/He at 523 K 29

Figure 10 Titration of ϵ–$Fe_{2.7}N$ Surface with Hydrogen After 5 minutes of Synthesis Sequence: $3H_2$/CO/He (5 min) → $9H_2$/Ar at 523 K 31

Figure 11 Steady Stte Activity of C_5 Hydrocarbons Conditions: $3H_2$/CO at 523 K and atmospheric pressure 33

Figure 12 Mössbauer Spectra of α–Fe Reacted at 458 K 42

Figure 13 Mössbauer Spectra of γ–Fe_4N Reacted at 458 K 46

Figure 14 Mössbauer Spectra of ϵ–Fe_xN Reacted at 458 K 49

Figure 15 Mössbauer Spectra of ς–Fe_2N Reacted at 458 K 51

Figure 16 Effect of CO Pretreatment on First Minute of Synthesis over ς–Fe_2N Sequence: NH_3–CO (1 min) →$3H_2$/CO at 523 K 54

Figure 17 Mössbauer Spectra of Pre-oxidized ς–Fe_2N Reacted at 523 K 61

page

Figure 18 Hydrogenation of ϵ–$Fe_{2.7}N$ Catalyst After 12 hours of Synthesis 66

Figure 19 Hydrogenation of ς–Fe_2N Catalyst After 12 hours of Synthesis 68

Figure 20 Mössbauer Spectra of α–Fe Carburized at 523 K 71

Figure 21 Mössbauer Spectra of Nitrides Treated in CO at 523 K 77

Figure 22 Mössbauer Spectra of ς–Fe_2N Carburized at 523 K 82

Figure 23 Mössbauer Spectra of γ'–Fe_4N Carburized at 523 K 88

Figure 24 Step change from H_2 to 4/1 NH_3 /He over reduced iron powder at 400 ° C 96

Figure 25 Initial minutes of reaction of 2:7:3 CO:H_2: NH_3 at 500 ° C over a prenitrided iron powder 98

Figure 26 Initial minutes of reaction of 2:7:3 CO:H_2 :NH_3 at 500 ° C over reduced 4% Fe/SiO_2 99

Figure 27 Decay of activity over a 4% Fe/SiO_2 catalysts as measured by gas chromatography 100

Figure 28 Acetonitrile production during a pulse of 2:7:3:1.5 CO:H_2: $^{15}NH_3$: Ar into 2:7:3:1.5 CO:H_2: $^{14}NH_3$: He at 500 ° C over Fe/SiO_2 102

Figure 29 Room Temperatur Mössbauer Spectra of 4.5 wt% Fe Supported on Carbolac 105

Figure 30 Room Temperature Mössbauer Spectra of 4.08% Fe Supported on CSX203 Carbon 106

List of Tables

page

Table 1 Mössbauer Parameters (298 K) Single Phase Nitrides 14

Table 2 Mössbauer Parameters (298 K) for Single Phase Nitrides 18

Table 3 Activity and Selectivity Results After 12 Hours of Synthesis at 523 K 35

Table 4 Iron and Iron Nitrides Kinetics at 458 K 38

Table 5 Mössbauer Parameters (298 K) for Catalysts Reacted at 458 K 43

Table 6 Iron and Pre-oxidized ς-iron Nitride Kinetics at 523 K 59

Table 7 Mössbauer Parameters for Pre-oxidized ς-Fe_2N 62

Table 8 Mössbauer Parameters (298 K) of Carburized Iron 72

Table 9 Mössbauer Parameters (298 K) of CO Treated Nitrides 75

Table 10 Mössbauer Parameters (298 K) of H_2/CO Treated ς-Nitride 83

Table 11 Mössbauer Parameters (298 K) of H_2/CO Treated γ'-Nitride 89

Table 12 Mössbauer Spectral Parameters 104

Table 13 Mössbauer Spectral Parameters 104

ABSTRACT

Our study of iron nitrides has included the preparation, stability, and catalytic kinetic behavior of these materials as Fischer-Tropsch synthesis (FTS) catalysts. Preparation of the three major phases (γ'–Fe_4N, ϵ–Fe_xN $2< x <3$, ζ–Fe_2N) is achieved by flowing NH_3/H_2 mixtures over reduced iron powders in the temperature range 250 - 500 ° C. The pure phases are easily identified by Mössbauer spectroscopy. Using constant velocity Mössbauer spectroscopy and mass spectral analysis we have i) observed the expected fast decomposition of the nitrides in hydrogen, ii) shown that restricted access of hydrogen to the surface in the initial stages of the decomposition can account for the low initial rate and the increase of the rate to a maximum, iii) shown that the pure nitride phases are also very unstable in CO/H_2 at Fischer-Tropsch reaction conditions, but in the presence of CO-containing gases the nitrides are converted to carbonitrides rather than α -iron. Loss of nitrogen from the carbonitrides during reaction is a slow process. Transient mass spectral analysis reveals that freshly prepared nitrides have an adsorbed NH_x species. On the fresh surface, hydrogen reacts preferentially with nitrogen rather than CO, removing approximately one monolayer of nitrogen before methane production begins. The reaction then proceeds on a surface containing essentially no reactive nitrogen.

The carbonitrides formed after steady state reaction over the three iron nitride starting materials have been identified by Mössbauer spectroscopy. Kinetics of FTS at atmospheric pressure and 3/1 H_2/CO over these phases are reported. The activity and

selectivity over iron nitrides are similar to those over reduced iron, although high initial activity, higher olefin to paraffin ratios, high CO_2 production rate and overall higher activity for the ϵ and ς catalysts were noted for the nitrides. Pretreatment of nitrided catalysts with CO resulted in a momentary inhibition of all activity, whereas O_2 pretreatment gave evidence of enhanced C_4 selectivity.

Addition of ammonia to synthesis gas over reduced or prenitrided iron at 500 °C produced acetonitrile. High deactivation rates over iron powders prompted the use of silica supported iron catalysts which are much more stable in activity. ^{15}N transient studies show the reaction to be governed by a small highly reactive pool of nitrogen on the surface.

Small particle iron on carbon catalysts showed unique stability of activity and nitride phase during FTS. Both the Mössbauer effect and chemisorption confirm the small size of the Fe particles on the reduced catalyst. A reduced, nitrided, reacted in FTS and rereduced iron on carbolac sample showed that the particles sinter during this cycle. Small particle nitrides and the production of nitrogen-containing compounds are the subject of continuing study.

1. OBJECTIVES AND SCOPE

1.1 Background

The feasibility of utilizing synthesis gas (CO + H_2) via the Fischer-Tropsch reaction pathway for the production of fuels and chemicals is well established. The SASOL ventures, for example, take advantage of abundant coal resources to produce both desirable synthetic automotive fuels and basic chemical feedstocks. The applicability of these chemical transformations is nonetheless limited. The present procedure requires extensive processing if the production of non-essential byproducts is to be avoided. The discovery and subsequent usage of improved catalysts would therefore be advantageous.

Experimental results published in the current literature show that nitrogen affects the performance of iron catalysts-catalysts which find widespread use in the Fischer-Tropsch synthesis route. Prenitriding of the iron catalyst has been reported to shift the product distribution to one exhibiting lower molecular weight fractions and enhanced alcohol yields (1). On the other hand, simultaneous introduction of ammonia (NH_3) with synthesis gas produces nitrogeneous compounds (2-5). Furthermore, and probably of greater importance, this addition of ammonia effects a reduction in the overall chain length of compounds in the product spectrum (2). It is of considerable interest, therefore, to study these and other characteristics of nitrided iron catalysts in order to gain a basic understanding of their behavior. Discovery of the new pathways in Fischer-Tropsch synthesis afforded by nitrogen will add to the fundamental knowledge from

which future synthesis-catalysts can be derived.

1.2 Objectives

The scope of the program may be broken down into two main areas of concern. Firstly, consideration must be given to the role of the surface nitrogen in

i. altering the product distribution and

ii. stabilizing catalyst activity

of the synthesis reactions. *In-situ* Mössbauer studies identify the various iron nitride phases and allow for examination of their stability during reaction. The Mössbauer results form the basis for detailed kinetic tracer experiments involving transient and isotope labeling analyses.

The second area of consideration involves the kinetic and catalytic effects observed during the addition of ammonia to the synthesis gas stream. Transient work is ideal for observing initial activity changes occurring as a result of NH_3 pulses. The transient kinetics of NH_3 addition also help clarify the most productive steady state experiments. The various analytical methods define interactions between surface and bulk nitrogen, and their role in effecting new reaction pathways.

The primary experiments which define our route to understanding which parameters influence the selectivity and alter the activity of synthesis reactions may, therefore, be outlined as follows:

i. Mössbauer and simultaneous kinetics of prenitrided iron catalysts are used to determine nitride phase stability and to correlate these phases to reaction

selectivity.

ii. Similar analysis of the effects of addition of NH_3 to the reactant stream are performed.

iii. Transient analysis and isotope tracer studies of synthesis reactions over prenitrided catalysts determine surface nitride stability. The stoichiometry at the surface and the influence of prenitriding on surface carbon inventory are sought.

iv. The effects of NH_3 addition to the reactant stream are similarly followed by transient tracer studies to determine possible alterations in reaction pathways invoked by the presence of NH_3.

2. Technical Progress

2.1 Summary of Results

We have separated our major results into three sections; stability of iron nitride catalysts (2.2), iron nitrides as Fischer-Tropsch catalysts (2.3), and modification of iron nitride chemistry by supports and by gas phase NH_3 (2.4). In the first section, we briefly review the reasons for interest in these catalysts and discuss our techniques for studying them. Preparation of the different phases from reduced iron powders can be achieved from NH_3/H_2 mixtures, but the nitrides are extremely unstable in pure hydrogen. In addition to the formation and decomposition of these structures, we report on the initial stability in H_2/CO mixtures.

In the second section, we report on our studies of the Fischer-Tropsch synthesis

at atmospheric pressure over nitrided catalysts. Both the phase behavior, (production of carbonitrides) and kinetic activity are discussed. CO and O_2 pretreatments, and hydrogenation of these catalysts after reaction were among the experimental studies.

The final section discusses modifications of both catalyst and synthesis reaction. Ammonia is added to synthesis gas and reacted over $Fe/si0_2$ based catalysts at 500 °C to produce acetonitrile. Small particle Fe/C catalysts were made to study its catalytic behavior for synthesis reactions.

2.2 Stability of iron Nitride Catalysts

2.2.1 Introduction

Iron nitride Fischer-Tropsch catalysts, originally investigated by Anderson and coworkers at the Bureau of Mines (1,6,7), reportedly provided higher activity, long life, somewhat shorter product chain lengths and significantly higher alcohol production rates than promoted fused iron catalysts. Recent studies by Yeh, *et al.* (8,9) indicate somewhat different selectivities but confirm the higher activities for a promoted catalyst at 7.8 and 14 atmospheres pressure for a 1:1 H_2:CO mixture. Most significant in both studies, however, is the extremely long life of bulk nitrogen in H_2/CO mixtures, whereas in pure H_2 nitrided catalysts are extremely unstable. The stability of these catalysts in various gas phase atmospheres is therefore a central issue in evaluating this catalyst for a particular reaction. In this report we examine the preparation and stability of the different unsupported

nitride phases, γ'–Fe_4N, ϵ–Fe_xN ($2<x<3$) and ς–Fe_2N, in an effort to understand differences in the Fischer-Tropsch behavior caused by nitriding iron catalysts.

Preparation of the three major phases of iron nitride, γ'–Fe_4N, ϵ–Fe_xN ($2<x<3$) and ς–Fe_2N can be accomplished by varying the NH_3/H_2 nitriding compositions and/or temperature, as reported by numerous authors (7,10-12). The different nitride stoichiometries are easily identified by their characteristic Mössbauer spectra, studied most recently by researchers at Northwestern (8,9,13). Also, stoichiometries and phase identification can be confirmed by X-ray diffraction and mass spectrometric measurement of the ammonia evolved during decomposition in hydrogen.

The Mössbauer effect is ideal for characterizing both steady state and dynamic forms of the catalyst under various conditions. Transient mass spectrometry, in tandem with the Mössbauer results, describes the dynamic chemistry that has occurred at the surface. We summarize here the preparation and characterization of iron nitride powders, and consider the stability of these nitrides in different atmospheres.

The Mössbauer results indicate that the pure nitride phase is unstable both in hydrogen and synthesis gas, although the nitride is completely lost to ammonia and α-Fe in hydrogen, whereas in synthesis gas carbonitrides are formed. Results from mass spectrometric investigation of the dynamic surface chemistry during the Fischer-Tropsch synthesis reaction give possible explanations for the remarkable stability of nitrogen in the bulk of these catalysts, namely that carbon, resulting

from the dissociation of carbon monoxide, effectively blocks the sites necessary for hydrogenation of bulk nitride. Apparently no surface nitrogen is present during Fischer-Tropsch synthesis.

2.2.2 Experimental Techniques

The unsupported iron oxide catalyst precursors used for this study were prepared by precipitation of iron oxyhydride from a mixture of NH_4OH and a 0.17M $Fe(NO_3)_3$ nitrate solution. The filtered cake was dried and pulverized in air at 370K and then oxidized at 573 K to form Fe_2O_3. For a second batch of catalyst prepared for the Mössbauer studies, the oxidization was carried out at 500 K. For the Mössbauer experiments, 25 mg of iron oxide precursor and 200 mg of EH-5 silica, mixed in as a diluent, were mechanically pressed into a self supporting 1.5 cm diameter wafer, approximately 1.5-2.0 mm in thickness. For the transient mass spectrometry experiments, 100 mg of precursor was packed between pyrex wool plugs in a 6 mm i.d. pyrex reactor tube. Individual samples of catalyst precursor were reduced in flowing H_2 for at least 4 hours at 673 K before nitriding. The surface area of the reduced catalysts was determined by flowing BET(44); the samples used for the Mössbauer experiments (without the silica diluent) gave a nitrogen uptake at 77 K corresponding to 1.6 $\pm$ 0.1 m^2/ gram reduced Fe, and that of the samples to be used for transient mass spectrometry 4.3 $\pm$ 0.1 m^2/g.

Both constant acceleration and constant velocity *in-situ* Mössbauer spectra were obtained with an Austin Science S-600 spectrometer controller. Data were

acquired in 256 channels of a Nuclear Data model 62 multichannel analyzer. The 70 mCi gamma ray source, ^{57}Co diffused in a Rh matrix, was obtained from New England Nuclear. Zero isomer shift was referenced to the center of a 25 μm NBS Fe foil spectrum. Room temperature spectra were obtained after the sample had cooled to ambient temperature in the appropriate gas mixture. The stability of the individual nitride phases was investigated at reaction conditions using the constant velocity (transient) mode, in which the velocity at a particular peak was monitored rather than a scan of energies as in the more familiar constant acceleration mode (22).

Most constant acceleration spectra were computer fit with Lorentzian lineshapes using a variable metric minimization method. The program allows for linear constraints on dips, widths and positions of the peaks. These constraints are chosen so that the parameters conform to physics of the Mössbauer Effect. In this study all six line patterns have a core set of constraints. Specifically, they are equal dips for pairs of peaks and equal widths for all six, a 3:2:1:1:2:3 area ratio between the six peaks, and relationships between the positions of the peaks as demanded by symmetry of hyperfine and quadrupole splittings on the energy transitions to the excited nuclear spin states. For a doublet, the dips and widths are equal. Some constant acceleration spectra were also computer fit with a routine developed by Niemantsverdriet (14). The routine fits a predetermined number of six line patterns, singlets or doublets to the data with optionally fixed or variable parameters of isomer shift, quadrupole shift, hyperfine field, or line width. The

individual spectrum components are a function of these parameters such that they conform to the physics of the Mössbauer effect. The program employs a Levenberg-Marquardt nonlinear regression formula to converge on the least squares optimum fit. In addition, the program was modified by Gregg Howsmon in our laboratory to contain a computational procedure for evaluation of overlapping hyperfine parameter distributions as a probability density along a range of hyperfine fields (15,16). A distribution may be fit independently, as in this work, or in conjunction with additional singlet, doublet or six line components.

The transient kinetic apparatus consists of a glass tube reactor within brass sheathing heated by a Research Incorporated IR oven and controlled by a Micristar temperature controller. The reactor can be fed with gas from any of three manifolds or a pulse loop for introduction of isotopically labelled components. Products, or reactants passed through a reactor bypass, were analyzed by an Extranuclear Laboratories EMBA II modulated beam quadrupole mass spectrometer interfaced to a Digital Equipment Corporation MINC-11 minicomputer for data acquisition. The modulated beam design allows for detection of inlet components and discrimination against background gases within the mass spectrometer chamber, which allows for elucidation of troublesome wall absorbing gases such as NH_3 or H_2O.

X-ray Diffraction was performed on a Siemens Kistalloflex 4 spectrometer using Cu K-α X-rays. The three major nitride phases are easily differentiated via the unique diffraction patterns.

All gases used for these experiments were Matheson UHP grade. Molecular sieve and Mn oxygen traps further purified helium and hydrogen. Metal carbonyls in CO were removed in a molecular sieve trap at dry ice-methanol temperature (216 K).

2.2.3 Preparation of Iron Nitride Catalysts

Preparation of the individual bulk nitride phases can be accomplished at atmospheric pressure in different NH_3/H_2 mixtures and at different temperatures. Figure 1 shows the conditions necessary to produce each of the phases after 3-4 hours of nitriding. Our results are in general agreement with those of Eisenhut (11) and Lehrer (12). Both the ζ–Fe_2N and γ'–Fe_4N phases are easily formed over a variety of temperatures and ammonia/hydrogen gas phase compositions, whereas the ϵ–Fe_xN ($2<x<3$) phase is only produced in a narrow composition range ($90 \pm 5\%$ NH_3). At higher temperatures (>800K), the ammonia decomposition reaction becomes dominant and nitrides do not form (17, 18).

Characterization of each of the pure phases can be accomplished by Mössbauer spectroscopy and X-ray diffraction. Figure 2 shows the room temperature spectra of the different nitrides. The solid lines in the spectra are the result of careful computer fitting, with parameters summarized in Table 1. In these fits, all the parameters of line width, isomer and quadrupole shifts or hyperfine field are variables and not independently fixed except that the widths of all lines belonging to the same species are equal. In addition, XRD of the separate phases distinguish

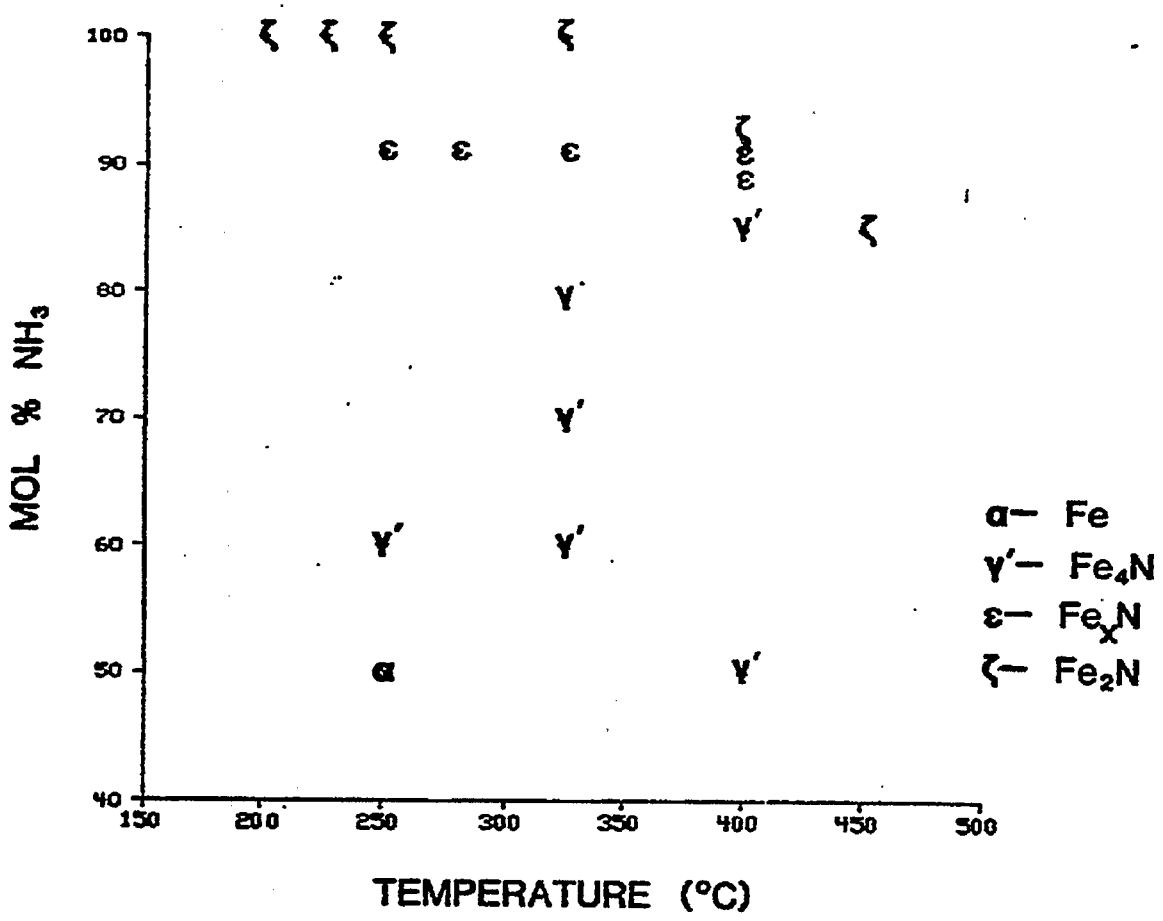

Figure 1 Nitriding Conditions

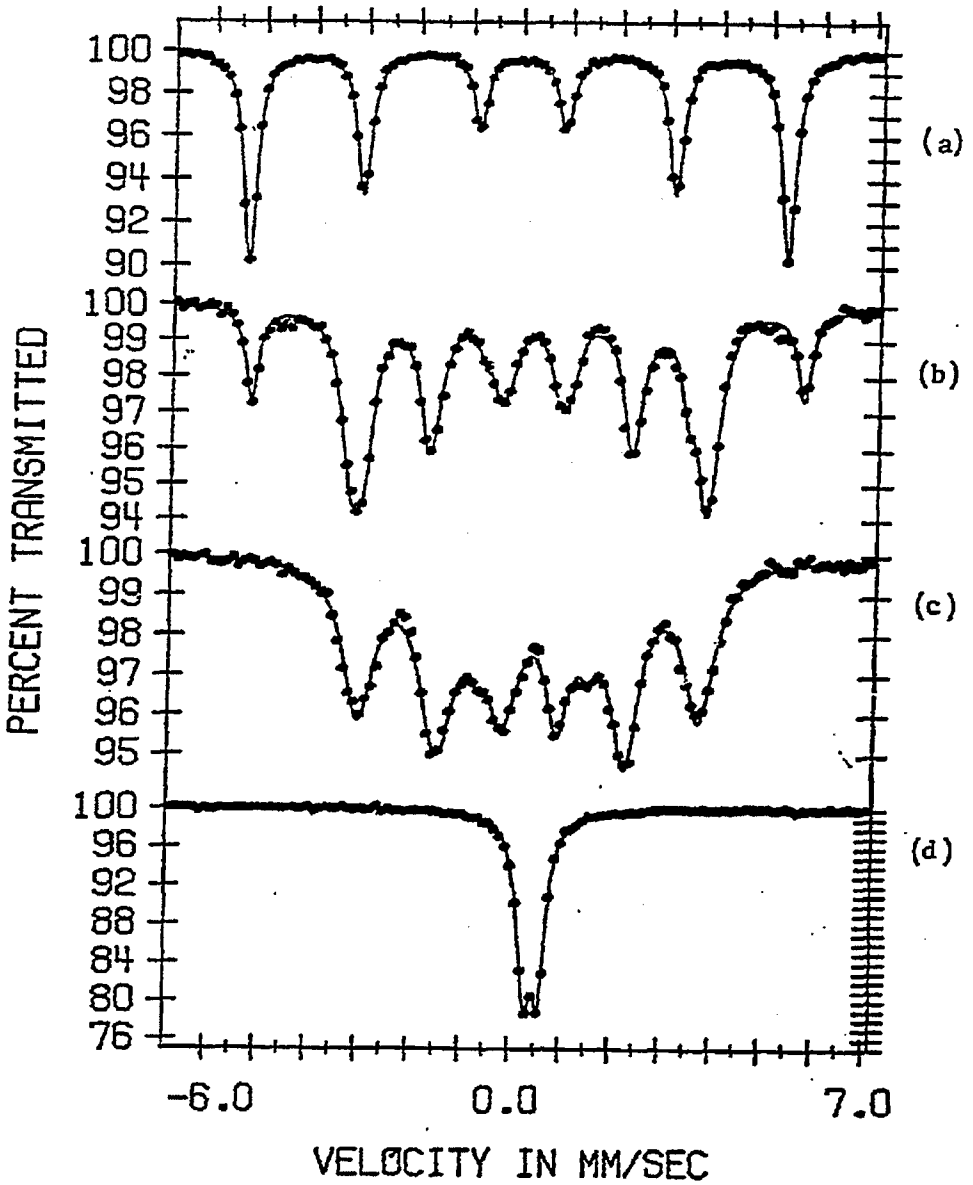

Figure 2 Mössbauer Spectra of Single Phase Nitrides.

a) α -Fe
b) γ'-Fe_4N
c) ε -$Fe_{2.52}N$
d) ζ -Fe_2N

TABLE 1

Mössbauer Parameters (298 K) Single Phase Nitrides

Phase	Figure	Iron Identity	IS (mm/s)	QS (mm/s)	HFS (kOe)	LW (mm/s)	RA (%)	TOTAL Area
α-Fe	2a	α-Fe	0.00	0.00	329.4		100.0	.2151
γ'-Fe_4N	2b	γ'-I	0.23	0.00	339.4		22.2	
		γ'-IIA	0.29	-0.14	218.1		49.9	
		γ'-IIB	0.31	+0.34	215.4		25.0	
		Fe-Q	0.29	1.37	---		2.9	
ε-$Fe_{2.52}N$	2c	ε-II	0.33	0.00	209.0	0.73	61.2	.2858
		ε-III	0.41	0.00	112.4	0.65	30.4	
		Fe-Q	0.32	1.15	---	0.53	8.2	
ζ-Fe_2N	2d	ζ-II	0.43	0.28	---	0.35	100.0	.1813

between the fcc, hcp, and orthorhombic structures of the γ', ϵ, and ς phases respectively, confirming the synthesis of a ς–Fe_2N sample from 100% NH_3 at 400 C, an ϵ phase from 85% NH_3 at 400 C, and a γ' phase from 75% NH_3 at 325 C.

The γ' nitride (Figure 2b) is identified by a characteristic eight line pattern arising from an overlap of Fe-I (zero nitrogen nearest neighbors = 0nn) and Fe-II (2nn) fields. The most positive velocity peak (5.71 mm/s) does not overlap either with iron or the nitrides and serves to indicate the presence of γ'–Fe_4N in complex, overlapping spectra. The γ' nitride can be fit with three different sextets (Fe-I, Fe-IIA and Fe-IIB). The Fe-IIA and Fe-IIB sextets both have the same hyperfine field, and frequently adequate fits can be made using Fe-I and only a single Fe-II site. Clauser (19) proposed that the 215 kOe field (Fe-II) sites IIA and IIB corresponded to face center iron atoms located either parallel to the field (two such atoms on opposite faces of a cube) or perpendicular to the field (the four atoms on the adjacent cube faces). The intensity of the IIA parallel sites therefore should be 1/2 that of the perpendicular IIB, and the QS of IIA equal to -1/2 of that of IIB.

The fitting of Figure 2b is made with all three sextets and a small central doublet, with the parameters reported in Table I. The Fe-Q doublet, necessary to achieve a close fit, appears in all the fits of the nitrides and is usually small (with the exception of certain ϵ nitrides). This component may arise from either the existence of small particle nitrides or non-uniformity in the distribution of the nitrogen in the matrix. Also, in Table I we have neglected any distributions of hyperfine fields that may exist for one particular iron site. This complication will

be considered in the discussion of the ϵ nitrides.

The hexagonal close packed nitrides, ϵ–Fe_xN ($2<x<3$) are shown in Figure 2c and Figure 3. The spectra of Figure 3 represent a range of stoichiometries in order of increasing nitrogen content. As the stoichiometry approaches Fe_2N, the magnetic field collapses to form a broad doublet (Figure 3e). Spectra of the ϵ nitride can be fit with a combination of 3nn and 2nn sites (Table 2) such that $H_{3nn} < H_{2nn}$, and an additional contribution of the nonmagnetic, quadrupole split component Fe-Q. The average stoichiometry of the ϵ-nitrides is estimated from the spectral areas of each of the three components, assuming equal recoil free fractions and 3nn Fe-Q composition. Note that the Fe-Q component increases with nitrogen content, and thus behaves as a nonmagnetic 3nn site that approaches the iron environment of the ζ nitride. The composition range in Figure 3 is then from $Fe_{2.52}N$ to $Fe_{2.14}N$, as indicated in Table 2. This approach yields a linear relation between the hyperfine field for both the Fe-II (2nn) and Fe-III (3nn) sites as a function of nitrogen content.

In these fits, we have assumed that the electric field gradient and hyperfine field remain constant for a particular iron site. However, the environment of an iron nucleus actually may vary in an ϵ nitride as a result of the wide range of stoichiometries possible for this phase. Accordingly, a distribution of hyperfine fields is expected from the random distribution of nitrogen surrounding each iron site. One method of approximating this distribution is given by Chen *et al.* (13) and Yeh *et al.* (8) who have used sextets with linewidths that are an increasing

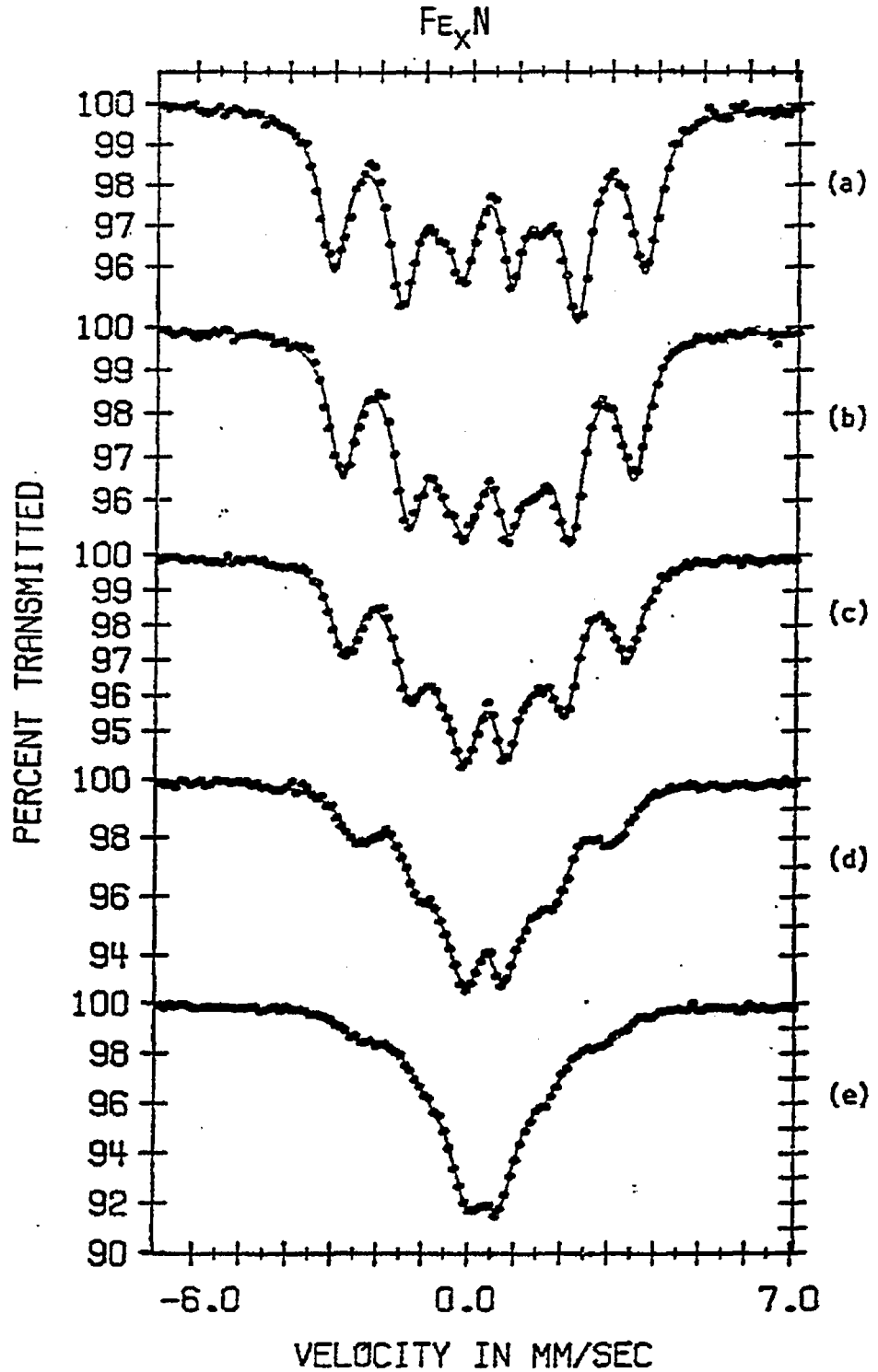

Figure 3 Mössbauer Spectra of ε-Fe$_x$N.

a) nitrided in 90% NH_3 at 598 K for 6 hours
b) nitrided (c) treated in 91% NH_3 at 523 K for 6 hours
c) nitrided (d) treated in 91% NH_3 at 553 K for 6 hours
d) nitrided (e) treated in 91% NH_3 at 598 K for 6 hours
e) nitrided in 91% NH_3 at 673 K for 6 hours

TABLE 2

Mössbauer Parameters (298 K) for Single Phase Nitrides

Phase	Figure	Iron Identity	IS (mm/s)	QS (mm/s)	HFS (kOe)	LW (mm/s)	RA (%)	Total Area
ε-$Fe_{2.52}N$	3a	ε-II	0.33	0.00	209.0	0.73	61.2	.2858
		ε-III	0.41	0.00	112.4	0.65	30.4	
		Fe-Q	0.32	1.15	---	0.53	8.2	
ε-$Fe_{2.39}N$	3b	ε-II	0.33	0.00	195.7	0.70	48.5	.2778
		ε-III	0.43	0.00	103.4	0.73	36.2	
		Fe-Q	0.37	1.10	---	0.92	18.3	
ε-$Fe_{2.33}N$	3c	ε-II	0.32	0.00	189.5	0.73	42.2	.2746
		ε-III	0.43	0.00	99.7	0.72	29.9	
		Fe-Q	0.35	0.97	---	0.83	27.9	
ε-$Fe_{2.25}N$	3d	ε-II	0.31	0.00	171.2	0.90	33.4	.2830
		ε-III	0.44	0.00	88.5	0.79	28.5	
		Fe-Q	0.36	0.87	---	0.90	38.1	
ε-$Fe_{2.14}N$	3e	ε-II	0.28	0.00	161.6	0.96	19.8	.2733
		ε-III	0.46	0.00	78.0	1.07	33.3	
		Fe-Q	0.34	0.68	---	0.93	59.9	

function of velocity to fit nitride spectra. A sextet with a slightly different hyperfine field would overlap a given spectra most at small velocities and overlap least for the outer peaks at high velocities, and thus when combined appear as a spectrum with greater linewidths as velocity increases.

Distributions of hyperfine field can also be fit by dividing the range of field into equal intervals (ΔH); the measured spectrum can then be fit with a probability distribution of discrete hyperfine fields. The method includes smoothness and zero factors to avoid the physically unrealistic solution caused by statistical fluctuations in the data (15, 16). We have fit the series of epsilon nitrides with distributions over the entire hyperfine field range (Figure 4). This necessitates using only one quadrupole and isomer shift for the entire distribution, thus the results can only be deemed as approximate. Nevertheless, Figure 4 graphically demonstrates the two separate fields, and the decay of the maximum at high hyperfine field with the corresponding growth of the inner maximum. Note also the increasing density near zero field. This represents the growth of the wide doublet Fe-Q, which may indeed be due to the onset of paramagnetism , i.e relaxation, for iron sites with 3 nitrogen nearest neighbors at room temperature. This effect is only markedly significant in the highest nitrogen concentration ϵ-nitride. Fits including the combination of a doublet and the distribution at higher fields did not significantly change the fitted parameters for Fe-Q, therefore indicating that the inclusion of a distribution of magnetic environments is not exclusively responsible for the spectrum density in the Fe-Q region.

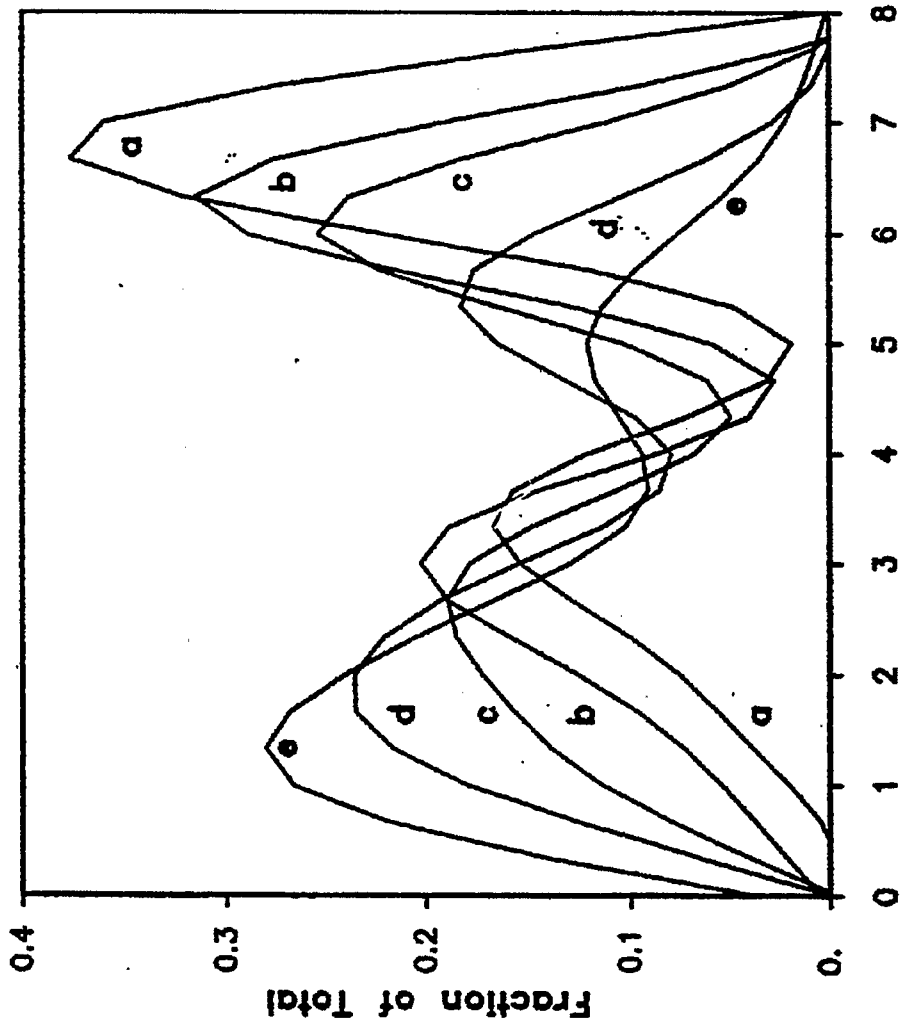

Figure 4 Fits of ε nitrides using 25 point distribution.
Letters a-e represent fits of spectrum of Figure 3a-e respectively.

The last nitride considered is the nitrogen rich phase ς–Fe_2N. This orthorhombic, paramagnetic phase is characterized by a central doublet, as shown in Figures 2d and 5b. In this phase all iron atoms have three nitrogen nearest neighbors. The spectrum does not split out even to 4.2 K (21). The room temperature spectrum, Figure 2d, has an isomer shift of 0.43 mm/s and a quadrupole splitting of 0.28 mm/s.

2.2.4 Iron Nitride Stability

Evaluation of the performance of a prenitrided catalyst for any reaction should asses what form the catalyst takes during that reaction. In this regard, the stability of the iron nitrides in different atmospheres is an important issue in studies involving them. Both Mössbauer spectrometry and transient mass spectrometry can follow the decomposition of these structures.

The collection of a Mössbauer spectrum can take between 4 and 24 hours depending on the strength of the source and the amount of ^{57}Fe in the sample. The usual constant acceleration mode of data accumulation is, therefore, much too slow for transient experiments. If, however, one measures the count rate at a carefully chosen single velocity, one can follow spectral changes on a time scale of minutes (22). Application of this technique to the denitriding and renitriding of ς–Fe_2N is shown in Figure 5. Choice of the constant velocity point at the minimum in the ς nitride doublet, spectrum 5-B, allows good sensitivity to changes in the amount of the nitride phase because this happens to be a region of the iron

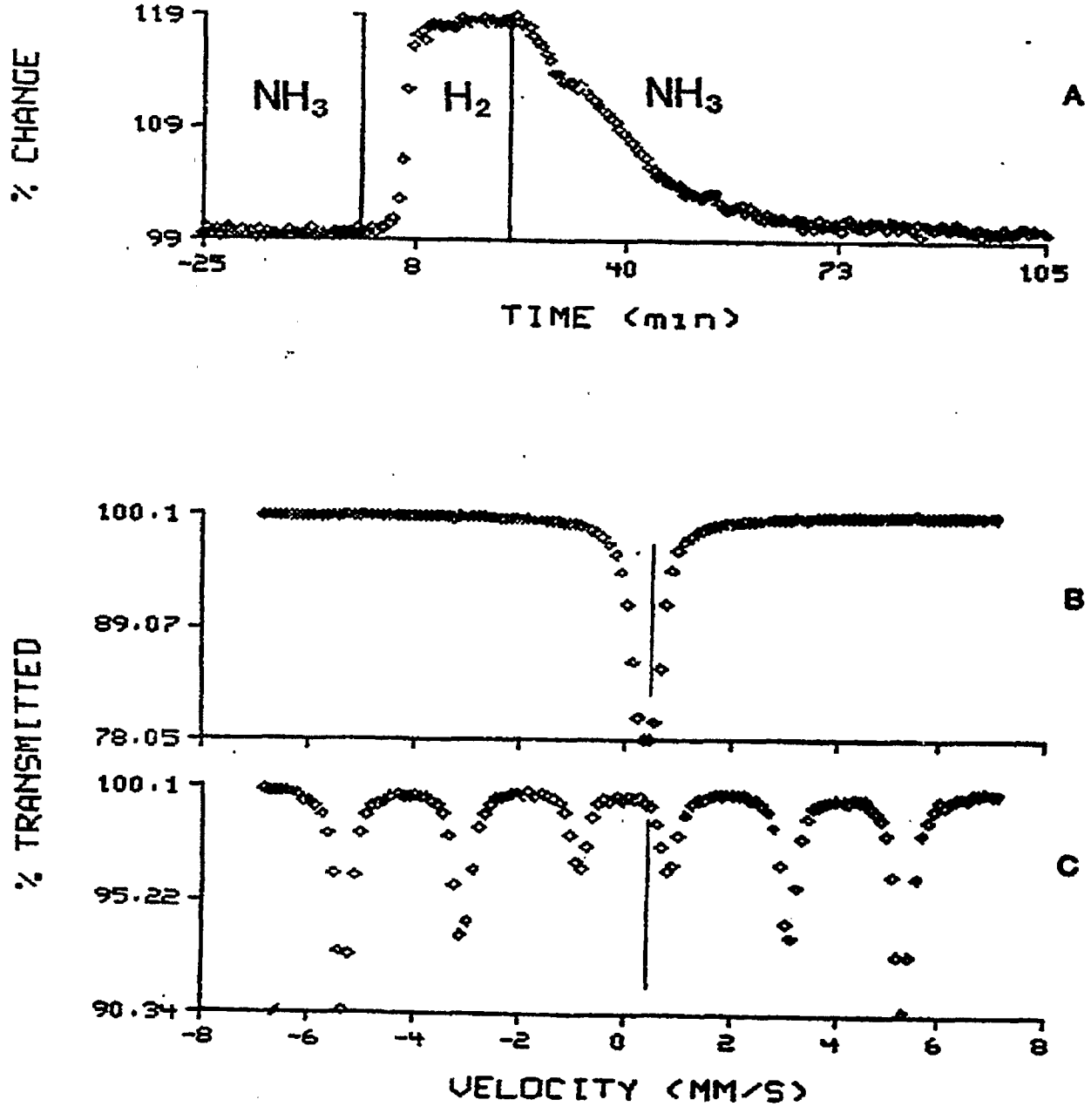

Figure 5 - Mössbauer spectra of ζ -Fe_2N during nitriding and denitriding. A) Constant velocity spectrum, at the velocity indicated by the lines in spectra B) and C), taken at 325°C during a switch from NH_3 to H_2 and back to NH_3. B) Spectra of the initial and final ζ-Fe_2N at 25°C. C) 25°C spectrum of α-Fe denitriding.

metal spectrum (Figure 5-C) where the transmission is nearly 100% (no peak). Curve 5-A shows very fast removal of nitrogen in the presence of pure hydrogen. In a matter of minutes, Fe_2N has become iron metal. Renitriding is slower because the nitrogen must penetrate the hexagonal close-packed nitride lattice rather than the more open bcc structure of α–Fe. The rapid nitride loss shown in Figure 5A is not surprising since the nitrides are known to be unstable in hydrogen (6,7,23).

Figure 6 displays the constant velocity spectra that indicate the stability of the pure nitride phases in different atmospheres. Surprisingly, the pure phase is not stable in CO/H_2 mixtures (Figure 6c). Comparison with Figure 6a shows that the time required for complete loss of the ζ–Fe_2N phase is barely retarded by the change from hydrogen to synthesis gas at 523 K. In this case, however, constant acceleration spectra after various times of exposure show that the nitride is not converted into the metal, but first into the ϵ nitride and then into a carbonitride. In pure hydrogen at 523 K, therefore, nitrogen is completely lost to the gas phase, whereas much of the nitrogen remains in the bulk after the nitrides are exposed to synthesis gas. Spectrum 6-d shows that the rate at which the pure nitride phase is lost can be slowed significantly if all the hydrogen is removed from the synthesis gas. Note that the greater scatter in this curve results from the change in scale.

We have studied the nitrogen removal process in some detail. Using computer-controlled mass spectrometry, the decomposition products in the effluent of a differential plug flow reactor can be monitored with time. Heating an iron nitride sample in flowing helium and monitoring the gas phase effluent for N_2 produces a

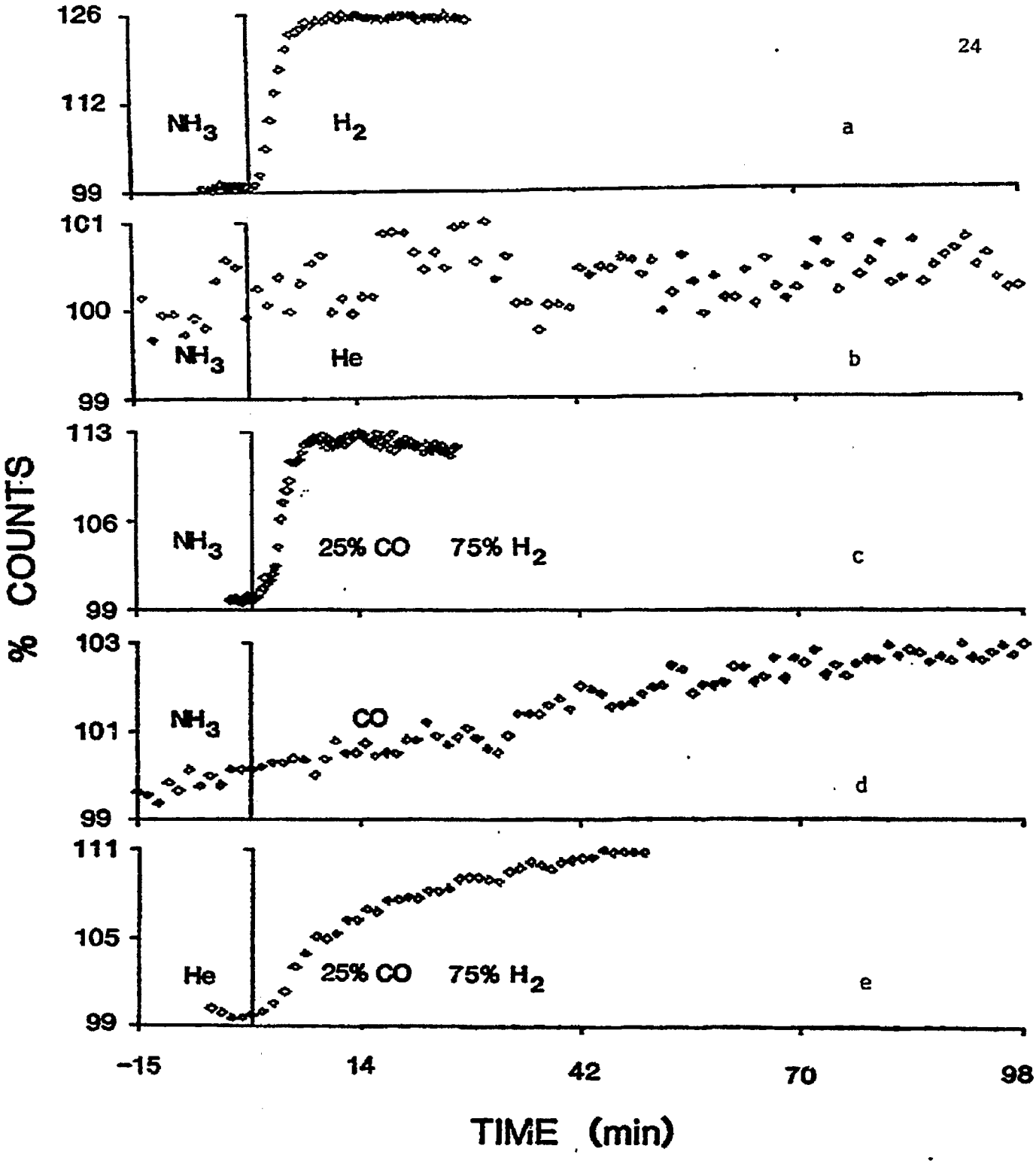

Figure 6 In Situ Analysis of ζ-Fe_2N Stability at 523 K.

a) step change to H_2 from NH_3
b) step change to He from NH_3
c) step change to $3H_2/CO$ from NH_3
d) step change to CO from NH_3
e) step change to $3H_2/CO$ from NH_3 over pre-oxidized ζ-Fe_2N

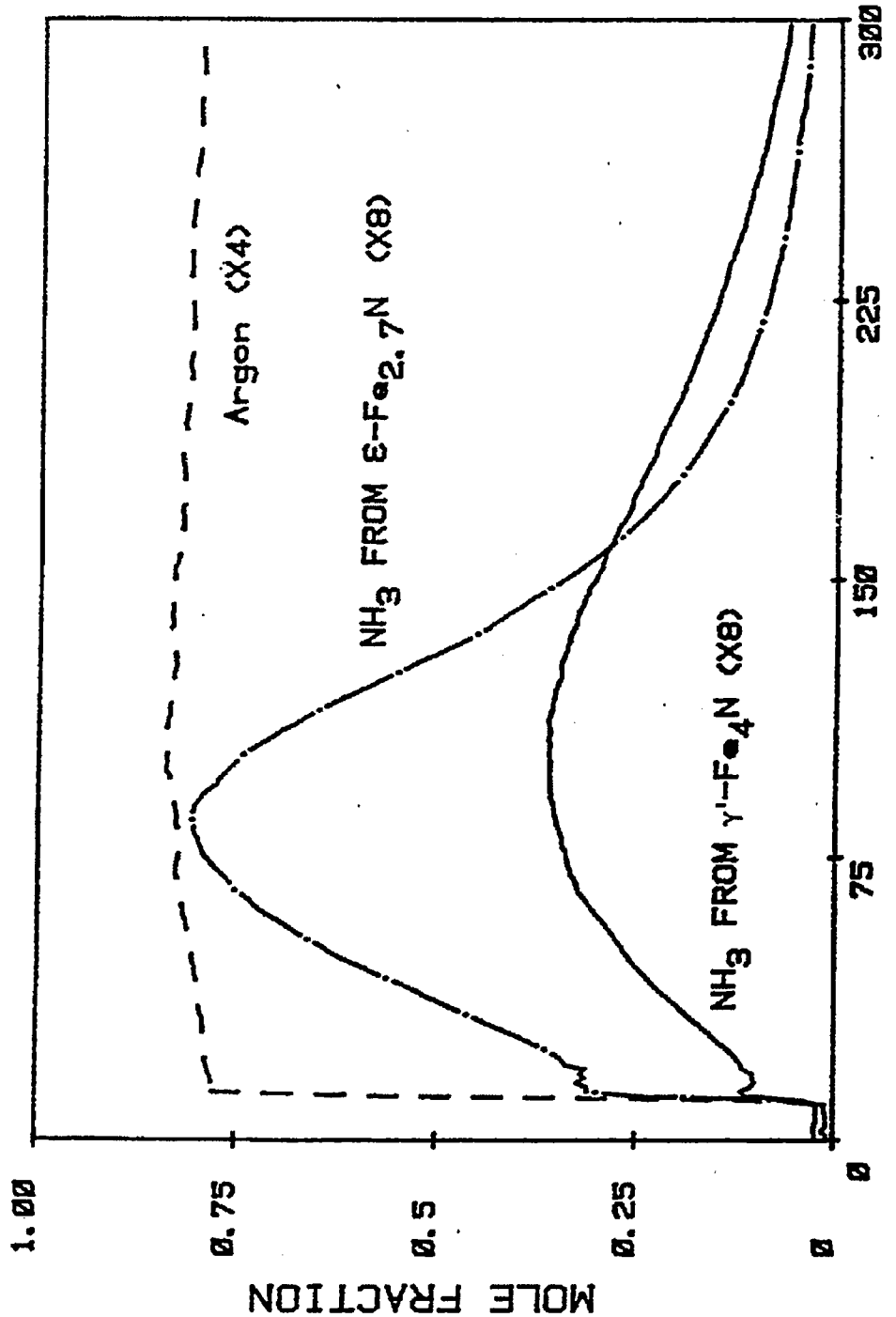

Figure 7 Decomposition of Iron Nitrides in Hydrogen
Sequence: He → H_2 at 523 K

temperature programmed decomposition spectrum of the nitride. Such experiments confirm the Mössbauer findings that at temperatures below 650 K the nitrides are stable in helium. When a freshly prepared nitride is flushed with a short pulse of He to remove the NH_3/H_2 synthesis mixture and then exposed to H_2 at 523 K, the ammonia concentration in the effluent is a measure of the nitride decomposition rate. Figure 7 displays the results of two separate experiments, the decomposition of an ϵ–$Fe_{2.7}N$ nitride and of a γ'–Fe_4N nitride in H_2 at 523 K. The complete removal of nitrogen after about five minutes is consistent with the instability of the nitrides in hydrogen as already discussed. The area under the NH_3 curve represents the total amount of nitrogen in the nitride, confirming the stoichiometry expected from the phase identification. In Figure 7, for example, the stoichiometry predicted by this method is $Fe_{3.9}N$ and $Fe_{2.7}N$ for the γ' and ϵ nitride decompositions respectively, which is correct for the phase within the uncertainty of the integration (10%).

The fact that the curves in Figure 7 slowly rise to a maximum rather than decaying from a maximum at the initial contact with hydrogen has been reported in the literature previously (23). This behavior shows clearly that nitrogen removal at these temperatures is not simply a diffusion limited process, which would have a maximum rate at the beginning when the transfer area is a maximum and the diffusion distance is a minimum. One model for this phenomenon would be a mechanism that includes competition for surface sites between adsorbed H and adsorbed N. Fast conversion of bulk nitrogen to adsorbed surface N initially limits

the amount of surface H and restricts the rate. As decomposition proceeds, the N arrival rate at the surface is slowed, surface hydrogen increases and therefore the rate builds to a maximum. On the right side of the maximum, the rate is limited by the concentration of surface nitrogen, a consequence of the decreasing amounts of bulk nitrogen.

To examine the surface species contribution to the very early time behavior shown in Figure 7, we exposed a freshly prepared ς-Fe_2N nitride to Ar then D_2 at 523 K. The results are shown in Figure 8. The Ar purge at 523 K removes the gas phase ammonia used for nitride synthesis. NH_x species on the surface are then reacted with deuterium. The presence of NH_xD_{3-x} in the effluent shows clearly that the fresh surface retains some hydrogen. The appearance of NH_3 first does not indicate that x=3, but is a result of chromatographic isotopic exchange at the leading edge of the deuterium pulse. The uncertainties introduced in calibration for the deuterated isotopes and in accounting for the small impurity concentration of hydrogen in the deuterium feed make determination of the total hydrogen from surface species difficult to ascertain from this experiment, but clearly a significant surface H concentration exists.

2.2.5 Nitride Stability During Fischer-Tropsch Synthesis

We have seen that some of the nitrogen in the pure nitrides is very labile. The transient mass spectrometric approach allows us to measure relative surface reactivities directly. Figure 9 shows the response of a freshly prepared and He-purged

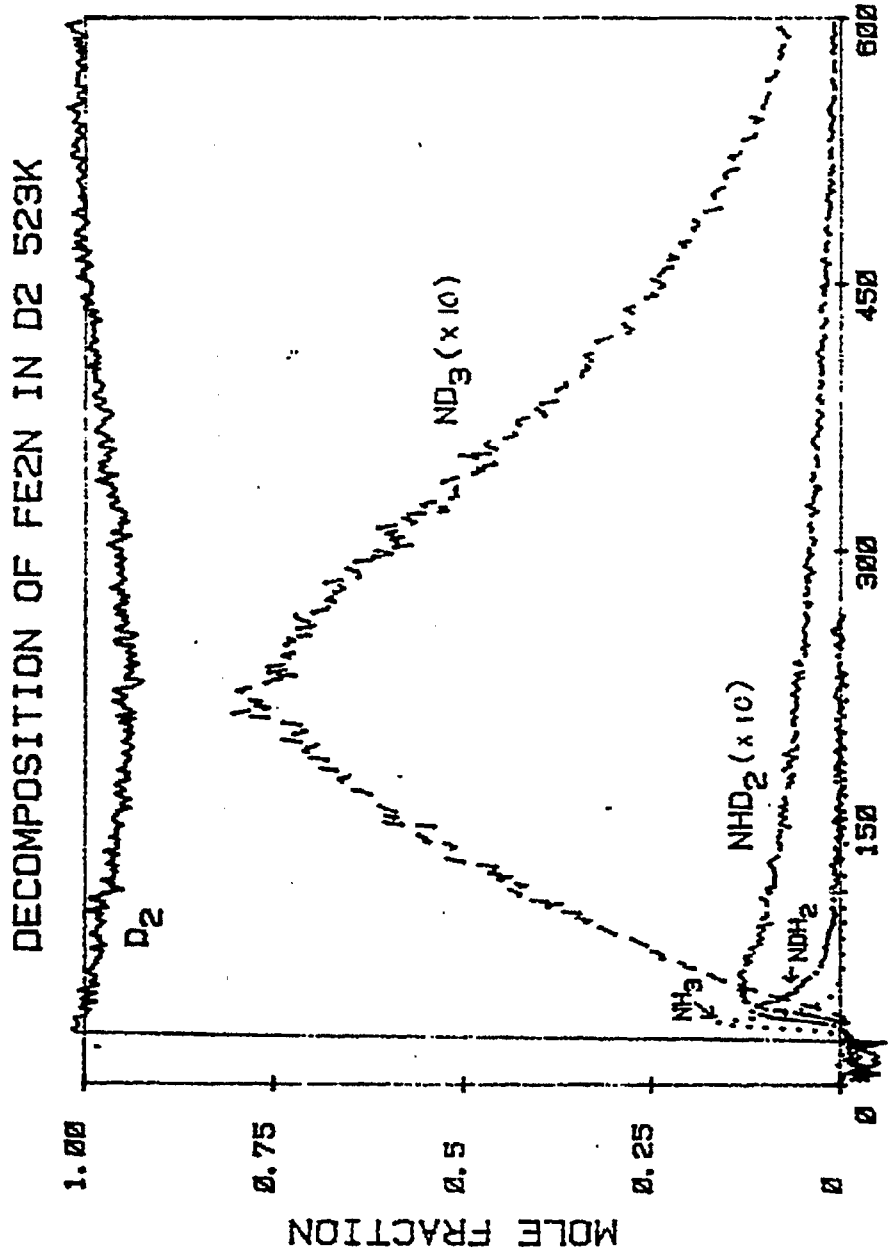

Figure 8 Decomposition of Fe_2N in Deuterium at 523 K.

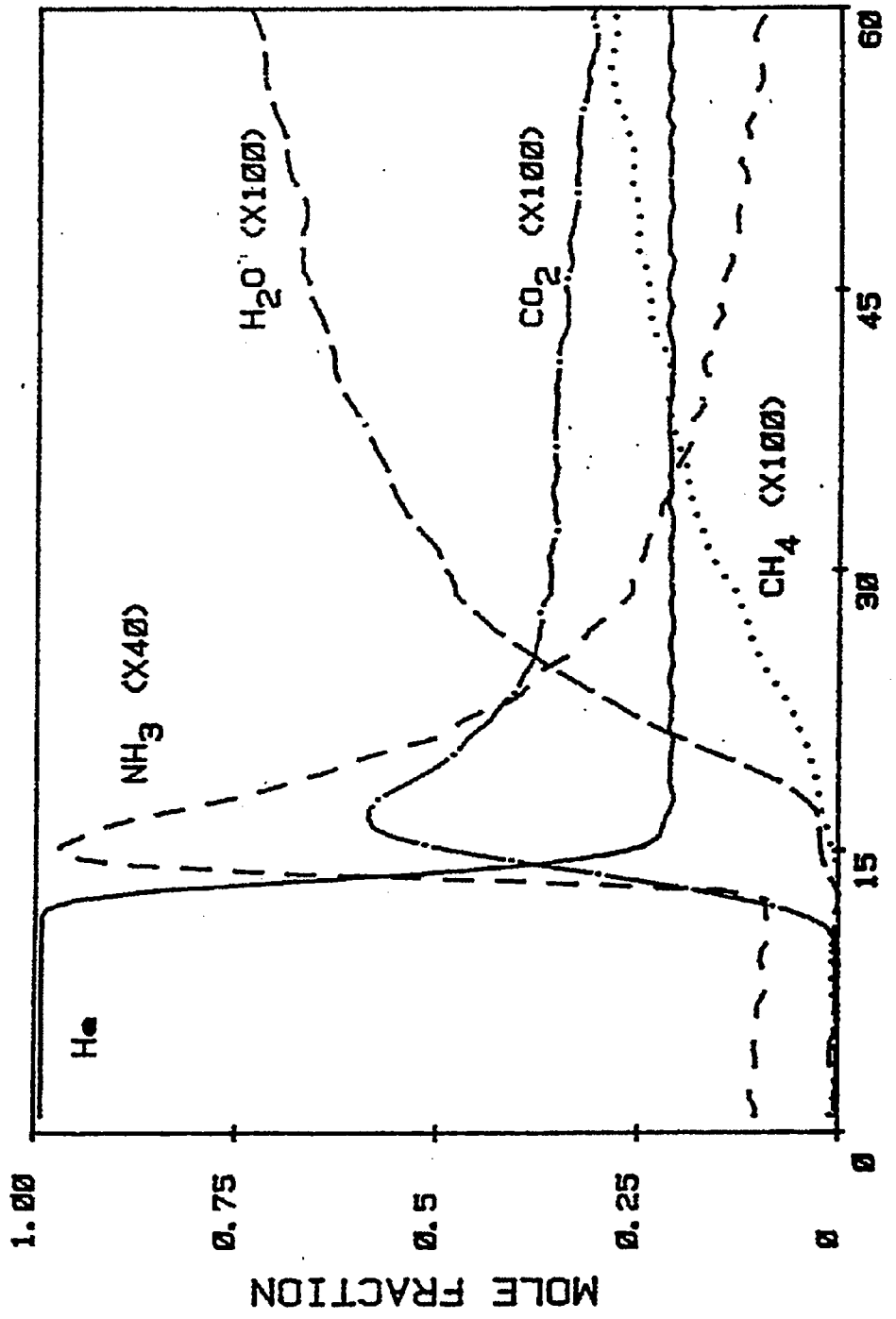

Figure 9 First Minute of Synthesis over ε-$Fe_{2.7}N$
Sequence: He → $3H_2/CO$/He at 523 K

surface to synthesis gas at 523 K with an H_2/CO ratio of 3. The curves show clearly that surface hydrogen reacts preferentially with surface nitrogen rather than surface carbon. Between 1 and 2 monolayer's worth of ammonia comes off before methane production starts. The CO_2 curve shows that carbon is being deposited on the surface by the Boudouard reaction while hydrogen is being scavenged by the surface NH_x groups. Surprisingly, further decomposition of the nitride does not occur to a measurable extent in Figure 9 after Fischer-Tropsch synthesis has begun.

The availability of surface species changes dramatically after five minutes on stream. Figure 10 shows the response of the reacting system to a short He pulse followed by a switch to hydrogen. The burst of methane is characteristic of excess surface carbon. Ammonia evolves only slowly from the catalyst. Because of the high reactivity of surface nitrogen species just demonstrated above, we take this result to indicate very low nitrogen content on the surface of the working catalyst.

2.3 Iron Nitrides as Fischer-Tropsch Catalysts

2.3.1 Introduction

In this section we investigate the properties of the pre-nitrided catalyst behavior during Fischer-Tropsch synthesis. We begin by examining the reaction at 523 and 458 K at atmospheric pressure, and examine the effect of pretreatment with CO or O_2 on the kinetic behavior and the bulk and surface phases present. Finally, we examine the nitrogen inventory in the form of carbonitride during reaction.

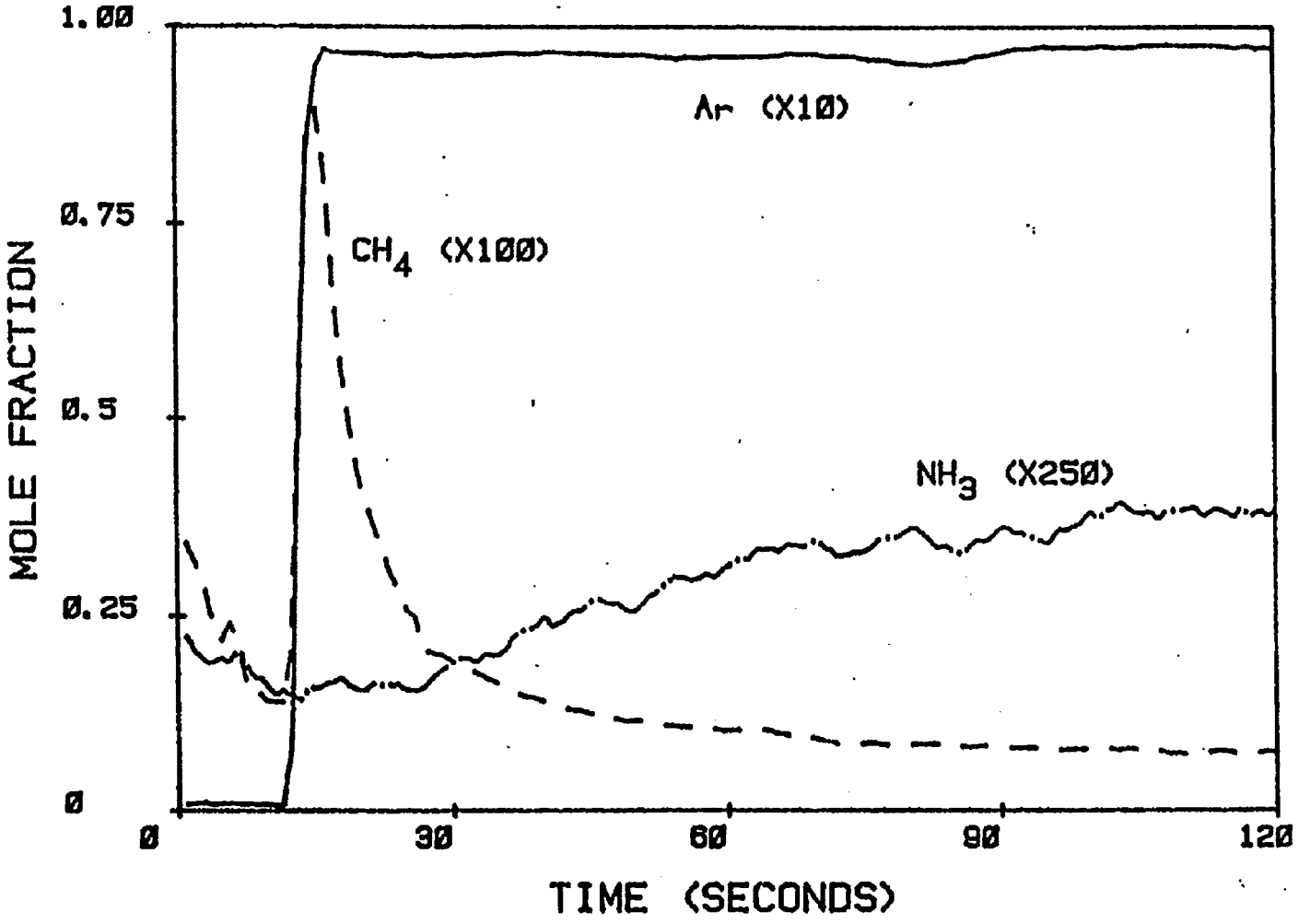

Figure 10 Titration of ε-$Fe_{2.7}N$ Surface with Hydrogen
After 5 Minutes of Synthesis
Sequence: $3H_2/CO/He$ (5 min) → He (5sec) → 9 H_2/Ar at 523 K

2.3.2 Steady State Fischer-Tropsch Reaction over the Iron Nitrides

It is clear that the available data on the kinetics of the Fischer-Tropsch reaction over the iron nitrides is scant (1,9 43). In addition the available data is not consistent. Anderson (1) reports a shift to lower molecular weight products and higher activity over promoted ϵ–Fe_xN nitride at 7.8 atm in synthesis gas, whereas recent studies at Northwestern (9) show a shift to higher molecular weight products and comparable activity at 7.8 atm and lower activity at 1 atm over an ϵ–Fe_xN catalyst. In an effort to clarify some of these issues, steady state data was taken for 12 hrs over each of the nitride phases separately. The conditions were held at 1 atm pressure, 3/1 H_2/CO at 250 ° C with a flow rate of 50 ml/min over approximately 200 mg of catalyst precursor, thus yielding a CO conversion of 1 - 10% to products.

Figure 11 displays the activity results referenced to the surface area of reduced Fe ($4.3m^2/g$) as found by BET. Interestingly, the initial activity is high for all three nitrides, indicating that the initial state of the nitride is more active than Fe metal. In kinetic data listed in a previous DOE report (24), the first point was low, in contrast to the results here. This seemingly contradictory result can be clarified by examining mass spectrometric data for the first few minutes of synthesis. These results show that the hydrocarbon production builds to a maximum only after the removal of surface nitrogen species (Figure 9). If the first sample was taken during this short period of nitrogen removal, the resulting FT activity would indeed by low. The length of this period is probably affected by conversion level

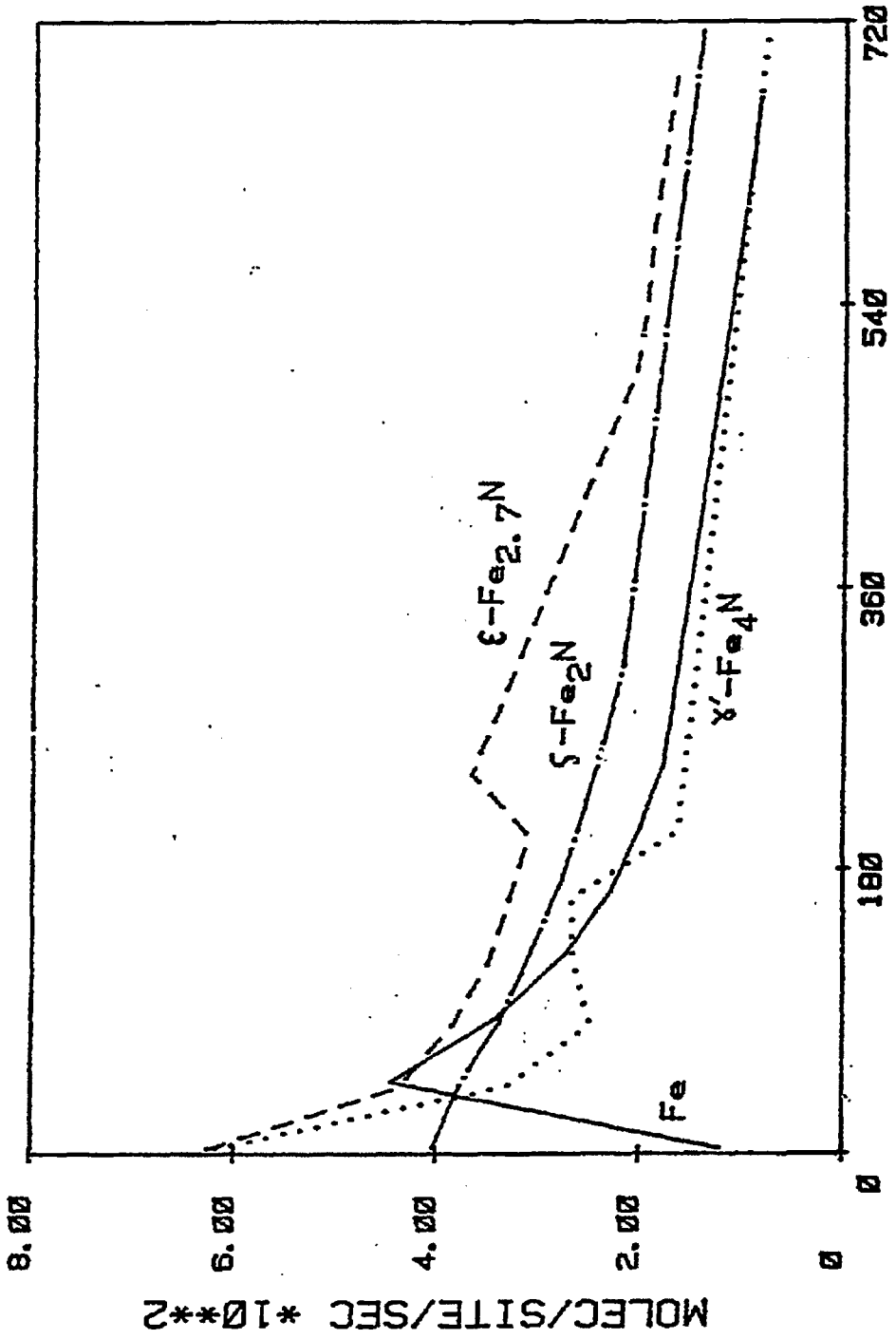

Figure 11 Steady State Activity to C_5 Hydrocarbons
Conditions: $3H_2/CO$ at 523 K and atmospheric pressure

and reactor design (CSTR of PFR), but in any case many changes occur during the first minutes of synthesis.

In addition, hydrocarbon selectivity over the nitrides indicates that the surface is somewhat hydrogen deficient during the first minutes of synthesis. The olefin/paraffin ratio at 4 minutes is higher than at 40 minutes, in spite of the fact that the conversion has decreased. The products are substantially methane poor, especially for γ'–Fe_4N. This behavior is perhaps indicative of a competition between carbon and nitrogen hydrogenation. It must be noted, however, that the activity for these nitrides is high, even though the data indicate that surface hydrogen concentration is low.

As Figure 11 shows, after eight hours of synthesis at these conditions, activity for all the catalysts reaches an essentially steady state. The position of a secondary maximum in activity increases in time for Fe, γ'–Fe_4N, and ϵ–$Fe_{2.7}N$ respectively, corresponding to an increase in nitrogen content. A maximum for ς–Fe_2N may exist, but data in the 360-540 minute range is not yet available for this catalyst.

Table 3 lists the activity and selectivity results for all catalysts after approximately 12 hours. The TON (CO_2 free) values reflect the activity results at the 12 hr point in Figure 11. Olefin/paraffin comparisons must be tempered by the total conversion level; high conversion lowers the olefin/paraffin ratio. Also, the selectivity results reflect total CO conversion with CO_2 included, therefore the relative selectivity between hydrocarbons will seemingly be less pronounced for high CO_2

Table 3

Activity and Selectivity Results After 12 Hours of Synthesis at 523 K

	Fe	$\gamma' Fe_4N$	ϵ–$Fe_{2.7}N$	ζ–Fe_2N
Total Conversion %	1.2	1.2	3.2	2.0
TON* (x 10^3)	10.2	9.6	22.6	16.4
TON (CO_2 free x $10^{3)}$	8.4	7.7	16.6	14.0
% CO conversion to products (% total hydrocarbons)				
CO_2	18	20	27	15
CH_4	33 (40)	32 (40)	35 (48)	39 (46)
C_2	22 (27)	20 (25)	15 (21)	18 (21)
C_3	18 (21)	15 (18)	14 (19)	17 (19)
C_4	8.8 (10.5)	7.3 (9.3)	6.4 (8.8)	8.8 (10.4)
Olefin/Paraffin Ratio				
C_2	1.0	1.0	0.5	1.0
C_3	5.2	4.9	3.7	7.2
C_4	3.2	2.2	1.8	2.9

* TON = turnover number = CO molecules converted to gas phase products per site per second includes all hydrocarbons to C_5

conversion (note the ϵ–$Fe_{2.7}N$ results).

The major overall conclusion from Table 3 is that the behaviors of the steady state catalysts are largely the same. The activity of the ϵ–$Fe_{2.7}N$ and ς–Fe_2N catalysts are respectively 2 and 1.6 times as much as that of Fe and γ'–Fe_4N, which suggests a significant advantage for the high nitrogen-containing catalysts.

Other observations that can be made from Table 3:

1. Fe and γ'–Fe_4N do not have significant differences in activity or selectivity after twelve hours of synthesis.

2. The ϵ–$Fe_{2.7}N$ and ς–Fe_2N catalysts produce more methane and correspondingly less C_2 hydrocarbons than Fe or γ'–Fe_4N; relative selectivity to the C_3 and higher hydrocarbons does not appear to be significantly affected.

3. The turn over number to CO_2 is increased over the ϵ and ς catalysts compared to Fe and γ'.

4. The olefin/paraffin ratio is enhanced for ς–Fe_2N for all carbon chain lengths, as compared to Fe and γ'–Fe_4N, even considering the high conversion level in the ς -nitride. The ratio for ϵ–$Fe_{2.7}N$ is too strongly affected by the high conversion level over this catalyst to be comparable.

These conclusions are in agreement with some of those listed by the Northwestern group (9), namely higher olefin/paraffin ratio and higher CO_2 production over an ϵ, ς–Fe_2N catalyst. We have found, however, that the activity is somewhat higher

for the high-nitrogen containing catalysts, although the difference is not substantial.

2.3.3 Kinetic Behavior at 458 K

Kinetics representative of the single phase nitrides are obtained by following CO hydrogenation in $3H_2/CO$, 458 K, and a total gas flow rate of 50 ml/min, measured at ambient conditions. The chromatographic analysis compares catalyst performance on the basis of CO conversion to CO_2 and C_1 through C_5 hydrocarbons. Molar selectivities are normalized to the total molar production. Due to small concentrations of C_4 hydrocarbons, the C_4 olefin to paraffin ratio is not included. No alcohol production was detected. Table 4 gives the kinetic results for the Fischer-Tropsch reaction over iron and over γ'-, ϵ-, and ς-iron nitrides.

The first G.C. sample at 10 minutes (.17 hr) after the switch to synthesis gas indicates a difference in kinetic behavior between the nitrides and iron. Over the iron catalyst, more than 23% of the products are hydrocarbons. No hydrocarbon production is detected over any of the nitrided catalysts, and the carbon monoxide conversion, x_{CO}, is derived from the Boudouard and water gas shift reactions. A significant, unidentified broad peak with an approximate retention time of 11.5 minutes is, however, present in the nitride chromatograms. This peak is absent from analyses after the 1.17 hr injection. It is unlikely that ammonia, which has a 10 minute retention time in the series Porapak G and Porapak R column, is solely responsible for this peak. The presence of other nitrogen containing gases is

TABLE 4

Iron and Iron Nitride Kinetics at 458 K

Initial Phase	Time (hr)	CO Conversion (%)	Molar Selectivity (%)										Olefin/Paraffin Ratio	
			C_1	CO_2	$C_2^=$	C_2	$C_3^=$	C_3	iC_4	nC_4	$2C_4$	C_5	$C_2^=/C_2$	$C_3^=/C_3$
α	.17	.110	10.9	76.7	1.9	0.7	3.1	0.6	4.0	0.2	0.1	2.0	2.8	5.2
γ'	.17	.108	---	100.0	---	---	---	---	---	---	---	---	---	---
ε	.17	.080	---	100.0	---	---	---	---	---	---	---	---	---	---
ζ	.17	.066	---	100.0	---	---	---	---	---	---	---	---	---	---
α	.73	.133	11.7	80.6	2.3	0.8	2.7	0.6	1.1	0.1	---	0.1	2.9	4.8
γ'	.75	.137	8.4	84.4	2.6	0.3	2.6	0.3	1.4	0.1	---	---	9.1	8.9
ε	1.00	.139	9.1	85.2	1.9	0.3	1.8	0.4	0.8	0.1	---	0.2	6.1	5.1
ζ	.73	.121	7.6	85.7	2.6	0.3	2.3	0.3	1.2	0.1	---	---	10.6	7.9
γ'	1.33	.155	10.6	80.4	3.3	0.4	3.2	0.4	1.6	0.1	---	---	8.5	8.6
ε	1.55	.137	11.5	81.7	2.4	0.5	2.3	0.4	1.0	0.1	---	0.1	4.4	5.3
ζ	1.33	.147	12.9	75.8	4.0	0.7	4.0	0.6	1.8	0.2	---	---	5.7	6.5

α ≡ α-Fe, γ' ≡ γ-Fe_4N, ε ≡ ε-Fe_xN, ζ ≡ ζ-Fe_2N

suspected.

The percentage CO conversion exhibits a trend; lower conversions occur with increasing nitrogen content, from 0.110% over iron to 0.066% over ς–Fe_2N. Two explanations could account for this. The dissociation of carbon monoxide could evoke a dual reaction: (1) carbon incorporation into the bulk and (2) surface carbon deposition. An hydrogenation pathway is minimal at 100% CO_2 selectivity. As carbon diffusion is slower in denser nitride phases, a decrease in the first reaction could lower the overall rate of CO dissociation. However, if the formation of surface carbon is not rate limited, i.e. a true competition exists between the two pathways, this explanation is inadequate. The CO would dissociate at the same rate, and more surface carbon would accumulate. A surface nitrogen competition effect is more likely to occur if nitrogen and carbon dissociation (recombination) sites are equivalent. As higher bulk nitrogen compositions should correspond to larger surface N concentrations under equilibrium conditions, the catalytic sites on ς–Fe_2N should experience a greater proximity of N than would those of γ'–Fe_4N. In a competition between CO dissociation and N removal, an increased nitrogen content should retard the reaction of CO and reduce the H availability. At sufficiently low nitrogen removal rates, N diffusion from the bulk to the surface would be sufficiently rapid to prevent immediate depletion of surface N.

The second and third reaction measurement points, are characterized by increasing hydrocarbon production over the nitrides. The lack of an unidentified nitrogen compound peak implies that CO hydrogenation has slowed the N removal

rate. Although reaction over the ϵ-nitride was temporarily interrupted by a stability problem with the GC, and the break in reaction continuity probably affected the catalyst, the level of CO conversion is comparable between all four phases at the second injection and between the nitrides at the third. The selectivities of the nitrides, barring ethylene and propylene, after 1.3 hours are quite similar to the iron selectivity after 0.75 hours. An induction period over the nitrides may exist; one in which hydrocarbon production starts after a decrease in the rate of N removal.

The remaining difference between the iron and nitrides is in the olefin to paraffin ratios. The mean $C_2=/C_2$ and $C_3=/C_3$ ratios over iron are 2.8 and 5.0, respectively. Table 4 shows C_2 and C_3 selectivities to olefins are higher for the nitrides, especially γ'- and ς-nitride. The increase is not as significant over the ϵ-nitride and may be due to the interruption in kinetic analysis. The ethylene to ethane ratio, particularly, is at least twice as high over the nitrides when compared to the iron. If olefin selectivity is indicative of large surface carbon pools, or a low hydrogen to carbon ratio on the surface, this trend is explained as the effect of initial competition between surface N-H and C-H reactions on the subsequent surface C/H ratio. Lower hydrogen availability would increase hydrocarbon unsaturation.

Barring the initial behavior when the nitride catalysts are first exposed to synthesis gas, and the higher $C_2=/C_2$ ratio, the nitride surfaces behave similarly to the iron surface. Although it is incorrect to extrapolate kinetic selectivities to higher temperatures, it is nonetheless interesting to note that Anderson and

coworkers reported enhanced olefin production by promoted, fused iron nitrides (6).

2.3.4 Phase Behavior at 458 K

The bulk catalyst phases are characterized by Mössbauer spectroscopy both before and after synthesis reaction. The room temperature spectra indicate the stability of the catalyst. This analysis tests the claim that the preceding kinetic results are indicative of the individual starting bulk phases.

2.3.5 α–Fe Carburization at 458 K

The room temperature Mössbauer spectra of the fresh and spent iron catalyst are presented in Figure 12. The Mössbauer parameters of the computer fits are given in Table 5. The starting catalyst is essentially reduced α–Fe whose six peaks can be fitted to 3:2:1:1:2:3 intensity and equal width constraints.

Unconstrained fitting, however, shows greater than expected spectral area in the two innermost peaks. This asymmetry is attributed to an oxide - one which persists after four hours of reduction at 673 K. This is more likely to be an unreduced species, rather than a reoxidized surface species because Mössbauer spectra of all reduced wafers were taken in positive pressures of H_2.

The spectra of this iron catalyst, after forty-five minutes of synthesis (Figure 12b), can be fitted with two different structural approaches. Both methods predict an 80% spectral area for α–Fe with the reduced 20% distributed as carbide phases. This residual is analyzed as either a combination of ϵ' and X (I, II, and III)

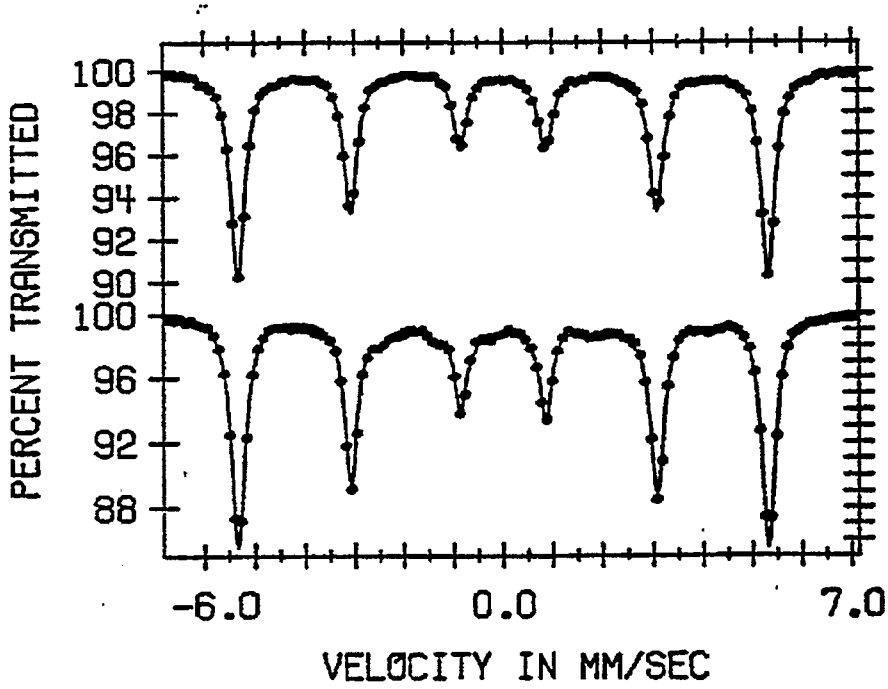

Figure 12 Mössbauer Spectra of α-Fe Reacted at 458 K.

a) α-Fe
b) treated in $3H_2/CO$ for 45 minutes

TABLE 5

Mössbauer Parameters (298 K) for Catalysts Reacted at 458 K

Figure	Iron Identity	IS (mm/s)	QS (mm/s)	HFS (kOe)	LW (mm/s)	RA (%)	Total Area
12a	α-Fe	0.00	0.00	329.4	0.32	100.0	.2151
12b	α-Fe	0.00	0.00	329.4	0.33	80.2	.3664
	carbide	unresolved				19.8	
13a	γ'-I	0.24	0.00	339.0	0.32	20.7	.3162
	γ'-IIA	0.31	-0.14	217.3	0.43	44.5	
	γ'-IIB	0.29	+0.40	215.2	0.43	22.3	
	Fe-Q	0.37	1.11	---	0.89	12.5	
13b	γ'-I	0.23	0.00	338.7	0.30	20.7	.2975
	γ'-IIA	0.30	-0.14	217.6	0.45	50.5	
	γ'-IIB	0.30	+0.36	214.4	0.45	25.2	
	Fe-Q	0.35	1.41	---	0.30	3.6	
14a	ε-II	0.32	0.00	193.2	0.59	27.3	.3567
	ε-III	0.40	0.00	102.2	0.77	34.3	
	γ'-I	(0.25)	(0.00)	(335.9)	(0.24)	(1.7)	
	γ'/ -II	0.35	-0.07	214.2	0.53	26.5	
	Fe-Q	0.33	1.06	---	0.42	10.1	

TABLE 5 (Continued)

Figure	Iron Identity	IS (mm/s)	QS (mm/s)	HFS (kOe)	LW (mm/s)	RA (%)	Total Area
14b	ε-II	0.32	0.00	207.5	0.78	48.2	.3700
	ε-III	0.41	0.00	115.1	0.60	20.3	
	γ'-I	(0.29)	(0.00)	(341.3)	(0.28)	(1.6)	
	Fe-Q	0.35	1.11	---	0.53	9.6	
	ε-II(CB)	0.36	-0.06	243.4	0.44	12.4	
	ε-III(CB)	0.45	-0.12	91.6	0.44	6.7	
	unknown	(0.40)	(-1.36)	(155.4)	(0.16)	(1.2)	
15a	ζ-III	as for Figure 2d					
15b	ε-II	0.35	0.00	209.9	0.86	17.4	.4544
	ε-III+	0.45	-0.31	108.1	1.36	22.9	
	ζ-III	0.44	0.28	---	0.34	53.4	
	Fe-Q	0.28	0.89	---	0.63	6.3	

carbides or as a combination of ϵ'- and Fe_xC carbides. Niemantsverdriet *et al.* (25) favor analysis with the amorphous Fe_xC carbide. They note that this transition carbide is characterized by a hyperfine field below ~275 kOe and that it transforms to other carbides soon after the disappearance of the α–Fe. The Fe_xC in Figure 12b would have a magnetic splitting of approximately 234 kOe. The χ–Fe_5C_2 carbide analysis approach will suffice as well, but the small contribution from each site, approximately 5% relative area, does not permit an authoritative assignment of the carbide. On the assumption that the iron and carbide have equal recoil-free fractions, one concludes, however, that the α–Fe is roughly 20% carbided after 45 minutes of reaction.

2.3.6 γ'–Fe_4N Carburization at 458 K

The γ'–Fe_4N catalyst was prepared by nitriding a reduced wafer in 80% NH_3 at 598 K for 6.5 hours. The room temperature spectrum of this catalyst is presented in Figure 13a and the Mössbauer parameters are given in Table 5. Two superimposed six line patterns, a zero nearest neighbor (340 kOe) and a two nearest neighbor (215 kOe), fit the spectrum adequately, but the fit is improved by considering two 2nn sites (IIA and IIB). In line with the theoretical analysis by Clauser (19), the two inequivalent 2nn magnetic sites are constrained to have relative intensities in the ratio 2:1. In addition, initial peak position assignments are made so as to bias the fitting to yield fields with opposite sign quadrupole interactions. The spectral area ratio in Figure 13a is 0.93:1.00:2.00 (I:IIB:IIA), as compared to the ideal 1:1:2 ratio for stoichiometric γ'–Fe_4N. In fitting this γ'-nitride

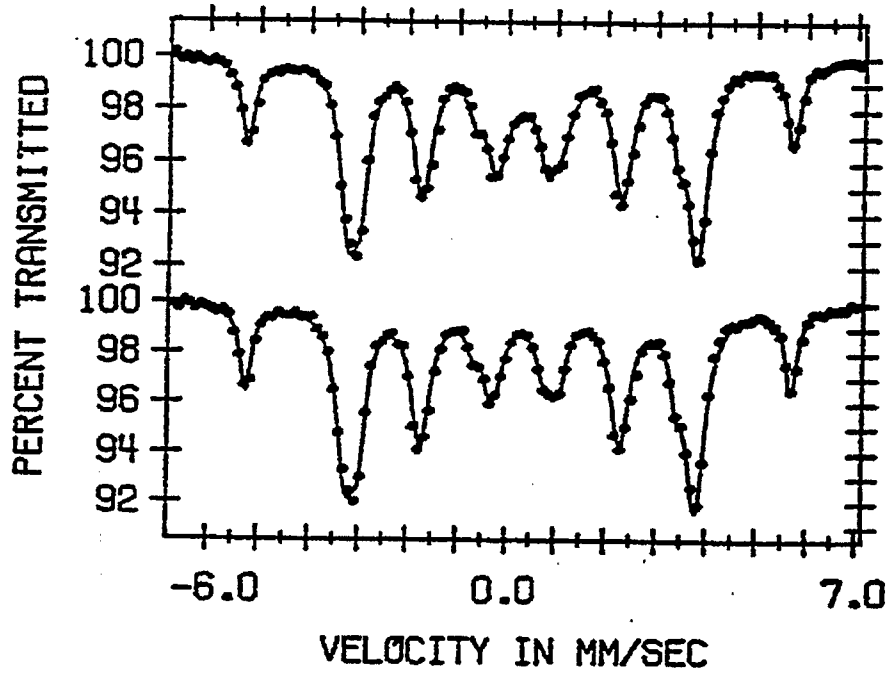

Figure 13 - Mössbauer Spectra of γ'-Fe_4N Reacted at 458 K.

a) γ'-Fe_4N

b) treated in $3H_2/CO$ for 85 minutes

spectrum, it is necessary to include a central doublet with an isomer shift of 0.37 mm/s and quadrupole splitting of 1.11 mm/s. The doublet, designated Fe-Q, accounts for 12.5% of the spectral area. Low temperature analysis should discern between this contribution arising from a small particle nitride or a non magnetic ϵ-nitride. The reducing atmosphere of the NH_3/H_2 nitriding mixture precludes such a large amount of iron oxide phase.

The Mössbauer characterization of the γ'–Fe_4N catalyst after 80 minutes reaction at 458 K is shown in Figure 13b and spectral parameters are given in Table 5. Only the eighteen peaks from the γ'-nitride, and the Fe-Q doublet, could be determined from the computer fit. The IS, WS, and HFS values for these three sites are in accordance with the starting catalyst. The 2nn sites, although still constrained to a 2:1 relative area ratio, are 10-15% greater in area than those in the fresh γ'–Fe_4N. The area of the γ' 0nn site is unchanged. An additional carbonitride or carbide contribution, unresolved at the present spectrum resolution, would account for this increased area fraction. A better statistical fit is given if one reverses the -1:2 QS symmetry expected in pure γ'-nitride. A similar fitting to the virgin γ'–Fe_4N spectrum would not converge. Even during synthesis reactions at 523 K over the γ'-nitride, no differentiation between the χ-II carbide site (~218 kOe) and the γ'-II sites could be made. So, although some γ'-carbonitride and carbide formation is expected, the probable inhomogeneity of the phase prevents its identification in the spectrum fit. Furthermore, a decrease in the non-magnetic contribution is seen between Figure 13a and 13b. The increase in the quadrupole

splitting from 1.1 to 1.4 mm/s, signifies greater charge asymmetry at this Fe site. One can speculate that addition of carbon in the vicinity of this site can reorder a portion of the domain as magnetic and further polarize the electronic state of the paramagnetic domain. The degree of carbon incorporation would account for less than 10% of the spectral area. As such, the kinetics are representative of a bulk γ'–Fe_4N.

2.3.7 ϵ–Fe_xN *Carburization at 458 K*

The ϵ-nitride catalyst was synthesized by nitriding a reduced wafer in 21% NH_3 at 653 K for 6 hours. The Mössbauer parameters for the computer fit to the room temperature spectrum (Figure 14a) are given in Table 5. In addition to the ϵ-II and ϵ-III fields, a small γ' 0nn contribution is evident. The small spectral area of this site (1.7%) is responsible for the deviation from the expected HFS value (~340 kOe). The associated 2nn site, identified as γ'/ϵ-II in Table 5, although characterized by a typical γ' magnetic splitting of 214.2 kOe, is not solely a γ'-II site. The 1.7% area contribution from γ'-I limits the total Fe_4N area to below 8%. Constraining the area of this six line pattern to three times that of the higher γ' field, rather than reducing the γ' 2nn area, increases the 0nn area unreasonably. Therefore, we attribute this two nearest neighbor contribution to an inhomogeneous mixture of γ' precipitates in hcp ϵ–Fe_xN. The ϵ-nitride inhomogeneity can be visualized by considering a distribution of hyperfine fields. The variation in statistical placement of nitrogen neighbors in the first (nearest) higher coordination shells of each iron atom will generate nonuniform fields at their nuclei. Chen *et al.*

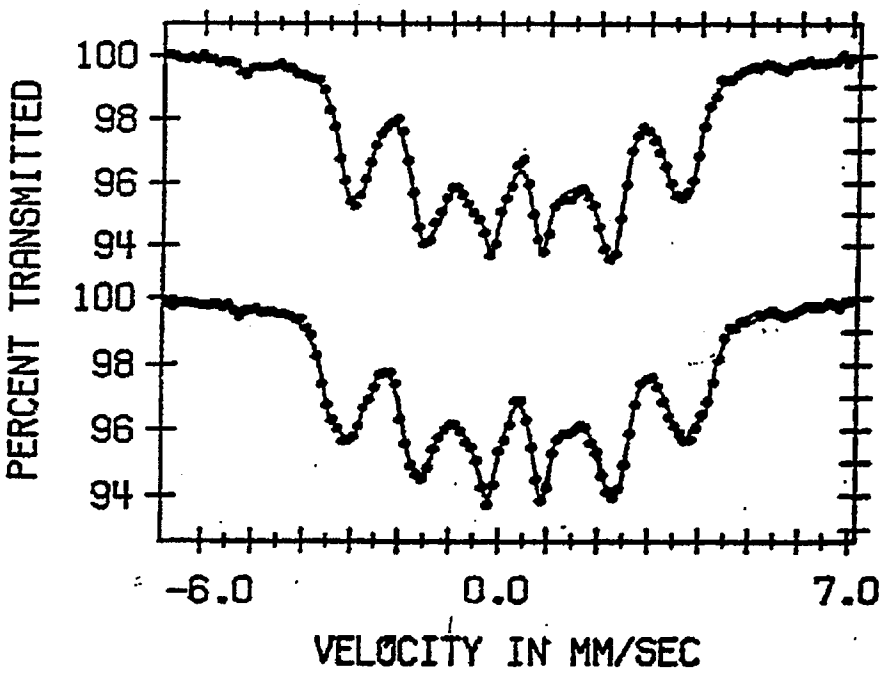

Figure 14 Mössbauer Spectra of ε-Fe_xN Reacted at 458 K.

a) ε-$Fe_{2.49}N$
b) treated in $3H_2/CO$ for 85 minutes

(13) and DeCristofaro and Kaplow (26) favor this distribution of magnetic fields approach. The nonmagnetic Fe-Q site should thus correspond to underestimated innermost peak intensities encountered when fitting field broadened spectra with 3:2:1 area constraints. Yeh *et al.* (8), in addition to fitting with HFS distribution, also require a nonmagnetic doublet in their room temperature Mössbauer spectra.

The ϵ-nitride catalyzed CO hydrogenation for approximately 1.5 hours. The room temperature spectrum of the spent catalyst (Figure 14b) still exhibits a small γ'-Fe_4N contribution. A majority of the starting nitride, ϵ-II, ϵ-III, and Fe-Q, is also retained. The hyperfine fields of ϵ-II and ϵ-III are higher than those in the starting nitride, indicative of N loss. Furthermore, the spectral area of the ϵ-III site has decreased from 34 to 20%.

The computer fitting also identified three new magnetic species in the carburized sample. A low spectral area and overlapping peak positions of the third site, however, does not warrant its discussion. The remaining two species, ϵ-II and ϵ-III, are attributed to ϵ-carbonitride sites having two and three interstices occupied. Foct *et al.* (27) identified a (CNV) carbonitride with a isomer shift of 0.30 mm/s and a magnetic field of 243 kOe. The ϵ-II site has similar parameters. The actual identification of these transition carbonitrides requires a greater reaction length so that greater definition is given each proposed site. One may say though, that Fe sites with carbon neighbors account for roughly 20% of the spectral area.

2.3.8 ζ-Fe_2N *Carburization at 458 K*

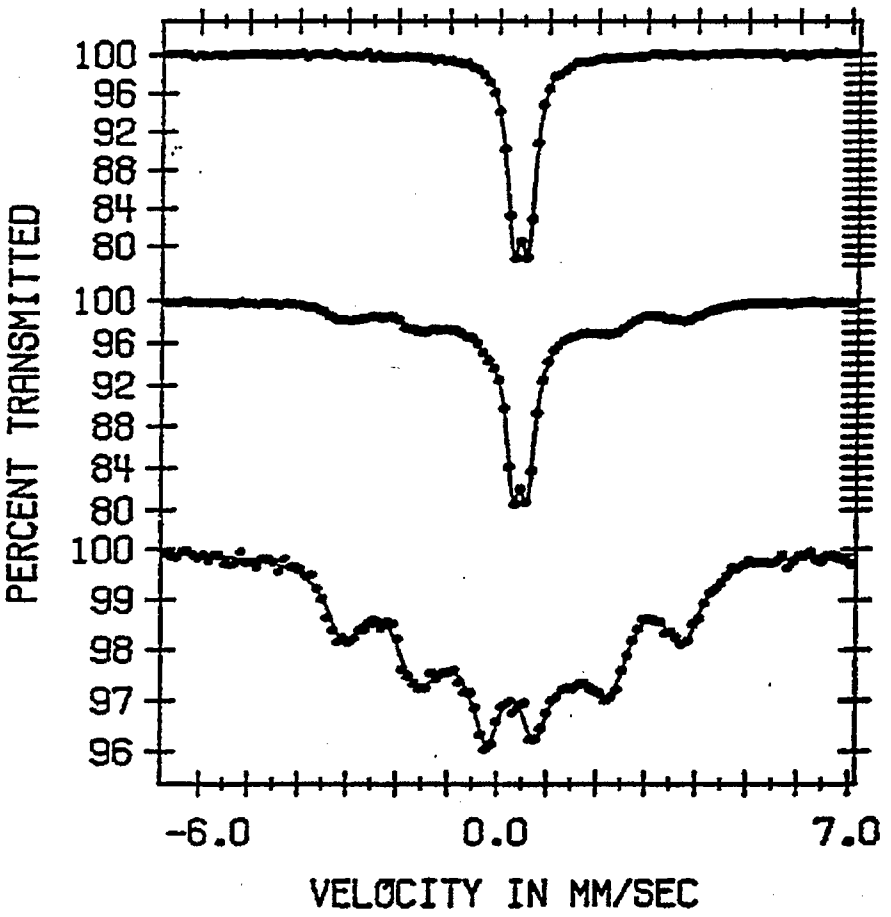

Figure 15 Mössbauer Spectra of ζ-Fe_2N Reacted at 458 K.

a) ζ-Fe_2N

b) treated in $3H_2/CO$ for 85 minutes

A ς-nitride catalyst was synthesized by flowing pure NH_3 at 673 K for 8 hours over a reduced iron powder. The computer fitted room temperature Mössbauer spectrum is given in Figure 15a. The Mössbauer parameters (Table 5) for this fit indicate a single phase paramagnetic ς–Fe_2N. The spectrum of the catalyst after 80 minutes of the reaction (Figure 15b) exhibits magnetic ordering in addition to pure ς-nitride. By subtracting the ς–Fe_2N contribution and expanding the spectrum scale, the background becomes substantially more clear (Figure 15c). Two magnetic fields and a single doublet are predicted in fitting this 'residual'. The two magnetic sites have hyperfine splittings characteristic of iron with 2 and 3 nearest nitrogen neighbors. The lower field site has a quadrupole splitting of -0.30 mm/s, and could not be fit with a physically meaningful zero quadrupole split six line pattern. Nor could a separate magnetically ordered site be introduced into the fit. This 108.1 kOe field is attributed to overlap between an ϵ-III site and a less intense ϵ-carbonitride site, probably of NNC structure. As a spectral area of ten percent or more is normally detectable, the carbonitride contribution to spectral area of the reacted zeta–Fe_2N may be estimated as less than 10%. This would be less than the spectral areas of carbon phases in iron, γ′-nitride, and ϵ-nitride.

2.3.9 Effect of CO Pretreatment on Fischer-Tropsch Synthesis

In Section 2.3.2, the steady state data over each of the nitrides was presented. Most significant was the initial high rate of reaction over all three of the nitrides as compared to α-Fe. This behavior was attributed to the existence of a nitride core, which blocks the competitive carburization of the bulk. In the relatively open bcc

lattice of α-Fe, this carburization reaction is so rapid that it inhibits the hydrogenation reactions. After a few minutes of synthesis over the nitrides, however, the activity drops; this could presumably be caused by nitrogen loss during this period and a corresponding increase in competitive carburization. Mössbauer spectroscopy has shown that the loss of the nitride phase is extremely rapid during the first few minutes of synthesis. Furthermore, transient mass spectrometry has revealed the existence of a surface adlayer of a nitrogen containing species that is immediately hydrogenated upon introduction of synthesis gas (Figure 9). Since this nitrogen has been lost, this "opens the door" for carbon to diffuse into the bulk, which causes the competitive carburization reaction of increase and the hydrogenation reaction to decrease. If the first few layers of nitride could somehow be retained, perhaps the initial high activity could also be maintained.

One conceivable way of protecting the bulk nitride is to deposit a carbon overlayer before the catalyst is exposed to hydrogen containing atmospheres. When this pretreated catalyst is exposed to synthesis gas, the bulk is not as readily hydrogenated since nitrogen must now diffuse through the carbon layer. An experiment of this nature was attempted and is shown in Figure 16. A freshly prepared ς-Fe_2N nitride was given a one minute pre-exposure to CO at 523 K before exposure to synthesis gas. The CO pulse denotes this interval of pre-exposure. Ammonia tails quite badly as it desorbs from the system. In previous experiments in this chapter, this artifact was removed by long exposures to inert gases. The introduction of $3H_2/CO$ is denoted by the fall in the CO signal. The slight shift in

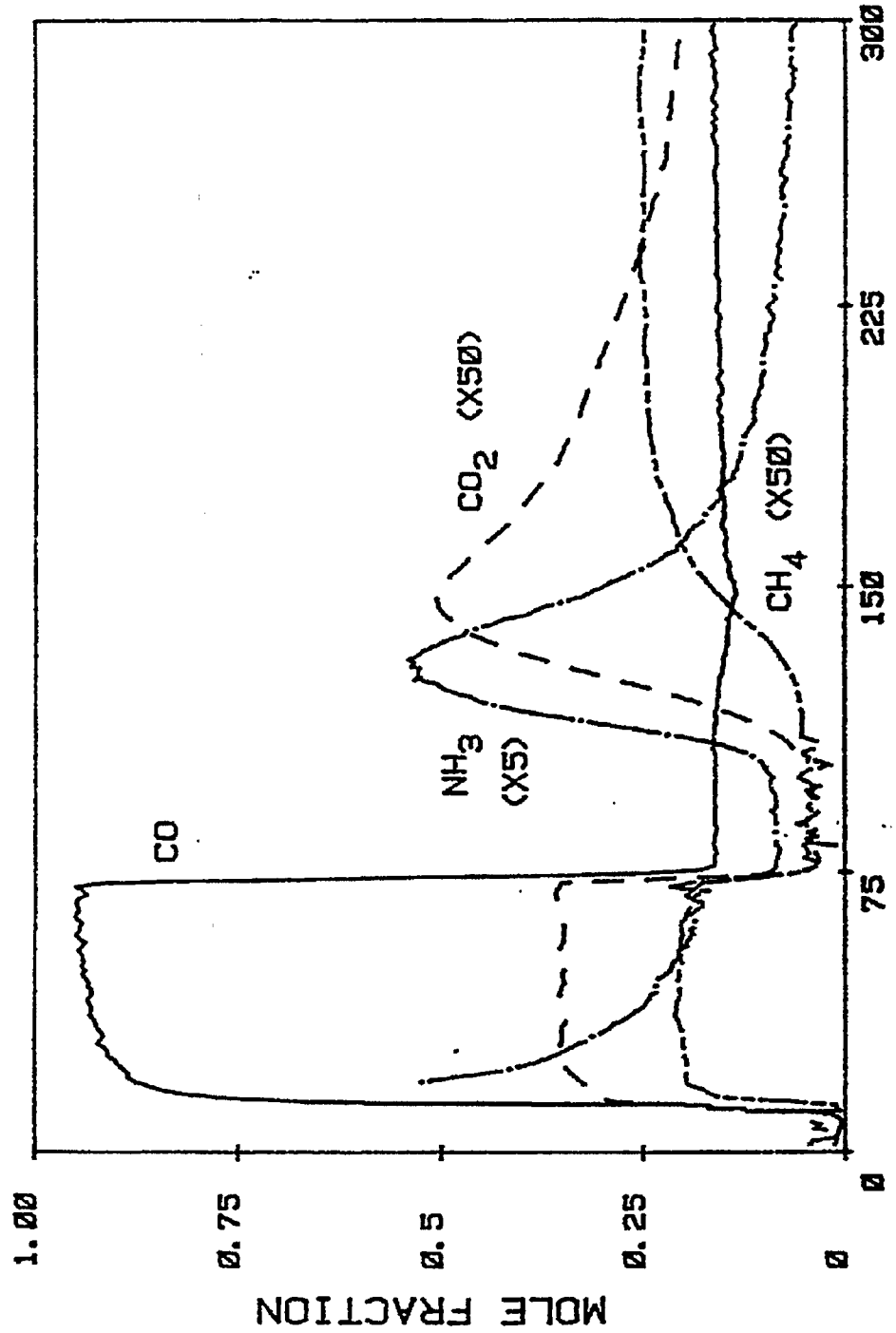

Figure 16 Effect of CO Pretreatment on First Minute of Synthesis over ε-Fe_2N
Sequence: NH_3 + CO (1 min) + $3H_2$/CO at 523 K

ammonia at this point is an artifact of the flow geometry for the experiment; in $3H_2/CO$ virtually all tubing that had previously been exposed to ammonia was bypassed.

During the CO pulse, CO_2 is being produced according to the reaction:

$$2CO_{ads} \rightarrow CO_2 + C_{ads}$$

and thus lays down the same amount of carbon as CO_2 produced. The rate of CO_2 production here is 1.9×10^{-2} molecules CO_2 produced/site/sec, and thus in 60 seconds 1.1 monolayers worth of carbon were deposited. Some of this carbon left in the form of methane, however, produced from hydrogen from NH_x species and residual ammonia in the system. The amount of methane corresponds to 0.7 monolayers, thus a total of 0.4 monolayers of carbon has been deposited on the surface. The surface NH_x species only amounted to 1 monolayer of hydrogen, and since 2.8 monolayers worth of hydrogen (four times the carbon) were produced in the methane product, the surface must be catalytically reacting NH_3 and CO to produce methane. Since the masses for CO and N_2 overlap, it is not known where the nitrogen that has lost its hydrogens to methane is going. Recall that nitrogen desorption at 523 K is insignificant due to the high activation energy. If the surface NH_x species are still present, as the ammonia peak later in the experiment suggests, it is indeed puzzling as to where the CO disproportionation reaction and the methane production reaction occurs. Also, the hydrogens on the NH_x species could have been stripped to form methane during the CO pulse. Nevertheless, it would seem that there are insufficient open sites for the steady state CO_2 produced

and the resulting surface carbon.

Upon exposure of the CO treated catalyst to synthesis gas, no products, other than the continued desorption of NH_3 , are observed for the first 20 seconds. If ammonia were being produced from hydrogenation of surface NH_x species during this period, open sites would be formed and the reaction would rise exponentially. This does indeed happen, but only after the 20 second induction period. One could speculate that CH_4 is being produced but at a low value (below detection limits), and thus is within the uncertainty of the experiment. Once enough open sites are available for H_2 adsorption onto active sites (this might be a very small number of open sites), ammonia starts to be produced and the surface is quickly cleared. The amount of ammonia in this peak corresponds to about 3 monolayers worth of material, which is uncertain by about 1 monolayer due to the ammonia in the background. This amount is about one monolayer higher than in the ϵ–$Fe_{2.7}N$ experiment of Figure 9.. Interestingly, the extra nitrogen is about the same amount of nitrogen that was "deposited" during the production of methane in the CO pulse.

On the heels of the ammonia peak, CO_2 rises to a later maximum. This phenomenon can be explained by considering the role of CO during NH_x hydrogenation. As NH_3 is removed, CO is selectively adsorbed from the gas phase. On iron, this species will quickly dissociate. The O_{ads} species can now react with the incoming CO and eventually remove all the surface oxygen, causing the overshoot in CO_2 production. The O_{ads} species does not react with H_{ads}, since this species is

selectively producing NH_3. Likewise, the C_{ads} species is not removed as methane until sufficient ammonia has been removed. Note that the production of methane (and water, which is not shown) is not significant until both ammonia and carbon dioxide have begun to decay. Water, however, does lag in any experiment due to adsorption in the system.

It would seem that preadsorbed carbon did indeed inhibit the hydrogenation of surface nitride, but only for a brief period. Unfortunately, the preadsorbed carbon inhibited hydrocarbon production as well, and thus essentially rendered the catalyst inactive until it was at least partially removed. Interestingly enough, however, it is seen that the NH_x species did not inhibit the formation of CH_4 and CO_2 during the CO pretreatment, whereas it is clear that NH_x species need to be removed for significant hydrocarbon production in H_2/CO mixtures.

Other curious phenomenon are observed in Figure 16 as well. As soon as the gas phase mixture is changed from CO to a H_2/CO mixture, the CO_2 production immediately drops. Since CO is still in the gas phase, and no other significant products are being produced, this must mean that H_2 has replaced the active species for CO_2 production. Paradoxically, this would suggest that the surface now has ample surface hydrogen to catalyze the production of ammonia and other products. Since this is not the case, the sites that produce CO_2 and adsorb hydrogen in CO/H_2 mixtures cannot be active sites for methanation or ammonia production.

This experiment has emphasized the notion that the surface of the iron nitride catalyst is heterogeneous. CO_2 and CH_4 can be produced from residual ammonia

in a CO atmosphere regardless of the blockage of surface sites by NH_x species, but both of these carbon products are inhibited as soon as H_2 enters the gas phase. Once the NH_x species is removed, we start to form Fischer-Tropsch synthesis products at the high initial rate characteristic of the nitrides. Bennett's two site mechanism for methane production over iron (28), and Bell's observation of large pools of seemingly inactive hydrogen on unsupported ruthenium during synthesis (29) both emphasize surface heterogeneity. Apparently adsorption and reaction need not occur on the same type of site.

2.3.10 Kinetic Behavior of Preoxidized ς-Fe_2N

Preoxidation of iron catalysts has been reported to markedly improve activity as compared to conventional iron catalysts (30). The Fe_2O_3 phase, however, is inactive until reduced to lower oxidation states in synthesis gas (31), suggesting that it is the partially oxidized surface phases that are of catalytic interest. Preoxidation of an original ς-Fe_2N catalyst offers a new route to the preparation of a partially oxidized surface.

A preoxidized nitride catalyst was prepared by oxidizing a fully nitrided ς-Fe_2N in 1% O_2/He at 473 K for 6 minutes. The CO hydrogenation kinetics over this catalyst and over a ς-nitride were monitored during the first hour of reaction. The synthesis conditions were atmospheric pressure, $3H_2/CO$, 523 K, and 66 ml/min total gas flow rate at ambient conditions. Discussion of the behavior of the nitride bulk, monitored by Mössbauer spectroscopy, follows these kinetic dis-

TABLE 6

Iron and Pre-oxidized ς-iron Nitride Kinetics at 523 K

Initial Phase	Time (hr	CO Conversion (%)	Molar Selectivity (%)										Olefin/ Paraffin Ratio		
			C_1	CO_2	$C_2^=$	C_2	$C_3^=$	C_3	$1C_4^=$	nC_4	$2C_4^=$	C_5	$C_2^=/C_2$	$C_3^=/C_3$	$C_4^=/C_4$
a	.17	0.37	6.1	89.8	1.3	0.4	2.4	---	---	---	---	---	3.5	---	---
b	.17	0.85	19.9	54.9	3.1	1.7	3.9	0.4	6.5	3.8	3.6	2.2	1.8	9.1	2.7
a	.81	1.16	46.1	24.7	5.7	4.9	8.3	1.6	1.9	1.8	0.9	0.2	1.2	5.1	1.6
b	.73	1.20	39.6	28.6	4.7	4.2	6.7	1.3	5.2	4.0	3.1	2.6	1.1	5.0	2.1

a ≡ α - Fe, b ≡ preoxidized ς-Fe_2N

cussions.

When compared to kinetics over ς nitride at the same conditions, the preoxidized nitride catalyst is seen to produce significantly more C_4 and C_5 hydrocarbons during the first hour (see Table 6). The GC analysis at .17 hr shows the ς forming no hydrocarbons above propylene and being 90% selective towards CO_2 production. The CO conversion over the preoxidized catalyst is twice as great as that over the ς nitride during this first analysis, and is even greater on a CO_2 free CO conversion basis.

By 0.75 hour, overall CO conversions are nearly equal. The olefin to paraffin ratios of each catalyst are essentially the same for C_2 and C_3 selectivity, but 30% larger for C_4 selectivity over the preoxidized catalyst. The preoxidized nitride is more than twice as selective towards total C_4 and C_5 hydrocarbon make, but is approximately 20% less selective towards C_1–C_3 production. Indeed, the nitride produces some 12% C_4 hydrocarbons, yet only 8% C_3 product. Should the active surface indeed by an iron nitride, this trend for higher molecular weight products is contrary to that seen by Anderson (1), but similar to the trend observed by Yeh *et al.* (9).

2.3.11 Phase Behavior of Preoxidized ς–Fe_2N

The six minute treatment in 1% O_2 at 473 K has a marked effect on the nitride bulk, as seen by Figure 17a. While the prominent center peak is the contribution from the remaining Fe_2N, two large hyperfine fields are clearly visible. As shown

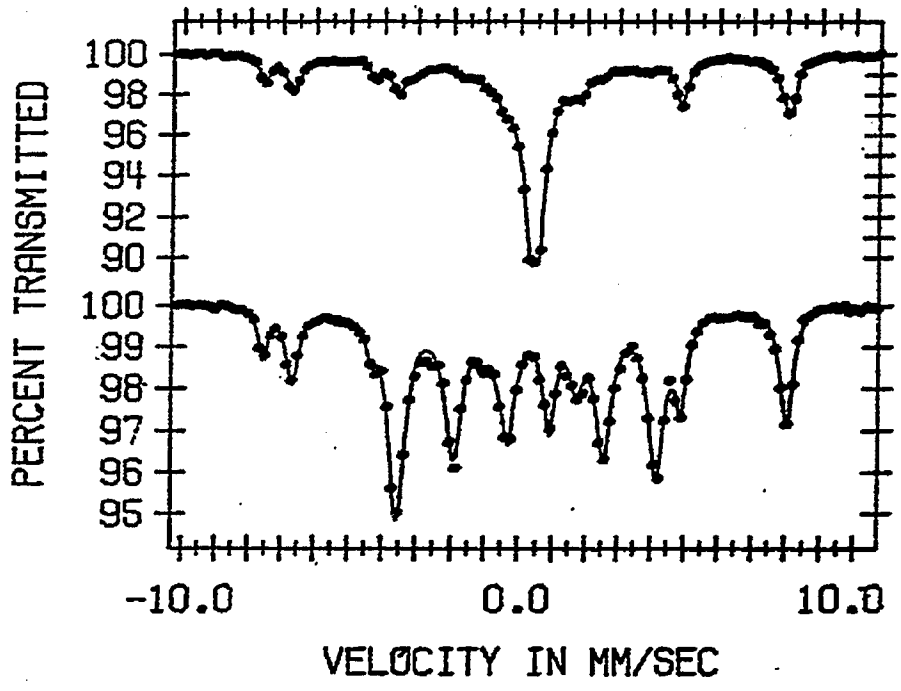

Figure 17 Mössbauer Spectra of Pre-oxidized ζ-Fe_2N Reacted at 523 K.

a) ζ-Fe_2N treated in 1% O_2/He at 473 K for 6 minutes

b) Pre-oxidized ζ-Fe_2N treated in $3H_2$/CO for 50 minutes

TABLE 7

Mössbauer Parameters for Pre-oxidized ζ-Fe_2N

Figure	Iron Identity	IS (mm/s)	QS (mm/s)	HFS (kOe)	LW (mm/s)	RA (%)	Total Area
17a	Fe_3O_4 A	0.29	0.00	486.4	0.30	10.2	.2702
	B	0.65	0.00	457.3	0.52	22.9	
	ε-II	0.35	0.00	217.3	1.19	16.6	
	ζ-III	0.43	0.27	---	0.39	24.7	
	Fe-Q+	0.43	0.34	---	1.68	25.6	
			unresolved			3.6	
17b	Fe_3O_4 A	0.28	0.00	485.2	0.33	9.1	.2700
	B	0.66	0.00	454.9	0.47	19.8	
	ε-II	0.31	0.00	238.8	0.62	55.3	
	ε-III+	0.37	0.00	172.3	0.59	11.2	
	Fe-Q	0.31	1.19	---	0.33	4.6	

in Table 7, these two offset fields have isomer shifts of .29 and .65 mm/s, hyperfine splittings of 486.4 and 457.3 kOe, and no quadrupole interaction. These parameters are consistent with magnetic Fe_3O_4. According to Greenwood and Gibb (32), Fe^{3+} in tetrahedral sites (A sites) and Fe^{3+} plus Fe^{+2} in octahedral sites (B sites) exhibit fields of 491 and 453 kOe respectively. The residual background to Figure 17a is computer fit with equal statistics to two different environments. Both procedures predict a 218 kOe field with isomer shift between 0.33 and 0.35 mm/s. Due to the broadness of the peaks for this site, with half widths of 0.8 mm/s and greater, the existence of a quadrupole interaction could not be ascertained. This fit gives a 17% area contribution from this site. A lower area is predicted by a second fit because it uses an extremely broad (Γ /2 > 9 mm/s) superparamagnetic species accounting for almost 25% of the spectral area. Both fits require a central (IS = .34 - .43), broad (Γ /2 = 1.1 - 1.6 mm/s) doublet. This is too broad to be attributed solely to the nonmagnetic Fe-Q species. Including a fourth magnetic site of approximate 70 kOe field (ϵ -III) in either fit gives nonphysical peak positions. The broadness of the doublet could arise rom a superposition of the Fe-Q species and a magnetically unresolved ϵ -III site, although an oxynitride species can not be ruled out. Some relaxation effects are probably being seen and the ill-defined nature of these sites arises from attempting to fit them to full Lorentzian line shapes.

The spectrum of the catalyst after 50 minutes of synthesis (Figure 17b) shows that the two Fe_3O_4 sites remain, but the orthorhombic Fe_2N phase has been

depleted. The total spectral area of site A and site B oxide is 15% less in the spent catalyst. In addition, two magnetic fields (239 and 172 kOe) and a 4-5% Fe-Q contribution are found. The two magnetically ordered sites could be fitted without quadrupole interactions. On a basis of their isomer shifts alone, a 2 and 3 nn ϵ -nitride assignment is likely. The magnitude of the 172 kOe HFS, however, makes an homogeneous ϵ -II and ϵ -III assignment difficult. A one nitrogen nearest neighbor ϵ -I site, although reported by Chen *et al.* (13) and DeCristofaro and Kaplow (26) has not been seen before in this nitride system. Furthermore, the well developed 239 kOe peaks (Figure 17b) favor an absence of domain inhomogeneity. A plausible assignment for this more intense field is low nitrogen containing ϵ -nitride ($\sim Fe_{2.75}N$), and although an ϵ -III site must be associated with this stoichiometry, its lower intensity and smaller field could be masked by higher field components. The 172 kOe contribution has isomer shift too large for ϵ' -carbide, and carbide formation is not expected in high nitrogen containing nitrides. The presence of an oxynitride cannot be discounted. Without low temperature spectra, and associated Debye temperatures, further phase identification is too speculative.

The different behavior of the nitride bulk in this pre-oxidized sample compared to the behavior of non-oxidized ϵ -nitrides clearly indicates a stabilizing effect of the oxygen upon the nitride bulk during reaction. Although the surface phase cannot be authoritatively assigned to a uniform Fe_3O_4 covering, a comparison of kinetic trends over oxidized iron surfaces is helpful. Teichner *et al.* (30, 33) have reported preoxidized iron catalysts to be more active toward hydrocarbon synthesis

than reduced iron. Krebs and coworkers (34) studied magnetite during CO hydrogenation but did not characterize the catalyst during reaction. Indeed, the kinetics over the pre-oxidized ς–Fe_2N are similar to kinetic results over an Fe_3O_4 surface reported by Knoechel (35). The preoxidized nitride was operated at a higher CO conversion than the Fe_3O_4 surface, but still produced higher olefin to paraffin ratios. Additional characterization of the pre-oxidized nitrides during reaction will be necessary, and, based upon the unusual product distribution, worthwhile.

2.3.12 Hydrogenation of Catalysts After Reaction

How different are iron nitride catalysts after 12 hours of reaction in H_2/CO at 523 K? If the bulk nitride were completely gone by this point, the catalysts might be expected to have the same behavior after they equilibrate from the loss of nitrogen. Figure 18 shows that this is not the case, however, since ammonia can still be produced from the used ϵ–$Fe_{2.7}N$ catalyst.

In this experiment the reactant is hydrogen, and the initial temperature is low (473 K). The catalyst has previously been used for 12 hours of reaction in 3/1 H_2/CO at 523 K, and then passivated in helium and finally exposed to air. Part of the catalyst was oxidized, and therefore produces water during the decomposition in hydrogen. The decomposition also produces methane from carbide that formed during synthesis, but the rate of production was extremely small during the entire course of the experiment, and is not shown in Figure 18. At the end of the experi-

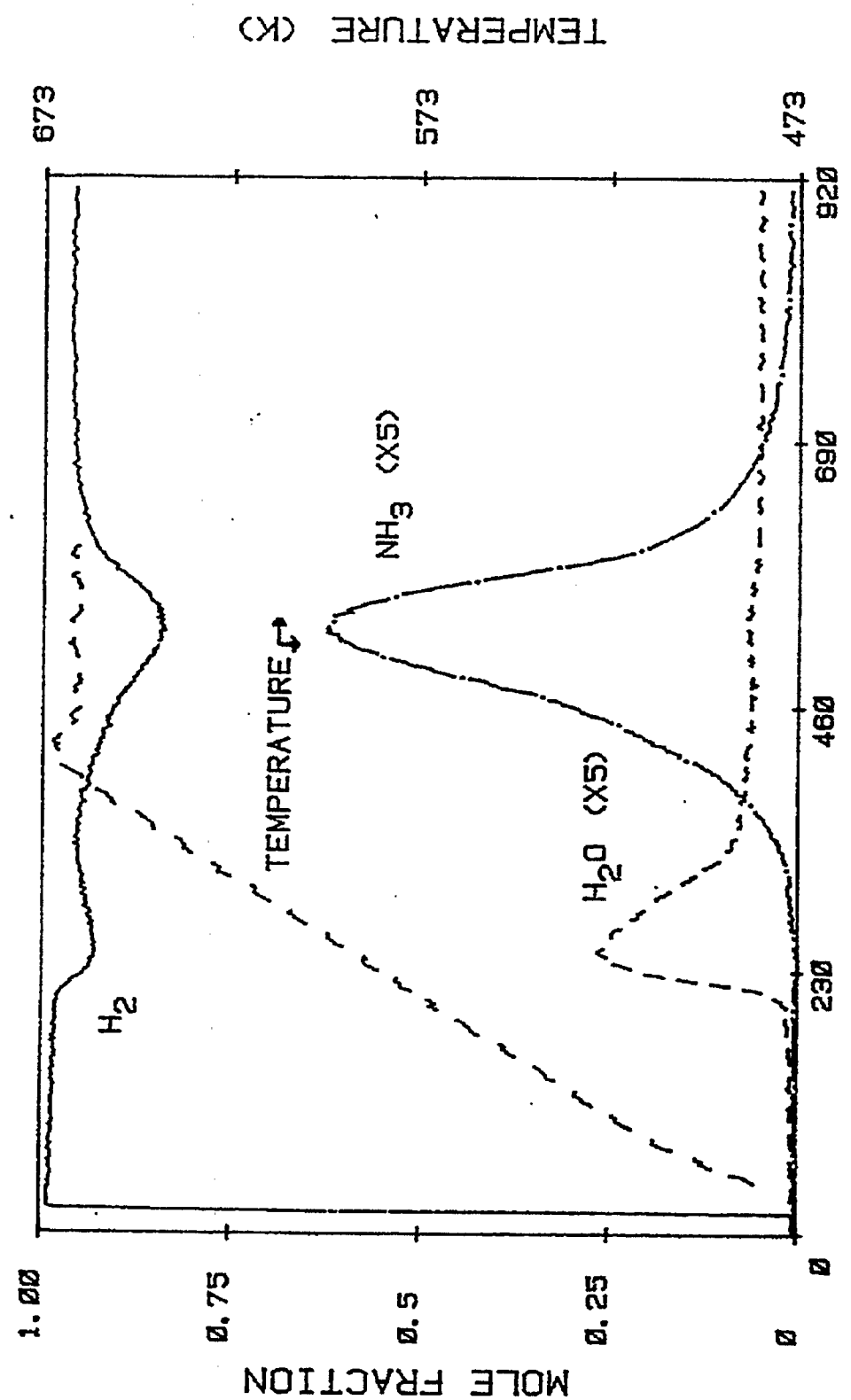

Figure 18 Hydrogenation of ε-$Fe_{2.7}N$ Catalyst After 12 Hours of Synthesis

ment (15 minutes), methane was beginning to rise, indicating that the carbide was finally available for hydrogenation. It is not clear why carbide hydrogenation took so long to commence, but the significant background level of water might be a cause of the inhibition. Unreactive surface graphite could also block methanation sites. Our other transient studies suggest that NH_3 is produced exclusively when both N and C are available to react with hydrogen at the surface. This selectivity could also play a role in the present experiments.

Figure 19 displays the analogous experiment over used ς-Fe_2N. Here, the amount of water is much less (note the scale difference between H_2O in Figures 18 and 19), indicating that the passivation procedure for this catalyst was more effective at preserving the bulk. Also, methane appears in Figure 19, after both ammonia and water have virtually disappeared. Much more ammonia was produced over the carburized ς catalyst as well. As will be shown subsequently, a greater percentage of nitrogen from the ς -nitride survived during 12 hours of Fischer-Tropsch synthesis.

Interestingly, the product formed during the temperature ramp is quite selective to hydrogen at different periods of the decomposition. In both Figure 18 and 19 water is the first product, appearing at approximately 573 K and at a maximum production rate at 600 K. Ammonia, meanwhile, begins to appear when water starts to decline. Methane waits until both these products have disappeared. The order of the products could be the result of a number of processes. Since the catalyst was passivated, oxygen is at the surface, and is available to hydrogen first.

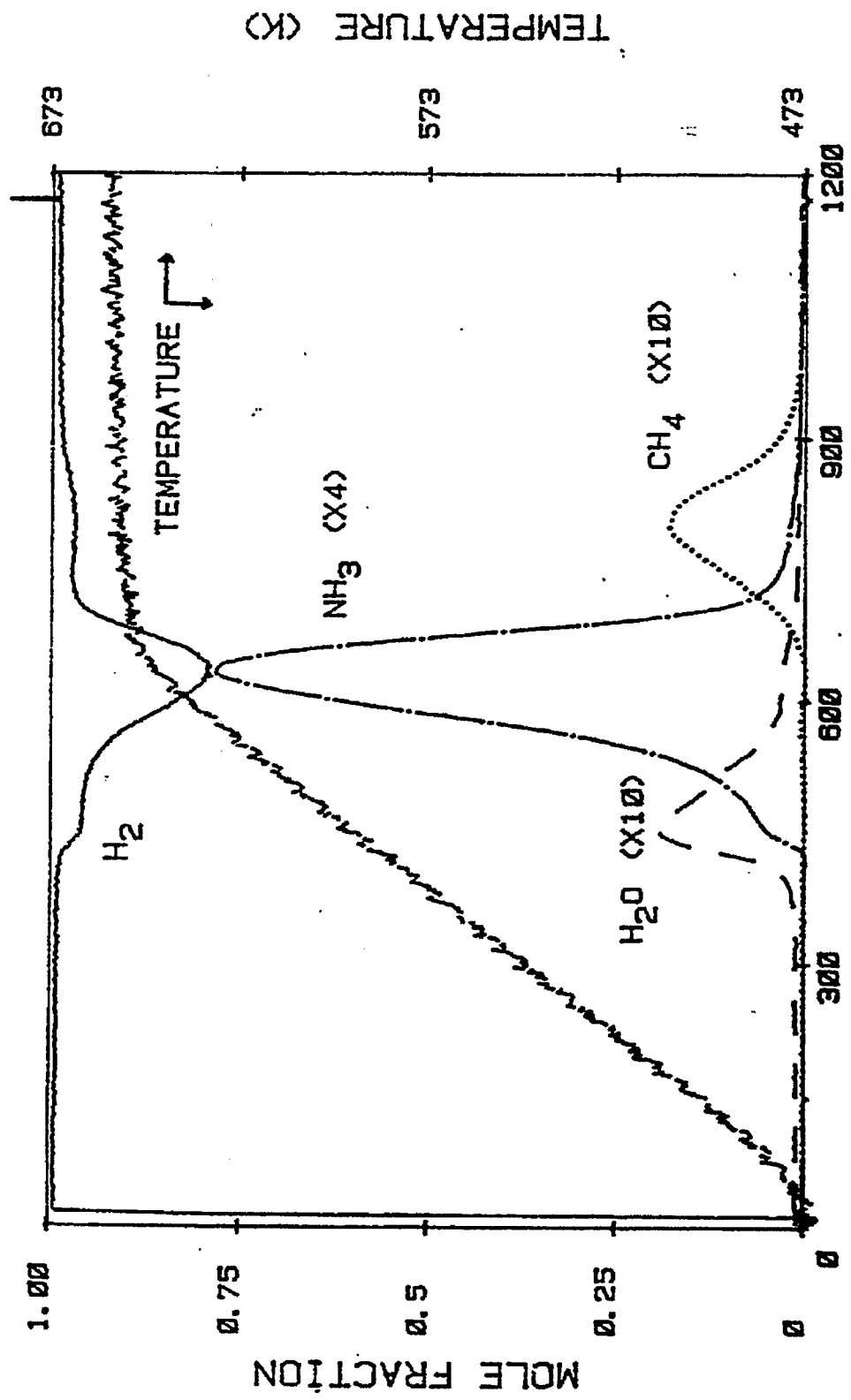

Figure 19 Hydrogenation of ϵ-Fe_2N Catalyst After 12 Hours of Synthesis

From the kinetic experiments of the initial minute of synthesis at 523 K over the ϵ nitride, we know that water is not produced in significant quantities until the rate of ammonia production declines. This would suggest that the rate of ammonia production is higher than water production with all reactants available on the surface. In Figure 18 and 19 however, nitrogen is apparently not available at the surface of the passivated catalyst, since the reaction favors water initially. As soon as enough of the surface is open to the nitride (or carbonitride) core, ammonia comes barreling out, leaving carbon behind. Carbon, slower to react, must wait for available surface hydrogen. Diffusion could be a factor, since carbon is slower to diffuse than nitrogen (36, 31), but at these high temperatures the diffusion rates are too rapid (10^{-10} cm^2/sec in α -Fe for nitrogen) to account for the delay.

The integrated amounts of the products give a rough estimate of the stoichiometry of the catalyst after 12 hours of synthesis. For the original ϵ–$Fe_{2.7}N$ catalyst, the amount of nitrogen left after 12 hours of synthesis corresponds to a Fe/N ratio of 5.0, indicating that 24% of the original nitride has been lost. Oxygen accounts for an Fe/O ratio of 10, which is substantial enough to place considerable uncertainty in the assessment of stoichiometry. During the passivation process, both nitrogen and carbon could have been lost. For ς–Fe_2N, the Fe/N ratio of 2.4 after reaction, indicates that only 15% of the original nitride has been lost. The Fe/O ratio is 25, which is not very significant. The Fe/C ratio is also 25, indicating that very little of the nitride has actually been carburized. The stoichiometry for the ς sample is thus $Fe\ N_{0.42}C_{0.04}O_{0.04}$, and adds to a net intersti-

tial stoichiometry of Fe_2X, in fair agreement with carbide stoichiometries by Anderson (1) and researchers at Northwestern (9). In order to estimate the carbon in the ϵ sample, we assume a Fe_2X stoichiometry, and thus the stoichiometry becomes $Fe\ N_{0.2}C_{0.2}O_{0.1}$. It is not known how oxygen replaces the other species, or if it simply adds as an oxide overlayer. These stoichiometries are somewhat nitrogen rich in comparison with those estimated by Wilson (see next section) using Mössbauer spectroscopy. After 12 hours of reaction, the catalysts had apparently reached a kinetic steady state with regard to the Fischer-Tropsch reaction. We see from these experiments, however, that a great deal of nitrogen still remains in the bulk, as predicted by the early experiments of Anderson (1). By exposing these used catalysts to hydrogen at higher (> 600 K) temperatures, nitrogen immediately vacates the bulk. Apparently the bulk nitrogen lies poised to react during the Fischer-Tropsch reaction, but carbon monoxide in the gas phase and the resulting carbon overlayer prevents decomposition.

2.3.13 Carburization of Iron and Iron Nitrides at 523 K

The addition of carbon to the iron nitride lattice produces carbonitride interstitial compounds and carbides after extended carburization. As a mechanism for carbonitride formation, Anderson and coworkers (6, 37) proposed that before significant nitrogen removal occurred in a CO/H_2 environment, carbon first diffused into an ϵ–nitride lattice, producing iron with few nearest neighbor vacancies. The behavior of the nitride is liable to be less stable in $3H_2/CO$ mixtures, where an increased percentage of H_2 can increase nitrogen removal as NH_3. A

blockage of surface sites by either C_xH_y or carbidic species would severely reduce NH_3 desorption. In studying this phenomenon, the difference between nitride phase stability under CO versus $3H_2/CO$ atmospheres is investigated. As a means of comparison, α–Fe stability is studied briefly to provide an insight into potential carbide formation in the iron nitrides.

Figure 20 shows the constant acceleration Mössbauer spectra of an iron powder carburized in 66 ml/min CO for 4 hours (Figure 20a) and then for an additional 6 hours (20b). The spectrum of the iron powder after 4 hours reaction 66 ml/min $3H_2/2He/CO$ is shown in Figure 20c. The temperature is 523 K during all reactions. As expected, the rate of carbide formation is accelerated in the presence of H_2. Table 8 shows that the catalyst carburized for 10 hours retains a 14% α–Fe spectral area. The carbides are fitted to ϵ'–$Fe_{2.2}C$ (ϵ') and χ–Fe_5C_2 (χ–I,χ–II,χ–III) structures. A wide doublet is used in Figure 20c to simulate the outer Fe_xC peaks. The slight misfit at -4 mm/s velocity in Figures 20a and b indicates a small Fe_xC contribution too.

The spectrum of the 4 hour carburized catalyst shows a 28% α–Fe contribution. The χ– and ϵ'–carbide parameters do not correspond exactly to those reported by Niemantsverdriet *et al.* (25). The χ–HFS values are close to the expected 189, 218, and 110 kOe for χ–I, II, and III, respectively, but the ϵ' –$Fe_{2.2}C$ field is slightly low. A discrepancy in the carbide isomer shift values is influenced by the unconstrained quadrupole splitting. As no Fe_xC inner peak contributions are included, the inner 4 peaks of the carbides are free to move to minimize this

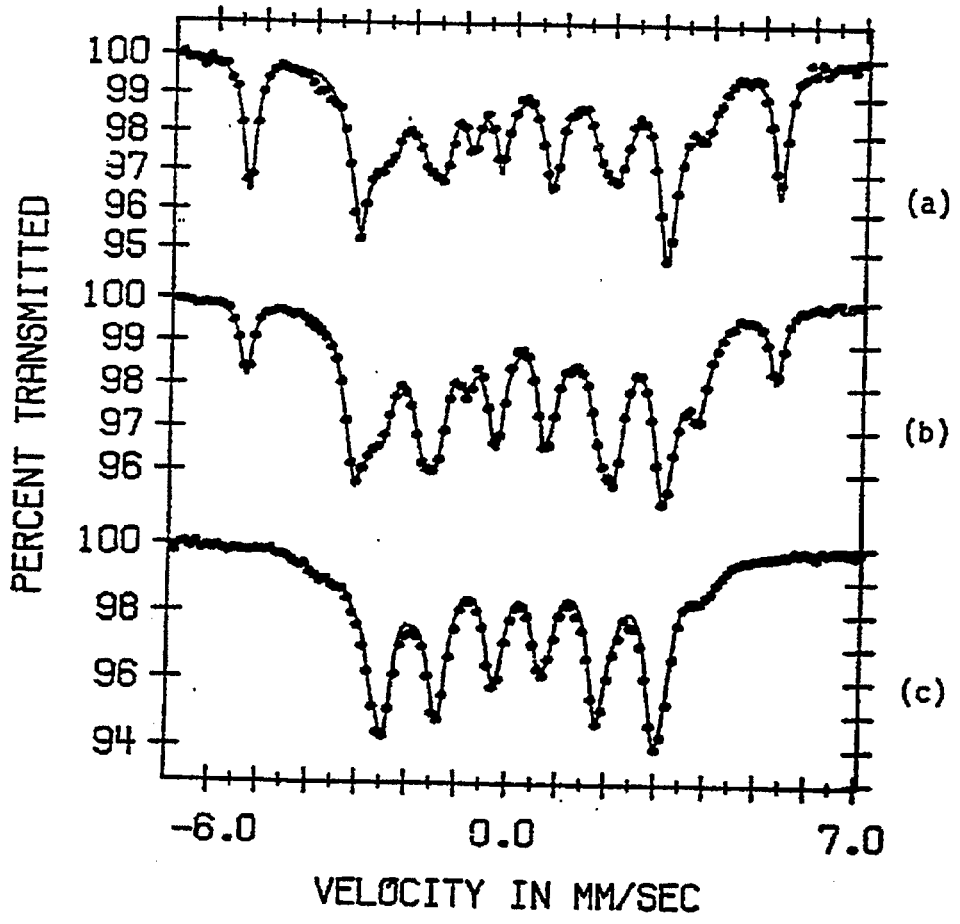

Figure 20 Mössbauer Spectra of α-Fe Carburized at 523 K.

a) treated in CO for 4 hours
b) treated in CO for 10 hours
c) treated in $3H_2/2He/CO$ for 4 hours

TABLE 8

Mössbauer Parameters (298 K) of Carburized Iron

Figure	Treatment	Iron Identity	IS (mm/s)	QS (mm/s)	HFS (kOe)	LW (mm/s)	RA (%)	Total Area
20a	CO	α-Fe	0.01	0.00	330.3	0.31	28.0	.2403
	523 K	X-I	0.26	-0.06	184.7	0.51	39.0	
	4.0 hr	X-II	0.23	+0.20	218.1	0.68	10.3	
		X-III	0.31	-0.31	114.7	0.46	13.9	
		ε'	0.22	+0.21	167.7	0.41	8.4	
		Fe-Q	(0.21)	(0.99)	---	(0.13)	(1.4)	
20b	CO	α-Fe	0.00	0.00	330.0	0.31	13.6	.2436
	523 K	X-I	0.27	-0.20	188.5	0.45	18.2	
	10.0 hr	X-II	0.23	+0.21	215.7	0.55	30.5	
		X-III	0.29	-0.45	114.5	0.45	10.4	
		ε'	0.21	+0.14	172.1	0.49	24.7	
		Fe-Q	0.18	0.92	---	0.23	2.6	
20c	$3H_2/2He/CO$	X-I	0.22	-0.05	182.0	0.42	23.2	.2600
	523 K	X-II	0.22	+0.70	217.1	0.35	3.8	
	4 hr	X-III	0.27	-0.13	121.5	0.96	10.5	
		ε'	0.23	+0.10	167.5	0.42	46.6	
		Fe_xC	(0.16)		(232.7)	(1.18)	(9.3)	
		Fe-Q	0.31	1.12	---	0.39	7.1	

absence. Negative QS values for χ–I and χ–III are thus predicted by the computer fitting, whereas Tau *et al.* (38) reported positive QS for these sites when they included 6 peaks for Fe_xC. The similarity in χ–I (183 kOe) and ϵ' (173 kOe) fields makes area assignments to each site difficult. Variations in the relative concentration of each carbide in a single hybrid six line pattern would not produce constant Mössbauer parameters and this combined site approach is avoided.

A non-magnetic contribution is found in all three spectra. With an IS in the range 0.18 - 0.31 mm/s, this is not an Fe^{2+} species, but Fe^{3+} or superparamagnetic carbide. Amelse *et al.* (39) reported significant superparamagnetic χ–carbide during their study of Mössbauer spectroscopy of silica supported iron. By cooling these carbided iron samples assignment of the central doublet might be possible. A superparamagnetic carbide species would alter the room temperature ϵ'/χ carbide area ratio. The spectral parameters for Figure 20c predict a high percentage of ϵ'–carbide, which may arise from reacting with $3H_2/CO$ and He. The inert reduces the reaction rate and carburization of the catalyst to χ–carbide is slowed.

The room temperature Mössbauer parameters for iron nitride phases carburized in 66 ml/min CO at 523 K are given in Table 9. Figures 21a-c show the room temperature spectra of a γ' –Fe_4N catalyst carburized for 2.5, 4.0, and 9.5 hours respectively. Figures 21d-e show the difference carburizing for 4 hours has on an ϵ–$Fe_{2.53}N$ versus a ς–Fe_2N sample. The γ'–spectra show the slow decay of the Fe_4N nitride. The outer 0nn sextet peaks progressively lose intensity and are essentially absent after 10 hours in CO (Figure 21c). The peaks positioned at -3.15

and +3.75 mm/s, γ' 2nn values, also decrease during carburization. The two innermost peaks at -0.25 and 0.70 mm/s become more symmetric with prolonged carburization.

The carburized Fe_4N spectra are fit to five magnetic sites and an Fe-Q site. A preliminary four magnetic site fit is used to simulate the γ' 0nn contribution; the parameters allow subtraction of the 340 kOe field and the residual spectrum to be fitted with 26 peaks rather than 32. Such a subtraction is not possible for Figure 21c, as the γ' 0nn contribution was too small to detect accurately. For this sample, this site is not reported in Table 9. Of the remaining four hyperfine fields, the 216 and 125-135 kOe sites were constrained to zero QS. The spectral parameters for the γ' 0nn and γ' 2nn are close to the expected values. However, due to inaccuracy arising from a small spectral area, the isomer shift and magnetic splitting of the γ'–I site in the 4 hr CO treated sample are lower than normal. The ratio of the 0nn to 2nn site area is considerably lower than the expected 1:3 value. This may be due to an additional magnetically ordered phase being superimposed upon the γ'–II contributions. The Mössbauer parameters for this proposed ill-defined phase would likely be similar to those for γ'–II, otherwise a deviation in the combined parameters would be expected.

The three non–Fe_4N sites are characterized by magnetic fields of roughly 157, 129 and 39 kOe and isomer shifts greater than 0.31 mm/s. The quadrupole splitting of the 129 kOe site in unconstrained fits was always in the range +0.02 to -0.06 mm/s, and constraining the QS to zero had no detectable effect. In assigning

TABLE 9

Mossbauer Parameters (298 K) of CO Treated Nitrides

Figure	Treatment	Iron Identity	IS (mm/s)	QS (mm/s)	HFS (kOe)	LW (mm/s)	RA (%)	Total Area
21a	γ'-Fe_4N	γ-I	0.24	0.00	340.6	0.33	5.2	.2398
	2.5 hr	γ-II	0.30	0.00	217.3	0.69	32.1	
		α-III	0.32	-0.17	157.1	0.64	32.4	
		β-III	0.33	0.00	123.5	0.63	21.2	
		δ-III	0.26	-0.27	88.9	0.36	7.3	
		Fe-Q	0.25	0.73	---	0.41	7.0	
21b	$'$-Fe_4N	γ-I	0.21	0.00	337.8	0.30	3.5	.2409
	4.0 hr	γ-II	0.30	0.00	215.9	0.69	25.0	
		α-III	0.34	-0.21	156.5	0.71	42.4	
		β-III	0.35	0.00	127.2	0.58	15.0	
		δ-III	0.29	-0.51	88.6	0.46	10.7	
		Fe-Q	0.26	0.78	---	0.43	11.1	
21c	$'$-Fe_4N	γ-II	0.30	0.00	217.5	0.49	7.6	.2365
	9.5 hr	α-III	0.33	-0.25	160.0	0.75	40.6	
		β-III	0.32	0.00	137.5	0.74	29.7	
		δ-III	0.30	-0.37	87.6	0.56	14.0	
		Fe-Q	0.25	0.78	---	0.45	8.3	

TABLE 9 (Continued)

Figure	Treatment	Iron Identity	IS (mm/s)	QS (mm/s)	HFS (kOe)	LW (mm/s)	RA (%)	Total Area
21d	ε-$Fe_{2.53}N$	ε-II	0.31	0.00	200.3	0.83	51.8	.2815
	4.0 hr	α-III	(0.43)	(-1.25)	(160.5)	(0.33)	(3.2)	
		ε-III/β-III	0.39	0.00	115.4	0.56	19.6	
		δ-III	0.39	-0.16	92.8	0.58	15.5	
		Fe-Q	0.33	1.04	---	0.51	9.9	
21e	ζ-Fe_2N	ζ	unresolved					
	4.0 hr							

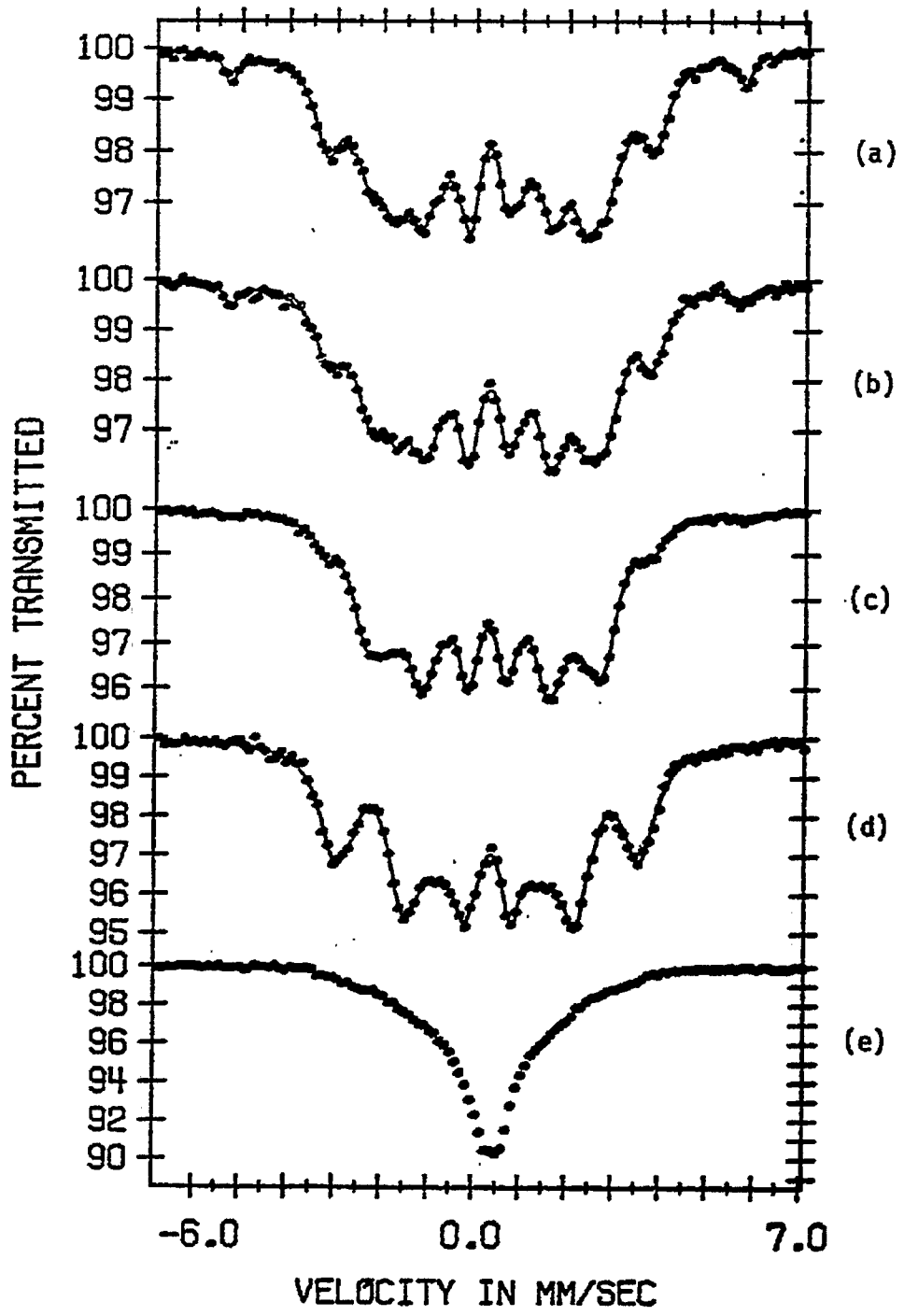

Figure 21 Mössbauer Spectra of Nitrides Treated in CO at 523 K

a) γ'-Fe_4N treated for 2 hours
b) γ'-Fe_4N treated for 4 hours
c) γ'-Fe_4N treated for 9.5 hours
d) ε-$Fe_{2.53}N$ treated for 4 hours
e) ζ-Fe_2N treated for 4 hours

homogeneous structures to each of the three sites, it is valuable to consider which phases cannot be present. No concentration of γ'–nitride nitrogen to form a higher ϵ–Fe_xN during carburization has been reported. Indeed, on the basis of hyperfine fields, only the 157 kOe sextet can arise from a ϵ–II nitride configuration. This magnetic splitting corresponds to ϵ–nitride of high nitrogen content. The ϵ–III environment (70-75 kOe) required to reach this high nitrogen stoichiometry is absent from the spectrum. Conversely, the 89 or 129 kOe sextets are associated with ϵ–II fields greater than 157 kOe. The three new fields must then arise from carbide and/or carbonitride structures. However, the IS values of the three unassigned sites are too large for the known carbides. The sites can then be attributed to a carbonitride species, as expected. Actual carbon and nitrogen nearest neighbor assignments will depend upon correlation to additional carburized spectra. The magnitude of the HFS for these sites, according to Foct *et al.* (27), is too low for 2nn carbonitrides. As such, the 3 sites will be tentatively assigned as 3nn carbonitrides, in a manner parallel to Foct's defining 2nn carbonitride sites, and designed as α–III (157 kOe), β–III (129 kOe), and δ–III (89 kOe).

A helium-treated ϵ–nitride was carburized in 66 ml/min CO at 523 K for four hours (Figure 21d). The spectrum of the carburized nitride shows a decrease in splitting and intensity of the outermost, ϵ–II field. Further structural rearrangement is evidenced by the increase in spectral intensity at -0.8 and -1.5 mm/s. The computer fit to Figure 21d requires two new hyperfine fields in addition to the nitride ϵ–II, ϵ–III, and Fe-Q contributions. All sextets are constrained to

3:2:1:1:2:3 peak intensities and the nitride ϵ–II and ϵ–III fields are constrained to zero QS. The IS and HFS values (Table 9) of the ϵ–II (200 kOe) and ϵ–III (115 kOe) sextets are within the expected range for pure nitrides. These room temperature parameters also confirm the decrease in ϵ–II hyperfine field from the starting 212 kOe value and the decrease in spectral area from 62 to 52%. Relative areas may be compared as the total spectral areas of starting and carburized spectra differ by less than 1.5%. The 2kOe decrease in ϵ–III field after carburization is not as high as predicted from the ϵ–II field decrease.

In pure ϵ–nitride, the decrease in hyperfine splitting is correlated to an increase in overall nitrogen content. This correlation may still hold when carbon has replaced a small percentage of the nitrogen, and represents a possible systematic concentration check in low C solubility carbonitrides. Although the ϵ–III field is 2kOe lower after carburization, if the nitrided phase is still relatively homogeneous and the ϵ–II field defines the interstitial concentration, an additional 6-8 kOe decrease is predicted. From magnetic splittings of the two remaining sites, 160 and 93 kOe, it is plausible to assign them as α–III and δ–III sites respectively. An approximate sample stoichiometry, $Fe_{2.43}(CN)$, is obtained by considering the two nearest neighbor site, ϵ–II, and the remaining three nearest interstitial sites. For a relatively homogeneous sample, this stoichiometry predicts ϵ–II and ϵ–III HFS of 198 and 104 kOe, respectively.

Extending this analysis, the higher than predicted ϵ–III field (115 kOe) could arise from a superposition of two magnetic splittings. A truly lower ϵ–III field

~105 kOe could, plausibly, be coupled to the ~129 kOe β–III carbonitride field in a similar way in which the ϵ'–$Fe_{2.2}C$ and χ–Fe_5C_2 (I) fields are occasionally coupled. The proposed β–III site is liable to have a similar isomer shift to that of the ϵ–III site. Through this assignment, the carburized nitride is visualized as essentially on hcp ϵ -iron nitride matrix with locally high concentrations of hcp carbonitride. The carbon distribution may be sufficiently homogeneous to be characterized by distinct nearest neighbor configurations, yet asymmetric enough to produce high negative quadrupole splittings.

The estimated nominal interstitial concentration, $Fe_{2.43}$ (CN) will provide an upper bound to the nitrogen remaining in the catalyst. Assuming no nitrogen loss during CO carburization, the carbonitride concentration becomes $Fe_{2.43}(C_{.04}N_{.96})$. If carbon addition accounts for between 18 and 28% of spectral area, this 4% interstitial carbon estimate is conservative. On the basis of spectral area, the γ'–Fe_4N catalyst is even less stable during 4 hours of carburization in CO. The lower nitrogen density in a more open fcc lattice is expected to facilitate faster C incorporation.

A comparison to the spectrum (Figure 21e) of ζ–nitride after 4 hours of carburization in 66 ml/min CO at 523 K can only be qualitative, as no reasonable fit could be generated. (Note the lack of peak definition in Figure 21e). Quantitatively, the carburized sample's spectrum exhibits a sharper ζ contribution with a narrower combined peak width. The extremely broad wings in Figure 21e indicate severe specimen inhomogeneity and probable relaxation effects. The widest

magnetic splitting still defined by 3:2:1:1:2:3 peak intensities, which would remain undetected in this background is 160 kOe. Computer simulation of this contribution predicts line widths of 1.0 mm/s and greater. Although no estimate of Fe_2N carbon uptake can be forwarded, the very lack of peak definition suggests stability of the ς phase in CO at 523 K.

The exposure of an iron nitride to a carbon monoxide and hydrogen environment at 523 K introduces three new considerations into a phase stability study: an increased carburization potential as evidenced earlier by a faster carbide formation over α–Fe, an inherent nitride instability in H_2, and C-H-N kinetics. The carburization of a ς–Fe_2N catalyst in 66 ml/min $3H_2/CO$ at 523 K, followed by constant acceleration Mössbauer spectroscopy (Figure 22), illustrates the first two complications. The progressive decay of the prominent peaks in Figure 22a, -3.2, -1.8, +2.4, and +3.9 mm/s, is clear evidence of structural alteration. The differences between the 13.5 hr spectrum (Figure 22d) and the 16.0 hr spectrum (Figure 22e) are less than differences between preceding spectra. Carbon addition is probably close to saturating the carbonitride lattice. The room temperature Mössbauer parameters of the carburized samples are given in Table 10. Figure 22a is fit with two magnetic sites and a non-magnetic, Fe-Q, contribution. The peaks in each sextet are constrained to 0 QS, equal peak widths, and 3:2:1:1:2:3 intensities. Two additional fields are required in the remaining spectrum fits; neither are constrained to zero quadrupole splitting.

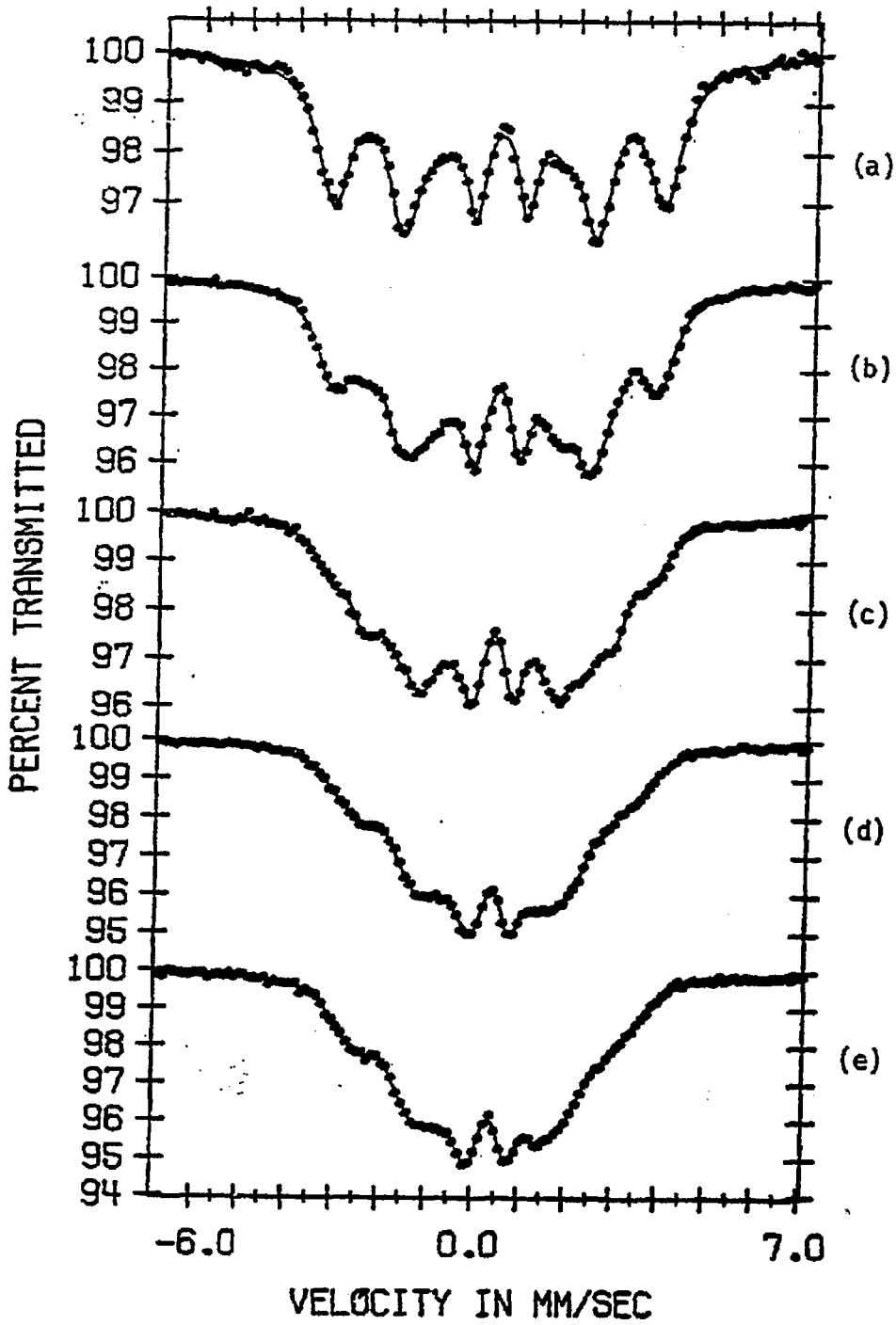

Figure 22 Mössbauer Spectra of ζ-Fe_2N Carburized at 523 K.

a) treated in $3H_2/CO$ for 17 hours
b) treated in $3H_2/2He/CO$ for 4 hours
c) treated in $3H_2/CO$ for 2.5 hours
d) treated in $3H_2/CO$ for 13.5 hours
e) treated in $3H_2/CO$ for 16 hours

TABLE 10

Mössbauer Parameters (298 K) of H_2/CO Treated ε-Nitride

Figure	Treatment	Iron Identity	IS (mm/s)	QS (mm/s)	HFS (kOe)	LW (mm/s)	RA (%)	Total Area
22a	$3H_2/CO$	ε-II	0.31	0.00	220.1	0.87	65.6	.2289
	523 K	ε-III/β-III	0.36	0.00	127.9	0.83	27.5	
	17 min	Fe-Q	0.32	1.07	---	0.41	6.9	
22b	$3H_2/2He/CO$	ε-II	0.30	0.00	215.8	0.89	40.7	.2683
	523 K	α-III	0.38	-0.54	165.3	0.80	15.3	
	4.0 hr	ε-III/β-III	0.35	0.00	122.5	0.82	30.1	
		δ-III	0.44	-0.62	93.1	0.45	6.0	
		Fe-Q	0.29	0.90	---	0.45	7.9	
22c	$3H_2/CO$	ε-II	0.30	0.00	213.0	0.88	20.1	.23651
	523 K	α-III	0.39	-0.42	166.5	0.80	31.6	
	2.5 hr	ε-III/β-III	0.32	0.00	123.7	0.71	20.0	
		δ-III	0.35	-0.44	95.9	0.55	16.1	
		Fe-Q	0.27	0.86	---	0.52	12.2	

TABLE 10 (Continued)

Figure	Treatment	Iron Identity	IS (mm/s)	QS (mm/s)	HFS (kOe)	LW (mm/s)	RA (%)	Total Area
22d	$3H_2/CO$	ε-II	0.32	0.00	196.6	0.93	19.4	.2654
	523 K	α-III	0.53	-0.83	160.8	0.77	17.6	
	13.5 hr	ε-III/β-III	0.28	0.00	111.3	0.91	17.5	
		δ-III	0.38	-0.34	91.4	0.80	29.2	
		Fe-Q	0.32	0.84	---	0.63	16.3	
22e	$3H_2/CO$	ε-II	0.32	0.00	193.8	0.86	15.7	.2627
	523 K	α-III	0.52	-0.78	159.8	0.86	23.0	
	16.0 hr	ε-III/β-III	0.27	0.00	107.9	0.76	18.6	
		δ-III	0.38	-0.39	90.4	0.72	23.2	
		Fe-Q	0.32	0.82	---	0.69	19.5	

The 220 and 128 kOe magnetic fields predicted in the 17 minute carburized ς–nitride of Figure 22a are in the acceptable range of 2nn and 3nn ϵ–nitride fields. The nominal stoichiometry of this interstitial catalyst is then $Fe_{2.56}$ (CN). A loss of N as NH_3 must occur to achieve this stoichiometry. Applying the HFS-composition correlation, the expected ϵ–II and ϵ–III fields for an homogeneous nitride with x = 2.56 are 216 and 117 kOe respectively. Again, the observed 3nn field (128 kOe) is higher. The 0.36 mm/s IS for this site is slightly below the 0.40 mm/s value seen for the single phase nitrides. The coexistence of an overlapping β–III carbonitride is plausible, and this 3nn field is assigned to an ϵ–III/zeta–III site. Based on the same argument this dual assignment is continued for the remaining four spectra. Higher carbonitride (2nn) fields may exist in the spectra but their intensities would be small. Their formation requires either addition into a 1nn ϵ–nitride lattice, or substitution into a 2nn environment. The former mechanism is, according to Anderson (1), more likely to occur in the early stages of reaction. In the noisy background to Figure 22a, a field could exist with outer peaks at approximately -5.3 mm/s and 5.6 mm/s. The background noise, however, prevents fruitful discussion of this possibility.

Figure 22b-c show the effect of decreased synthesis gas partial pressure on the ς–Fe_2N stability. The room temperature spectrum (Figure 22b) of Fe_2N carburized in 100 ml/min $3H_2$/2He/CO for 4 hours at 523 K shows more ϵ–nitride retention than in Figure 22c, where the ς–nitride is carburized in $3H_2$/CO at 523 K for only 2.5 hours. Both spectra exhibit similar Mössbauer parameters for the nonmagnetic

Fe-Q, ϵ–nitride, and hcp carbonitride sites. The spectral percentages of the α–III and δ–III contributions are 21% in Figure 22b but 50% in Figure 22c. On a 2nn and 3nn assignment, the stoichiometries for the 4 hour and 2.5 hour carburized samples are $Fe_{2.31}$ (CN) and $Fe_{2.14}$ (CN) respectively. Qualitatively, the lower syngas partial pressure reduces the transformation rate of ϵ–nitride to the 3nn carbonitride. In the first 4 hours of synthesis reaction, GC measurements show that the $3H_2/CO$ reaction produces twice the moles/min of CO_2 and is 10 times as active toward CO conversion as the $3H_2/2He/CO$ reaction. Without measuring both CO_2 and H_2O production during the reaction, a balance on O cannot be made to give the extent of carbon deposition. So, whether hydrogen-assisted removal of nitride nitrogen allows a faster ingress of carbon addition to the lattice, or whether faster CO reaction rates provide a higher driving force for C addition, is not clear from these two spectra. The requirement for interstitial mobility in a ζ–nitride, however, remains for the production of ϵ–II environments.

The spectra of the ζ–nitride after 13.5 hours (Figure 22d) and 16.0 hours (Figure 22e) in the $3H_2/CO$ show a continued, slower loss of nitrogen and an increase in overall interstitial content. Nominal stoichiometry of the latter catalyst is $Fe_{2.11}$ (CN). The inhomogeneous nature of the catalyst bulk is evidenced by decreased peak resolution and a more difficult estimation of individual site identification. Yeh *et al.* (8) reported Mössbauer spectra of carburized, silica-supported Fe_2N. Their 49 hour caburized nitride spectrum exhibits greater peak definition than Figure 22e and is more similar to Figure 22b. This could be due to stabilization of

the ϵ–nitride by the silica. Indeed, a γ'–Fe_2N dispersed on a high surface area carbon (40) support showed surprising stability under reaction conditions. The Northwestern group (8) also reports a non-magnetic spectral contribution which is attributed to amorphous Fe^{3+}. This would be a possible assignment of the Fe-Q site, as the IS is higher than expected for superparamagnetic carbide. The growth in area percentage suggests it is not solely a non-magnetic nitrogen 3nn site. The evaluation of nominal stoichiometries will assume, however, that it is a 3 nitrogen nearest neighbor site. Its actual identity cannot be determined with the available data.

Figure 23 illustrates the effect of decreased H_2/CO ratio on carbonitride formation in γ'–nitride. The starting γ' catalysts were prepared by nitriding an iron powder in 60% NH_3 at 598 K for the $3H_2/CO$ reaction (Figure 23a-b) and by nitriding in 50% NH_3 at 673 K for the $3CO/H_2$ reaction (Figure 23c). The latter catalyst showed a small 5% α–Fe contribution after two hours of nitriding, indicating a longer time is necessary under these conditions to ensure homogeneity. The $3CO/H_2$ ratio clearly stabilizes the nitride with respect to loss of γ' 0nn sites. The Mössbauer parameters for these carburized samples are given in Table 11, and indicate a different mechanism of carbon incorporation than carburization in either CO or $3H_2/CO$. The peaks within each sextet are constrained to 3:2:1:1:2:3 peak intensities and equal widths. Only the 340 and 216 kOe γ'–nitride fields were constrained to zero QS.

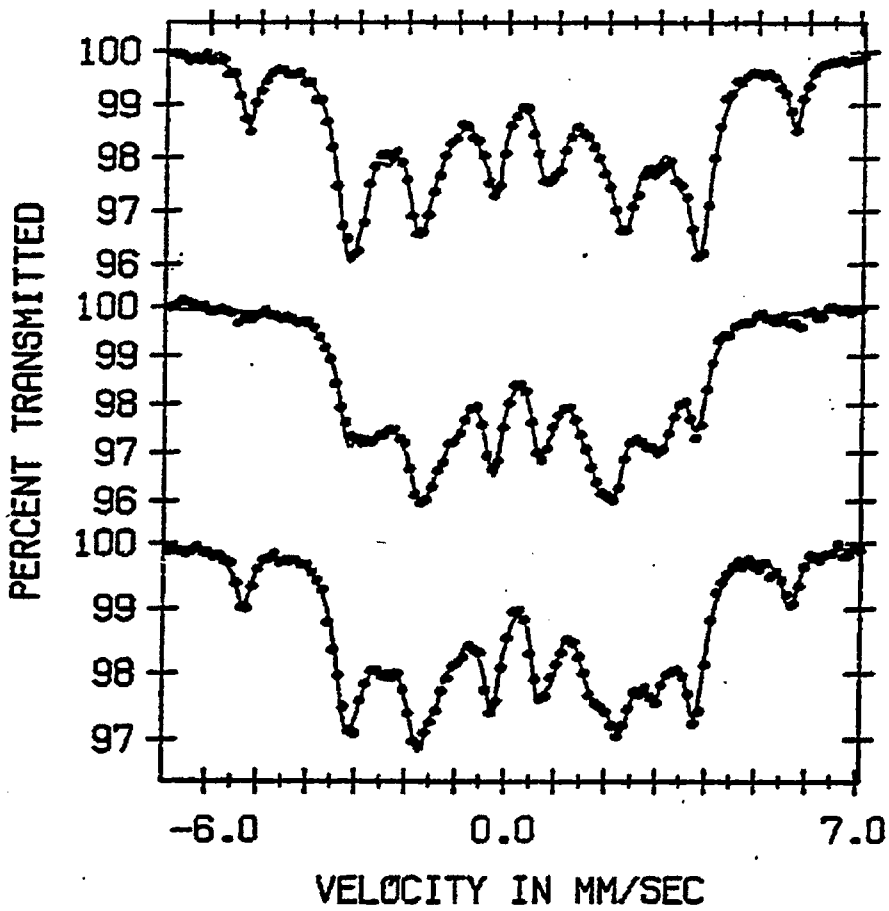

Figure 23 Mössbauer Spectra of γ'-Fe_4N Carburized at 523 K.

a) treated in $3H_2/CO$ for 17 minutes
b) treated in $3H_2/CO$ for 2.5 hours
c) treated in $3CO/H_2$ for 2.5 hours

TABLE 11

Mössbauer Parameters (298 K) of H_2/CO Treated γ'-Nitride

Figure	Treatment	Iron Identity	IS (mm/s)	QS (mm/s)	HFS (kOe)	LW (mm/s)	RA (%)	Total Area
23a	$3H_2/CO$	γ-I	0.24	0.00	339.5	0.38	13.9	.2250
	523 K	γ-II/χ-II	0.31	0.00	217.6	0.62	59.4	
	17 min	χ-I	0.25	+0.06	165.6	0.58	15.8	
		χ-III	0.23	-0.22	124.4	0.51	10.3	
		Fe-Q	0.23	0.87	---	0.24	2.0	
23b	$3H_2/CO$	α-II/χ-II	0.24	+0.20	216.7	0.48	24.4	.2310
	523 K	χ-I	0.29	-0.28	182.3	0.70	32.9	
	2.5 hr	unknown	0.27	-0.11	150.1	0.86	26.4	
		χ-III	0.22	-0.34	107.5	0.45	12.2	
		Fe-Q	0.20	0.86	---	0.32	4.1	
23c	$3CO/H_2$	γ-I	0.21	0.00	339.6	0.40	12.4	.1969
	523 K	γ-II/χ-II	0.31	0.00	216.1	0.56	40.5	
	2.5 hr	χ-I	0.10	-0.29	180.0	0.46	8.0	
		ε-II	0.24	+0.13	165.8	0.43	13.5	
		unknown	0.19	-0.01	146.9	0.42	7.0	
		χ-III	0.27	-0.15	118.4	0.58	15.2	
		Fe-Q	0.22	0.86	---	0.24	3.4	

The Fe_4N catalyst after 17 minutes carburization in $3H_2/CO$ at 523 K (Figure 23a) is fitted to two fields, 166 and 124 kOe, in addition to the starting nitride fields. The Mössbauer parameters for the nitride fields are indicative of γ'–Fe_4N. The area ratio of 2nn to 0nn contribution is larger than expected, which is attributed to overlap with the χ–II (218 kOe) field. Carbide formation is indicated by the IS = 0.25 mm/s, QS = +0.06 mm/s, and HFS = 166 kOe site. Although the α–III site possesses the same magnitude splitting, the IS and QS values are consistent with ϵ'–$Fe_{2.2}N$, or χ–Fe_5C_2 (I). The 124 kOe site has an isomer shift which is too low for β–III carbonitride and thus is attributed to χ–III. The corresponding χ–I and χ–II sites would then overlap with the 166 and 218 kOe fields, respectively.

The catalyst after 2.5 hours carburization (Figure 23b) retains little of the starting γ'–nitride. The 0nn 340 k0e contribution could not be accurately fit in this spectrum, although bumps in the background at approximately -5.2 and + 5.7 mm/s are attributed to Fe_4N. The 217 kOe field, although essentially χ–II according to IS and QS values, may then contain γ–II contributions. The 182 and 108 kOe fields are attributed to χ–I and χ–III sites. An unidentified 150 kOe field accounts for 26% of the spectral area. A similar field occurs in the $3CO/H_2$ sample (Figure 23c) after 2.5 hours carburization. The Figure 23c spectrum is fitted with γ'–nitride, χ–carbide and a 13% ϵ'–carbide contribution whereas no ϵ' is uniquely detected in the $3H_2/CO$ spectrum. We speculate that the different IS and QS values for this unknown phase in the $3CO/H_2$ as against the $3H_2/CO$ carburi-

zation arises from superposition of ϵ–II and the unknown phase in Figure 23b or from an inaccuracy in subtracting 8 peaks, γ–II and Fe-Q, from the Figure 23c spectrum.

An obvious assignment to this unknown would be a fcc carbonitride. Jack [41] and Bridelle [21] report different X-ray parameters for the γ'– and ϵ– carbonitrides. In a cubic carbonitride the four possible configurations are: 0nn for corner Fe atoms, and NN, CN, and CC for the 2nn face centered Fe. Moreover, the fields for these hypothetical cases are likely to be similar to those for 2nn ϵ– carbonitride fields. Foct *et al.* [27] proposed that such 2nn splittings are 200 kOe in magnitude and greater. As such the 148 kOe unidentified field may be too low. Any γ'– carbonitride peaks overlapping the 217 kOe γ' II contribution would be unresolved. The assignment remains in doubt but this explanation is plausible.

The mechanism of carbon incorporation in the three pure iron nitrides appears to depend both on the nitrogen density within the catalyst and the hydrogen partial pressure. In $3H_2/CO$ the ζ–Fe_2N nitride loses significant nitrogen before carbon addition is appreciable. The γ'–nitride forms pure χ– and ϵ'–carbides whereas the ζ–nitride forms appreciable hcp carbonitride. Carburizing Fe_4N in pure CO will, however, form the ϵ– carbonitride phase, but the Fe_4N does not lose sufficient nitrogen in CO in 4 hours to form a well defined carbonitride. In order to determine the actual nitrogen retention in the nitride, or the actual stability of the catalyst with the Mössbauer effect, a carbon-nitrogen nearest neighbor assignment must be made for the α–III, β–III, and δ–III carbonitride sites. Foct *et al.* (27)

identified 2nn ϵ– carbonitrides as having magnetic splittings increase in the order $H_{CCV}<H_{NNV}<H_{CNV}$. If a similar trend holds for 3nn sites, the expected ϵ–carbonitride ordering becomes $H_{CCC}<H_{NNN}<H_{NCC}$ and H_{NNC}. Yeh *et al.* (8), however, have proposed a linear variation in hyperfine field splitting between the saturation 3 nitrogen nn field (100 kOe) and the 3 carbon nn field (191 kOe). This goes against the extrapolated Foct *et al.* (27) trend.

By considering the CO carburized γ'–Fe_4N spectra (Figure 21a-c), a series of trial site assignments can be made. Assignments which predict higher nitrogen content than Fe_4N or an increasing interstitial nitrogen percentage are considered unacceptable. Three assignments are in accordance with the physical restraints:

(1) α–III $\equiv$ CCC, β–III $\equiv$ NNC, δ–III $\equiv$ NCC

(2) α–III $\equiv$ CCC, β–III $\equiv$ NCC, δ–III $\equiv$ NNC

(3) α–III $\equiv$ CCC, β–III $\equiv$ NNC, δ–III $\equiv$ NNN.

All three possibilities predict α as a three C environment and either β or δ as a NNC site. The first assignment, however, is more likely. The second assignment predicts an equal quantity of nitrogen after 2.5 and 4.0 hours of carburization, and loss after 4.0 hours. Anderson (1) and Jack (42) have seen greater initial nitrogen loss. The β–III site is favored as a NNC environment by Figure 22a, because if the β site does represent NCC, the NNC site should be detected. A second site, however, was not seen in Figure 22a. The negative quadrupole splittings (-0.62 to -0.15 mm/s) suggests an asymmetric environment not associated with ϵ–II or ϵ–III nitrides. The carbonitride NNN environment should behave similarly, and would have a zero, or small, QS.

From the above considerations, the first assignment is more likely. The ordering of this assignment, $H_{\alpha(CCC)} > H_{\beta(NCC)} > H_{\delta(NCC)}$ does not follow the trends of either Yeh *et al.* [8] or Foct and coworkers (27). Rather, we modify the two nearest neighbor approach of the latter to the 3nn carbonitride system and predict an ordering trend intermediate between that of each research group. The increasing Fe-Q contribution and the overlap between the β–III/ϵ–III sites in the carburized Fe_2N spectra (Figure 22) makes it difficult to validate the carbonitride. Additional experiments, possibly with low temperature spectra, will be needed to confirm this assignment.

2.4 Modification of Iron Nitride Chemistry by Supports and by Gas Phase Ammonia

2.4.1 Selectivity and Stability of Synthesis Reactions over Iron Nitrides

In previous work (45), we examined the stability, surface chemistry and catalytic behavior of the three iron nitrides, principally on unsupported iron powders. Stability of these structures in various gas phase atmospheres was found to be a vital issue when evaluating the dynamics of the catalysts or reactions on them. At 523 K in pure hydrogen, the nitrides decompose rapidly to Fe^0 and NH_3, whereas in synthesis gas slow replacement of nitrogen for carbon in the bulk results in the formation of carbonitride phases. A surface nitrogen species, deposited during the nitriding pretreatment in ammonia, was found to be extremely active, suggesting a possible surface synthesis route to nitrogen containing compounds when NH_3 is added to synthesis gas. Accordingly, the literature, along with several patents, reports the production of amines or nitriles with these reactants over iron catalysts (2-5).

We report here our studies to include the behavior of iron nitride catalysts and reaction kinetics of CO, H_2 and NH_3 reactions. It is known that at lower temperatures amines are formed (2), and at high temperatures (773 K) acetonitrile is selectively formed (3-5). Our research has emphasized studies of the reaction at 773 K over unsupported prenitrided catalysts, which deactivate quickly with accompanying high CO_2 production rates, and over Fe/SiO_2, which has stable activity and favorable selectivity to acetonitrile.

Iron supported on carbon has unusually stable activity for the Fischer-Tropsch synthesis (FTS) (40). In work in our laboratory, we have observed a corresponding stability of a prenitrided phase during FTS as well. We have begun investigation small particle iron on carbon catalysts for the Fischer-Tropsch reaction using Mössbauer Spectroscopy. X-Ray diffraction (XRD), hydrogen chemisorption and transmission electron microscopy (TEM) have been used to characterize a number of different iron on carbon catalysts, with good agreement between the techniques. We report here Mössbauer effect studies of Fe particle growth after nitriding and reaction.

2.4.2 Catalyst Preparation

The reduced or nitrided iron-based catalysts used for these experiments were prepared from either unsupported iron oxide powders, 4% Fe/SiO_2, or Fe/C samples. The supported catalyst precursors were prepared by incipient wetness with iron nitrate solutions and subsequent decomposition in hydrogen. In the work reported here, reduction was carried out at 400°–450°C in flowing UHP H_2, and nitriding at either 325 or

400°C in pure NH_3 (to produce the ς–Fe_2N phase) or at 500°C (to produce a high nitrogen ϵ–Fe_xN phase, $x \cong 2$). For some nitrided samples, iron oxide catalyst precursors were nitrided in NH_3 without prior reduction. The nitriding conditions have been confirmed to produce the reported phases by XRD, Mössbauer spectrometry, and quantitative decomposition in hydrogen as measured by mass spectrometry.

2.4.3 Addition of Ammonia to Synthesis Gas

We have spent considerable effort in preparation and identification of the iron nitride phases. By monitoring the conversion of NH_3 and the production of H_2 during the nitride formation reaction (Figure 24) or by following the dynamic changes in the catalyst bulk using Mössbauer spectrometry (Figure 5), we can not only identify the nitrides formed but also follow their evolution. In Figure 24, we display the initial minutes of nitriding over a prereduced unsupported iron powder at 400°C. From pure H_2, a switch to a 4/1 NH_3/He mixture is made, producing the initial products H_2 and a solid nitride phase. Note that NH_3 is initially adsorbed whereas He passes through unaffected, thus causing the observed overshoot in helium signal. The nitriding reaction occurs at a furious pace during the first minute; ammonia is decomposed to hydrogen and nitride only, since N_2 is not observed. At the two minute mark in the figure, the total amount of ammonia decomposed correlates approximately to an Fe_4N stoichiometry. Further nitriding at this temperature will yield the ς–Fe_2N nitride.

In an effort to take advantage of the active surface nitrogen species and also to investigate nitride stability in NH_3 and synthesis gas mixtures, we have recreated the

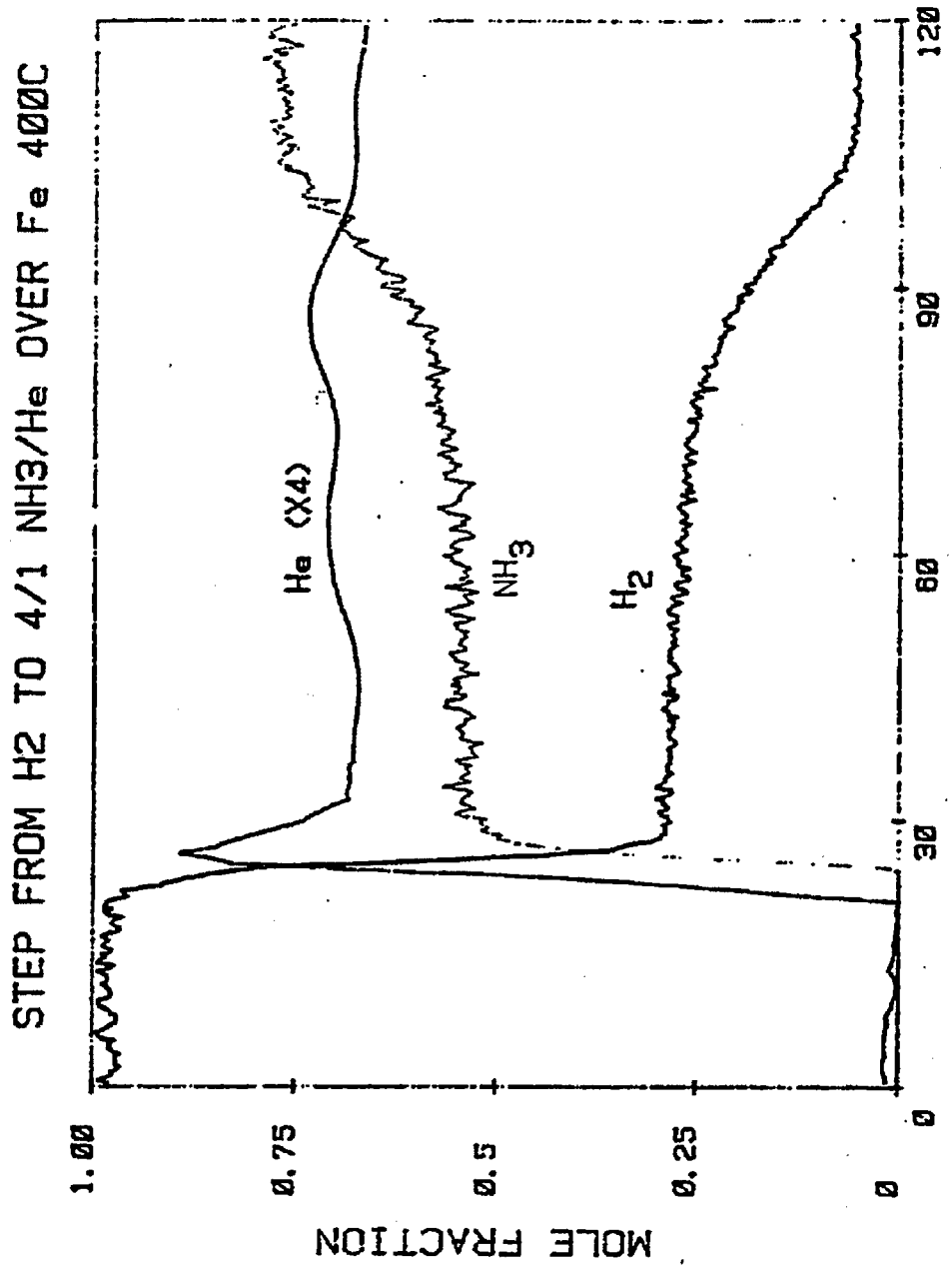

Figure 24 Step change from H_2 to 4/1 NH_3/He over reduced iron powder at 400°C. Fe_4N is formed as H_2 is evolved.

reaction conditions of the Monsanto patents (3-5) to produce acetonitrile, CH_3CN, selectively. Figure 25 shows the result of introducing a 2:7:3 $CO:H_2:NH_3$ mixture, with He as a diluent, over an iron powder catalyst prenitrided at 500°C directly from iron oxide. The N_2 and H_2 in the left portion of the figure depict substantial ammonia decomposition occurring over the catalyst. As the reactants are introduced, ammonia concentration drops slowly because the iron nitride decomposes rapidly in the reaction mixture, removing the majority of the nitrogen from the bulk and producing ammonia. This is indicated not only by the ammonia signal, but also by the excessive consumption of hydrogen. Simultaneously, the conversion of CO is substantial (75%) to CO_2 and H_2O, along with smaller (~1%) amounts of HCN and CH_3CN. The excessive CO_2 production deposits so much carbon that the activity to all products is virtually zero after one hour.

The situation is drastically different when a supported catalyst is used. Figure 26 shows the mass spectrometer signals for the initial minutes of reaction over a prereduced Fe/SiO_2 catalyst at 500°C. The rate of CO_2 production is an order of magnitude smaller than the rate exhibited over unsupported iron. CH_3CN is produced now at a higher rate, with comparable selectivity to CO_2. Accurate values of the production rates will require careful calibration for acetonitrile. Nevertheless, a significant rate is maintained for at least 20 hours into the reaction (Figure 27). In these results, He is only 10% of the gas stream. Prenitriding the supported catalyst yields similar results in activity profile. Thus, we suspect that the nitrided catalyst loses most of the bulk nitrogen quickly at these conditions (500°C in a hydrogen rich reactant mixture).

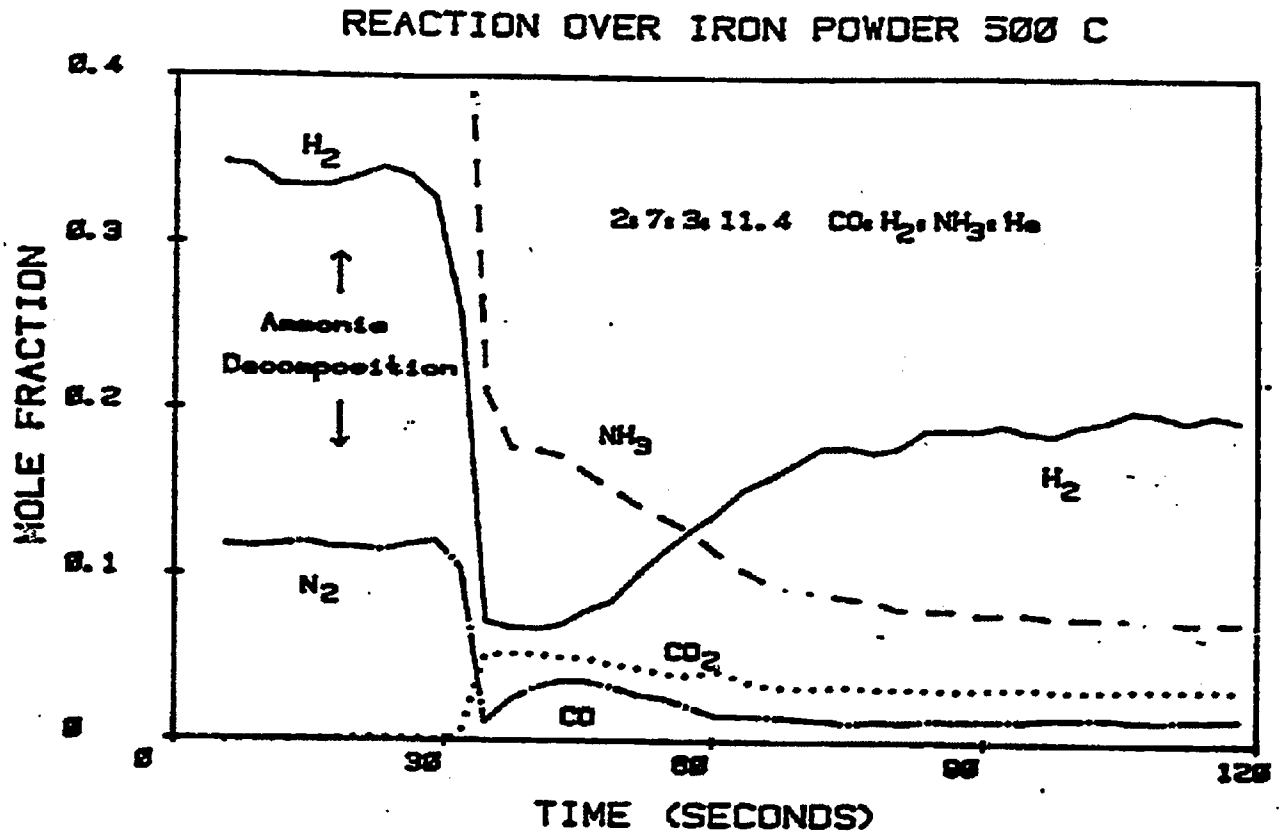

Figure 25 Initial minutes of reaction of 2:7:3 $CO:H_2:NH_3$ at 500°C over a prenitrided iron powder. Pure NH_3 is fed to the catalyst at the left of the figure, producing the ammonia decomposition products. The reaction mixture, with He as a diluent, is then stepped over the catalyst. N_2 and CO have the same mass and thus make up the same curve.

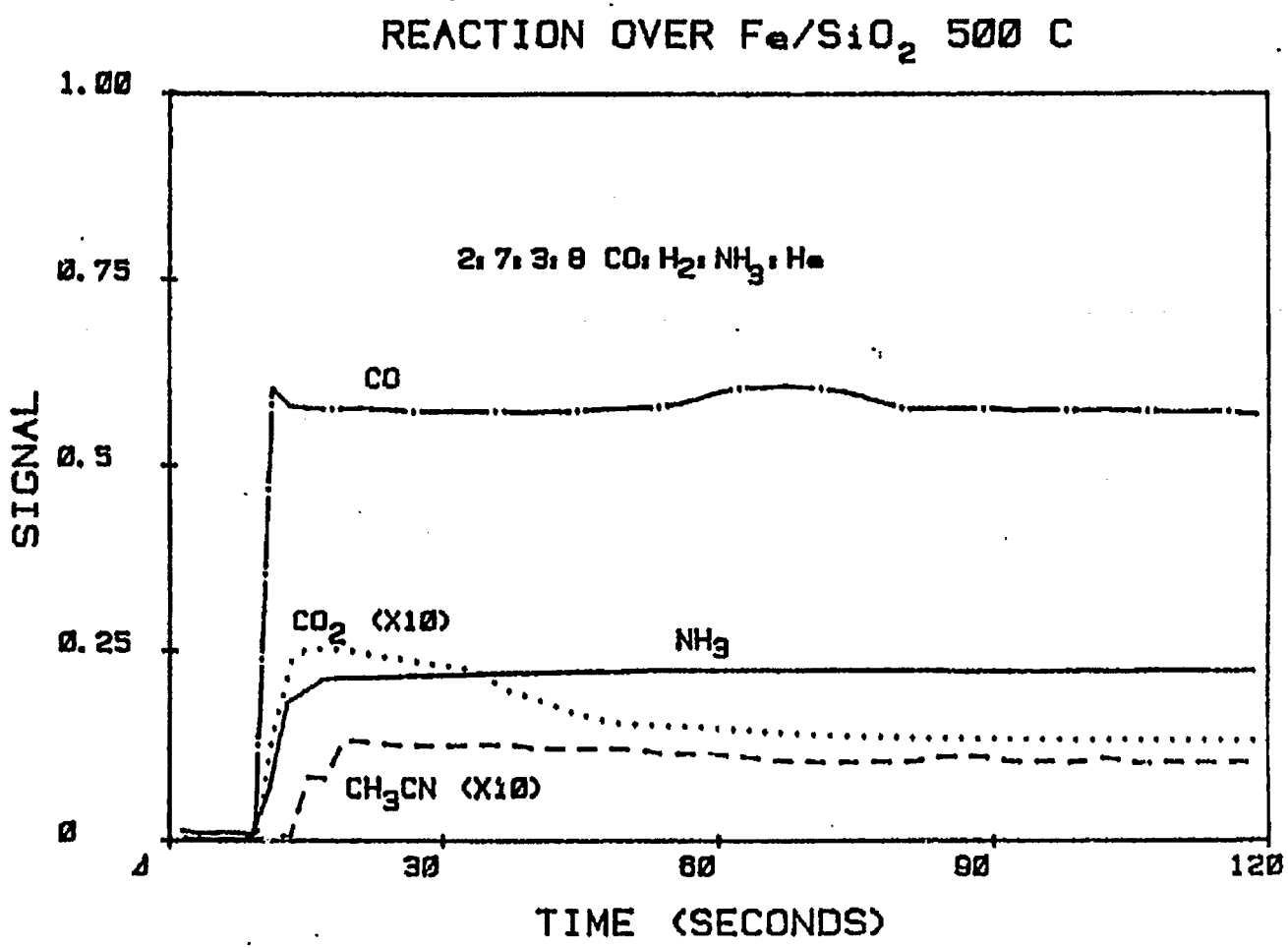

Figure 26 Initial minutes of reaction of 2:7:3 $CO:H_2:NH_3$ at 500°C over reduced 4%Fe/SiO_2. The reaction mixture, with He as a diluent, is stepped into H_2 (not shown). Note that signals have not been converted to mole fractions, and that mole fractions ratios do not correlate with signal ratios (CO/NH_3 is 2:3 in the feed, but > 1 in signal ratio.

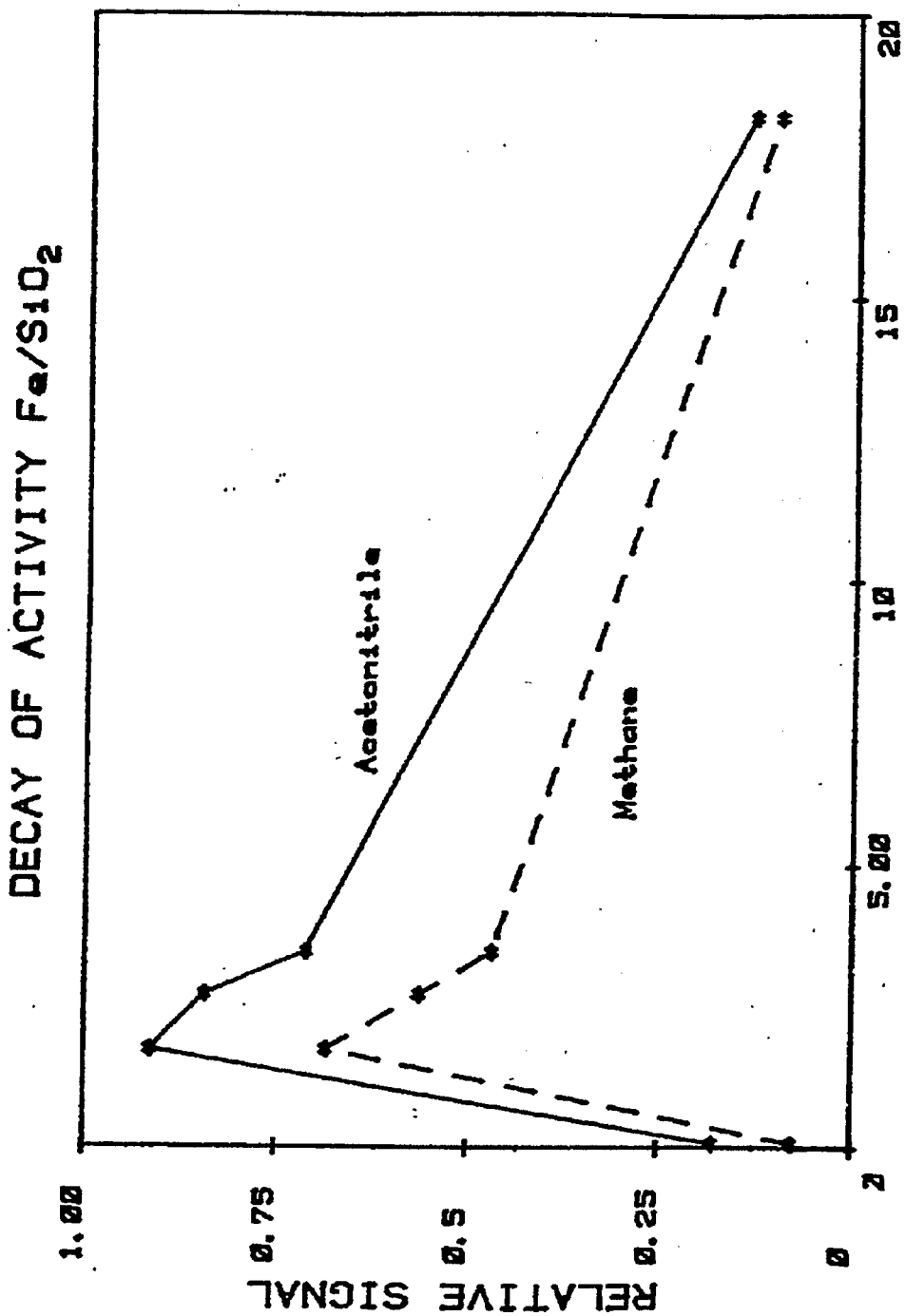

Figure 27 Decay of activity over a 4%Fe/SiO_2 catalysts as measured by gas chromatography. The reaction mixture is 2:7:3:1.3 CO:H_2:NH_3:He at 500°C. Other major products are H_2O, CO_2 and HCN.

Over this same catalyst after 2 hours of synthesis, the $^{14}NH_3$ and He in the reaction mixture (2:7:3:1.5 $CO:H_2:NH_3:He$) were substituted with $^{15}NH_3$ and Ar in a pulse with the remaining components unchanged. The reaction maintained steady state during this change. Figure 28 shows the result of this substitution on the acetonitrile product. The $CH_3C^{14}N$ decays during the pulse (denoted by the argon signal) and the corresponding isotope $CH_3C^{15}N$ comes up. Not only does this behavior confirm our identification of acetonitrile, but it also shows that the nitrogen pool that participates in the reaction is quick to exchange with gas phase ammonia. The data in Figure 28 show an influence of readsorption on the NH_3 response. If the problem can be eliminated, analysis of results like these will yield an approximate coverage of the nitrogen-containing surface species active in production of acetonitrile, and also the reaction rate constant of the rate limiting step.

2.4.4 Small Particle Iron on Carbon

We have also begun studying iron nitrides supported on carbon. A small-particle, 5% iron on Carbolac-1, which is a high surface area (1000 m^2/g) carbon support, was prepared and reduced in hydrogen for 16 hours at 400°C. The room temperature Mössbauer spectrum of this reduced catalyst is shown in Figure 29a, and the preliminary fitted Mössbauer spectral parameters in Table 12. The broad singlets at 0.0 mm/sec may be ascribed to superparamagnetic Fe^0. The typical six line pattern collapses to a superparamagnetic singlet when the relaxation time is short compared to the lifetime of the excited state of the nucleus. We may therefore conclude that our iron crystallites are small. The asymmetric nature of this spectrum is due to the

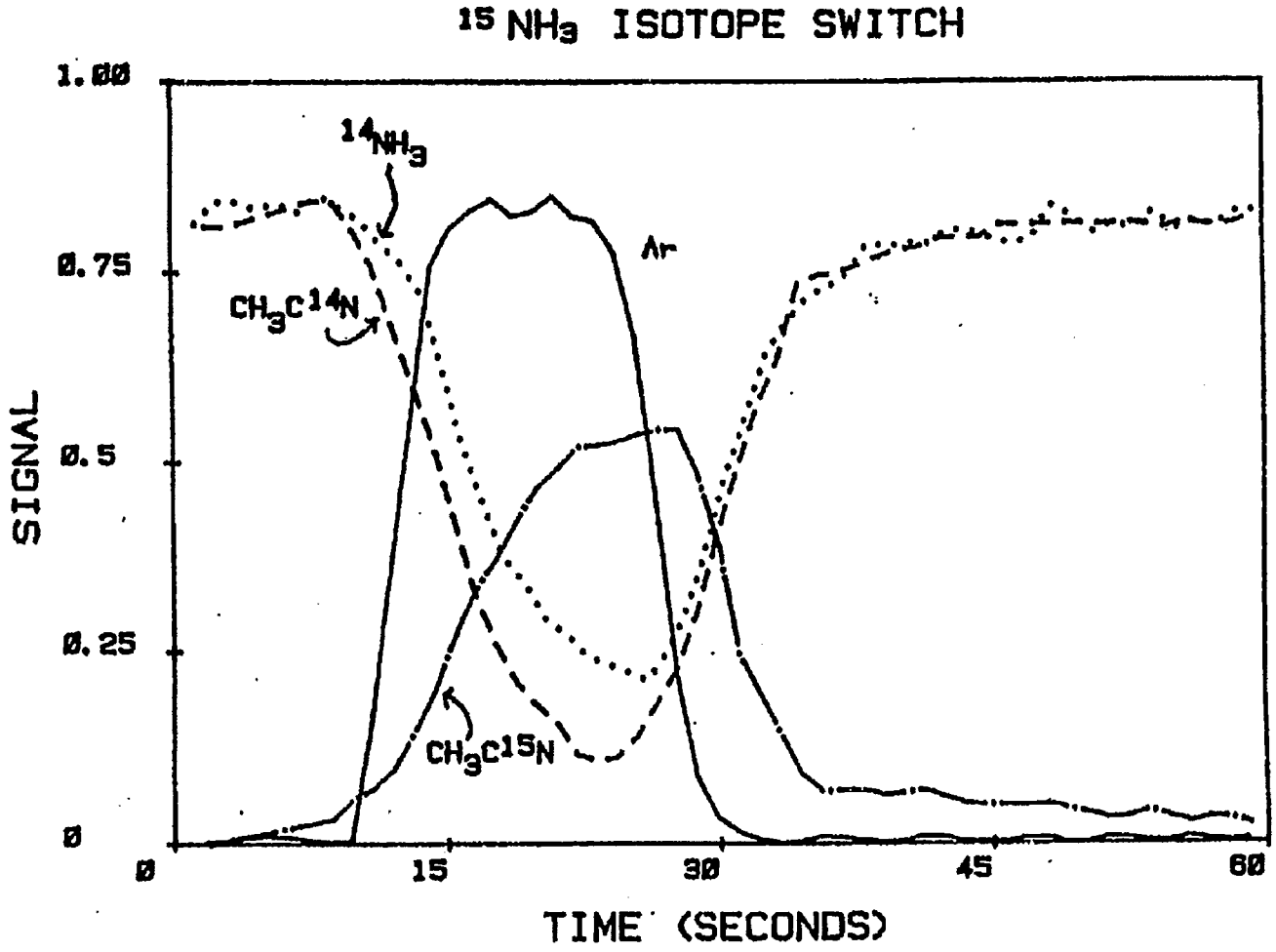

Figure 28 Acetonitrile production during a pulse of 2:7:3:1.5 $CO:H_2:{}^{15}NH_3$:Ar into 2:7:3:1.5 $CO:H_2:{}^{14}NH_3$:He at 500°C over Fe/SiO_2.

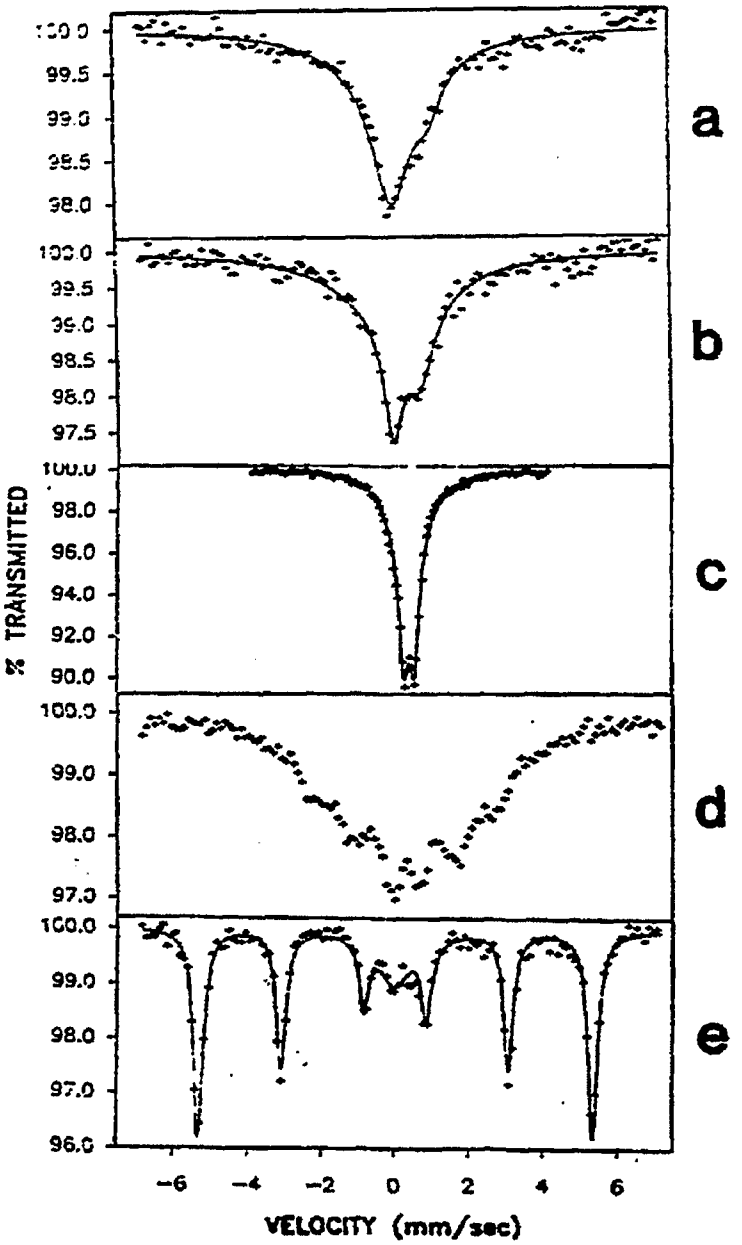

Figure 29 Room Temperature Mössbauer Spectra of 4.5 wt% Fe Supported on Carbolac.

a) Reduced in H_2 at 400°C for 16 hrs
b) Exposed to He at RT for 21 hrs
c) Nitrided to ε-Fe_2N using 100% NH_3 at 400°C for 8 hrs
d) Post - FTS at 250°C for 20 hrs
e) Rereduced in H_2 at 400°C for 4 hrs

TABLE 12

Mössbauer Spectral Parameters

FIG. 7	PHASE	IS (mm/sec)	QS (mm/sec)	HFS (kOe)	LW (mm/sec)	REL AREA (%)
7a.	sup α-Fe	0.0	-	-	1.2	41
	sup α-Fe	0.0	-	-	3.5	49
	Fe^{2+}	1.0	-	-	0.9	10
7b.	sup α-Fe	0.0	-	-	0.6	19
	sup α-Fe	0.0	-	-	3.5	61
	Fe^{2+}	0.74	-	-	0.9	20
7c.	ς–Fe_2N	0.40	0.29	-	0.29	36
	ς–Fe_2N	0.40	0.24	-	0.98	64
7e.	sup α-Fe	0.0	-	-	1.0	16
	Fe^{2+}	1.0	-	-	0.5	2
	α-Fe	0.0	0.0	330	0.31	82

TABLE 13

Mössbauer Spectral Parameters

FIG. 8	PHASE	IS (mm/sec)	QS (mm/sec)	HFS (kOe)	LW (mm/sec)	REL AREA (%)
8a.	sup α-Fe	0.0	-	-	1.3	84
	Fe^{2+}	1.0	-	-	0.86	10
	α-Fe	0.0	0.0	330	0.27	6
8b.	sup α-Fe	0.0	-	-	1.3	21
	ϵ'–$Fe_{2.2}C$	0.24	0.68	-	0.64	79
8c.	sup α-Fe	0.0	-	-	1.4	87
	Fe^{2+}	1.0	-	-	0.9	7
	α-Fe	0.0	0.0	330	0.27	6

contribution of Fe^{2+} at 1.0 mm/sec, which arises from incomplete reduction. Extensive (21 hrs) exposure to UHP He that was further purified in oxygen traps resulted in the spectrum of Figure 29b. The increased absorbence in the Fe^{2+} region indicates that the catalyst is passivated in helium with oxygen concentrations on the order of 1 ppb but assignment of the product to Fe^{2+} vs Fe^{3+} is not yet complete. This catalyst was nitrided in pure NH_3 at 400°C for 8 hours to produce the ς–Fe_2N phase, indicated by the doublet seen in Figure 29c. Figure 29d shows the result of exposure of this catalyst to 3/1 H_2/CO at 250°C for 20 hours. This spectrum has the same general appearance as those of unsupported nitrided samples following FTS and indicates a complex mixture of nitride, carbide and carbonitride phases. Rereduction of the sample given in spectrum 29d resulted in spectrum 29e, showing major contributions (84%) from a bulk Fe metal pattern. Thus, the iron crystallites have sintered during the nitriding-reaction-reduction process. In previous experiments, we have shown that small particle Fe_4N on carbon has stable activity during Fischer-Tropsch synthesis. Our results here suggest that high nitrogen content may diminish the stability of small particles in FTS.

In addition to the Carbolac samples, we have prepared a number of well characterized Fe/CSX203 samples. The CSX203 carbon has an extremely high surface area (1300 m^2/g). The Mössbauer spectrum of a reduced 4.08%Fe/SiO_2 sample, with dispersion of 47% and 18 Å particle diameter, is shown in Figure 30a. The vast majority of the iron displays superparamagnetic character (the fitted parameters are in Table 13). Subsequent reaction with synthesis gas yields a superparamagnetic carbide (Figure

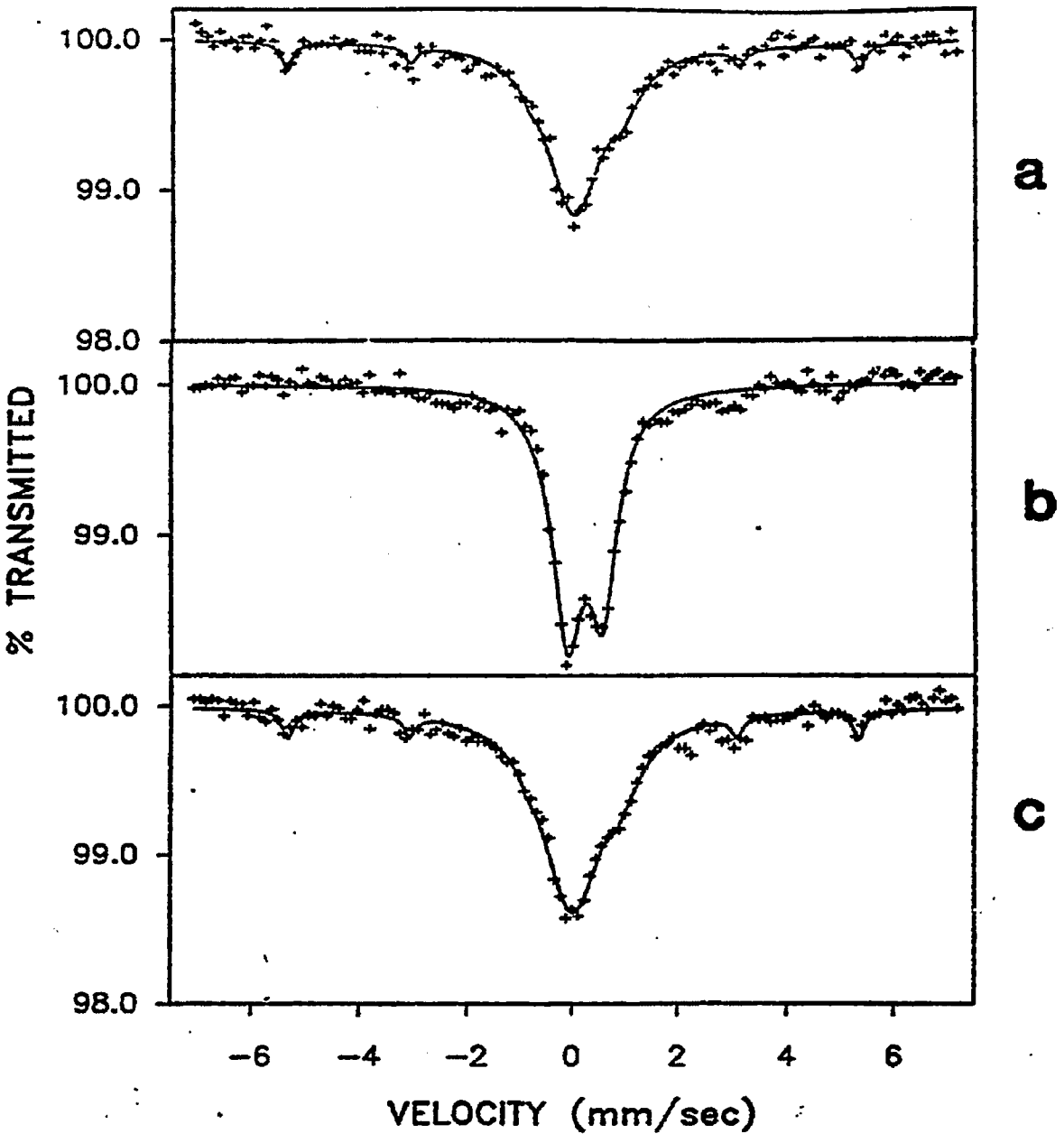

Figure 30 Room Temperature Mössbauer Spectra of 4.08% Fe Supported on CSX203 Carbon.

a) Reduced in H_2 at 400°C for 16 hrs

b) Post - FTS at 250°C for 23 hrs. Catalyst was not nitrided.

c) Rereduced in H_2 for 10 hrs at 400°C

30b). Rereduction of this sample shows no evidence of sintering (Figure 30c). Investigation of the effect of size on iron particle stability and on reaction rate is currently under way.

References

1. Anderson, R.B., Cat. Rev. - Sci. Eng., *21,* 53 (1980).
2. Olive', G. and Olive', S., J. Molec. Catal., *4,* 378 (1978).
3. Olive', G. and Olive', S., U.S. Patent 4, 179, 462, Dec. 18, 1979.
4. Gambell, J.W. and Auvil, S.R., U.S. Patent 4, 272, 451, June 9, 1981.
5. Auvil, S.R. and Penquite, C.R., U.S. Patent 4, 272, 452, June 9, 1981.
6. Anderson, R.B., Adv. Catal., *5,* 355 (1953).
7. Anderson, R.B., Shultz, J.F., Seligman, B., Hall, W.K. and Storch, H.H., J. Am. Chem. Sco., *72,* 3502 (1950).
8. Yeh, E.B., Jaggi, N.K., Butt, J.B., and Schwartz, L.H., J. Catal. *91,* 231 (1985).
9. Jack, K.H., Proc. Roy. Soc. (London), *A208, 200* (1951).
10. Eisenhut, O. and Kaupp, E., Z. Elektrochemie, *36 (6),* 392 (1930).
11. Lehrer, E., Z. Elektrochemie, *36 (6),* 383 (1930).
12. Chen, G.M., Jaggi, N.K., Butt, J.B., Yeh, E. and Schwartz, L.H., J. Phys. Chem., *87,* 5326 (1983).
13. Niemantsverdriet, H., PhD dissertation, Technische Hogeschool Delft, 1983.
14. Hesse, J. and Rübartsch, A., J. Phys. E. Sci. Inst., *7,* 526 (1974).
15. Wivel, C. and Morup, S., J. Phys. E. Sci. Inst., *14,* 605 (1981).
16. Ertl, G., Huber, M. and Thiele, N., Z. Naturforsch, *34A,* 30 (1979).
17. Logan, S.R., Moss, R.L. and Kemball, C., Trans. Faraday Soc., *54,* 922 (1958).
18. Clauser, M.J., Sol. State Comm., *8,* 781 (1970).
19. Lin, S.C. and Phillips, J., J. Appl. Phys., *58,* 1943 (1985).
20. Bridelle, R., Ann. Chem. Series 12, Number 10, 824 (1955).
21. Raupp, G.B. and Delgass, W.N., J. Catal., *58,* 348 (1979).
22. Emmett, P.H. and Brunauer, S., J. Am. Chem. Soc., *55,* 1738 (1933).
23. U.S. Department of Energy Quarterly Technical Progress Report, DOE/PC50804-3.
24. Niemantsverdriet, H.W., vander Kraan, A.M., van Dijk, W.L. and van der Baan, H.S., J. Phys. Chem., *84* 3363 (1980).
25. DeCristofaro, N. and Kaplow, R., Met. Trans. A., *8A,* 425 (1977).

26. Foct, J., LeCaer, G., DuBois, J.M. and Faivre, R., in "International Conference on Carbides, Borides, and Nitrides in Steels" Kolobrzeg, Poland, 1978.

27. Bianchi, D., Tau, L.M., Borcar, S. and Bennett, C.O., J. Catal. *84,* 352 (1983).

28. Winslow, P. and Bell, A.T., J. Cat., *86,* 158 (1984).

29. Reymond, J., Merlaudeau, P. and Teichner, S., J. Catal. *75,* 39 (1982).

30. Stanfield, R., Personal Communication.

31. Greenwood, N.N. and Gibb, T.C., "Mössbauer Spectroscopy", Chapman and Hal, Ltd., London, 1971.

32. Blanchard, F., Reymond, J., Pommier, B. and Teichner, S., J. Mol. Catal., *17,* 171 (1983).

33. Krebs, H.J., Bonzel, H.P., Schwartung, W. and Gafner, G., J. Catal., *72,* 199 (1981).

34. Knoechel, D.J., M.S. Thesis, Purdue University, 1983.

35. Schwerdtfeger, C., Grieveson, P. and Turkdogon, E.T., Trans. Met. Soc., *245,* 2461 (1969).

36. Hall, W.K., Dieter, W.E., Hofer, L.J.E. and Anderson, R.B., J. Phys. Chem., *74,* 638 (1952).

37. Tau, L.M., Borcar, S., Bianchi, D. and Bennett, C.O., J. Catal., *87,* 36 (1984).

38. Amelse, J.A., Grjnkewich, G., Butt, J.B. and Schwartz, L.M., J. Phys. Chem., *85,* 2484 (1981).

39. Jung, H.J., Walker, K. and Vannice, M.A., J. Catal. *75,* 416 (1982).

40. Jack, K.H., Proc. Roy. Sci., (London), *A195,* 41 (1948).

41. Jack, K.H., Proc. Roy. Soc., (London), *A195,* 34 (1948).

42. Borghard, W.G. and Bennett, C.O., I&EC Prod. Res. & Div., *18,* 18 (1979).

43. Amelse, J.A., PhD dissertation, Northwestern University, 1985.

44. Hummel, A.A., Hummel, K.E., Wilson, A.P. and Delgass, W.N., to be published.

APPENDICES

Distribution List

A) *Fred W. Steffgen* (3)
Project Manager
U.S. Department of Energy Pittsburgh Energy Technology Center
P.O. Box 10940
Pittsburgh, PA 16236

B) *Michael Hogan*
Acquisition & Assistance Division
U.S. Department of Energy
Pittsburgh Energy Technology Center
P.O. Box 10940
Pittsburgh, PA 16236

*C) U.S. Department of Energy
Technical Information Center
P.O. Box 62
Oak Ridge, TN 37830

E) U.S. Department of Energy
Patent Office
Office of General Counsel
Chicago Operations & Regional Office
9800 South Cass Avenue
Argonne, IL 60439

G) *Frank M. Ferrell, Jr.*
U.S. Department of Energy Fe-3 MS C-156 GTN
Washington, D.C. 20545

H) *Marilyn Keane* (3)
U.S. Department of Energy
Pittsburgh Energy Technology Center
P.O. Box 10940
Mail Stop 920-116
Pittsburgh, PA 15236

I) *A.A. Hummel*
Graduate Student
School of Chemical Engineering

Purdue University

J) *K. Hummel*
Graduate Student
School of Chemical Engineering
Purdue University

K) *Jerry L. Arnold*
Principal Research Metallurgist
Research and Technology
ARMCO Inc.
703 Curtis Street
Middletown, OH 45043

*Note: Grantee Shall obtain patent
clearance from
addressee "E" above
prior to forwarding
copies to TIC.
Include Statement
"Patent Cleared by
Chicago OPC on

_____"
Date

SATISFACTION GUARANTEED

NTIS strives to provide quality products, reliable service, and fast delivery. Please contact us for a replacement within 30 days if the item you receive is defective or if we have made an error in filling your order.

▲▲ E-mail: info@ntis.gov
▲▲ Phone: 1-888-584-8332 or (703)605-6050

Reproduced by NTIS

National Technical Information Service
Springfield, VA 22161

This report was printed specifically for your order from nearly 3 million titles available in our collection.

For economy and efficiency, NTIS does not maintain stock of its vast collection of technical reports. Rather, most documents are custom reproduced for each order. Documents that are not in electronic format are reproduced from master archival copies and are the best possible reproductions available.

Occasionally, older master materials may reproduce portions of documents that are not fully legible. If you have questions concerning this document or any order you have placed with NTIS, please call our Customer Service Department at (703) 605-6050.

About NTIS

NTIS collects scientific, technical, engineering, and related business information – then organizes, maintains, and disseminates that information in a variety of formats – including electronic download, online access, CD-ROM, magnetic tape, diskette, multimedia, microfiche and paper.

The NTIS collection of nearly 3 million titles includes reports describing research conducted or sponsored by federal agencies and their contractors; statistical and business information; U.S. military publications; multimedia training products; computer software and electronic databases developed by federal agencies; and technical reports prepared by research organizations worldwide.

For more information about NTIS, visit our Web site at **http://www.ntis.gov**.

NTIS

Ensuring Permanent, Easy Access to U.S. Government Information Assets

U.S. DEPARTMENT OF COMMERCE
Technology Administration
National Technical Information Service
Springfield, VA 22161 (703) 605-6000